NASA CONTRACTOR REPORT

NASA CR-2524

NASA CR-2524

LIGHTNING EFFECTS ON THE NASA F-8 DIGITAL-FLY-BY-WIRE AIRPLANE

J. A. Plumer, F. A. Fisher, and L. C. Walko

Prepared by
GENERAL ELECTRIC COMPANY
Pittsfield, Mass. 01201
for Flight Research Center

NATIONAL AERONAUTICS AND SPACE ADMINISTRATION • WASHINGTON, D. C. • MARCH 1975

1. Report No.	2. Government Accession No.	3. Recipient's Catalog No.
NASA CR-2524		

4. Title and Subtitle	5. Report Date
Lightning Effects on the NASA F-8 Digital-Fly-By-Wire Airplane	March 1975
	6. Performing Organization Code

7. Author(s)	8. Performing Organization Report No.
J. A. Plumer, F. A. Fisher, and L. C. Walko	SRD 74-068
	10. Work Unit No. 501-26-06

9. Performing Organization Name and Address	11. Contract or Grant No.
Environmental Electromagnetics Unit General Electric Company Corporate Research and Development Pittsfield, Massachusetts 01201	NAS 4-2090
	13. Type of Report and Period Covered: Contractor Report - Final

12. Sponsoring Agency Name and Address	14. Sponsoring Agency Code
National Aeronautics and Space Administration Washington, D. C. 20546	

15. Supplementary Notes

NASA Technical Monitor: Wilton P. Lock, Jr.

16. Abstract

This is the first program to experimentally determine the effects of lightning on a Digital Fly-By-Wire (DFBW) aircraft control system. The aircraft was a NASA operated F-8 fitted with a modified Apollo guidance computer. Current pulses similar in waveshape to natural lightning, but lower in amplitude, were injected into the aircraft. Measurements were made of the voltages induced on the DFBW circuits, the total current induced on the bundles of wires, the magnetic field intensity inside the aircraft, and the current density on the skin of the aircraft. Voltage measurements were made in both the line-to-ground and line-to-line modes. Voltages measured at the non-destructive test level were then scaled upward to determine how much would be produced by actual lightning. A 200,000 ampere severe lightning flash would produce between 40 and 2000 volts in DFBW circuits. Some system components are expected to be vulnerable to these voltages. The typical surge voltage measured on this aircraft was of a damped oscillatory nature of frequency roughly proportional to the length of the wires comprising the circuit. This report describes the physical processes by which lightning generates voltages, describes the experimental techniques used for measurements, and presents data on magnetic field intensities, currents, and voltages. It concludes with a discussion of results and recommendations regarding both this aircraft and future fly-by-wire aircraft.

17. Key Words (Suggested by Author(s))	18. Distribution Statement
Control systems Digital fly-by-wire Lightning effects	Unclassified - Unlimited Category: 08

19. Security Classif. (of this report)	20. Security Classif. (of this page)	21. No. of Pages	22. Price*
Unclassified	Unclassified	155	$6.25

For sale by the National Technical Information Service, Springfield, Va. 22151

CONTENTS

CONTENTS (Concluded)

ILLUSTRATIONS

ILLUSTRATIONS (Continued)

ILLUSTRATIONS (Continued)

ILLUSTRATIONS (Continued)

ILLUSTRATIONS (Continued)

TABLES

NOMENCLATURE

A/C	Aircraft
AGC	Apollo Guidance Computer
BCS	Backup Control System
DFBW	Digital fly-by-wire
DFCS	Digital Flight Control System
FCS	Flight Control System
IMU	Inertial Measurement Unit
LVDT-PRIM	Linear Variable Distribution Transformer-Primary
LVDT-SEC	Linear Variable Distribution Transformer-Secondary
MPC	Mode and Power Control
SAS	Stability Augmentation System
FUP	Secondary Actuator Follow-Up

LIGHTNING EFFECTS ON THE NASA F-8 DIGITAL-FLY-BY-WIRE AIRPLANE

By J.A. Plumer, F.A. Fisher and L.C. Walko

Environmental Electromagnetics Unit
GENERAL ELECTRIC COMPANY
Corporate Research and Development
Pittsfield, Massachusetts

SUMMARY

This is the first program to experimentally determine the effects of lightning on a Digital Fly-by-Wire (DFBW) aircraft control system. The aircraft was a NASA operated F-8 fitted with a modified Apollo guidance computer. Current pulses similar in waveshape to natural lightning, but lower in amplitude, were injected into the aircraft. Measurements were made of the voltages induced in the DFBW circuits, the total current induced on bundles of wires, the magnetic field intensity inside the aircraft and the current density on the skin of the aircraft. Voltage measurements were made in both the line-to-ground and line-to-line modes. Voltages measured at the non-destructive test level were then scaled upwards to determine how much would be produced by actual lightning. A 200,000 ampere severe lightning stroke would produce between 40 and 2000 volts in DFBW circuits. Some system components are expected to be vulnerable to these voltages. The typical surge voltage measured in these circuits was of a damped oscillatory nature of period roughly proportional to the length of the wires comprising the circuit. The driving mechanism that excited the voltages was the changing magnetic field inside the aircraft. The use of a single point ground philosophy does not eliminate such magnetically induced voltages even though it may reduce the exposure of circuits to the IR voltage produced by the flow of current through the structural resistance of the aircraft. Typically the latter were small compared to the magnetically induced voltages.

External magnetic fields were shown to be proportional to the amplitude of the lightning current. External field amplitudes were also determined by the shape and circumference of the adjacent structure upon which the currents were flowing.

The internal magnetic fields were much lower in amplitude than the external fields, but were not negligible. Magnetic fields penetrate to the interior through apertures and by diffusion through the skin of the aircraft. Aperture coupling is generally the more important. In the cockpit the measured magnetic fields were entirely due to aperture coupling. In a compartment with a removable cover, the amount of aperture coupling was shown to depend on the number of fasteners used to hold that cover in place. Around the gun bay these fasteners were about 0.3 m apart and the aperture coupled fields predominated. Around the battery compartment, the fasteners were about 0.04 m apart and the diffusion coupled fields predominated.

Currents on bundles of wires were, like the circuit voltages, shown to be predominantly oscillatory in nature. Amplitudes varied greatly. A cumulative distribution of currents measured in the gun bay showed 50 percent of the currents would exceed 250 amperes peak-to-peak with 10 percent exceeding 900 amperes peak-to-peak, when extrapolated to correspond with a 200,000 ampere stroke.

The voltages and currents produced by lightning on the DFBW circuits also appeared simultaneously on all three channels of the Backup Control System (BCS). These voltages and currents lasted for times on the order of 10 microseconds. These times are comparable to the memory cycle and computation times of the computer. Since a typical lightning flash is comprised of several strokes occurring at intervals of a few tens of milliseconds, several repeated bursts may occur during a complete computation cycle of the computer.

The implication of these tests is that a lightning flash has the potential of damaging or interfering with both the primary and the redundant channels of a fly-by-wire control system at the same time.

There are techniques available (shielding, grounding, surge suppression) to control lightning induced effects, but this study did not incorporate development of protective measures for this system.

It is recommended that the NASA F-8 DFBW or similar aircraft not be flown in areas where thunderstorms are in progress unless positive protective measures are taken to minimize possible lightning effects.

INTRODUCTION

Present practices in lightning protection of aircraft deal predominantly with what may be called the DIRECT EFFECTS of lightning, including burning, blasting and physical deformation of skins and structural elements. Existing lightning protection specifications, such as MIL-B-5087B (Bonding, Electrical, and Lightning Protection, for Aerospace Systems) concentrate on electrical bonding and its function in minimizing these effects. Other criteria, such as FAA Advisory Circular No. AC 25-3A (Protection of Transport Aircraft Fuel Systems Against Lightning) provide guidance for protection against lightning ignition of flammable fuel-air mixtures. Concern with these effects has been necessary since safety of flight in a lightning environment has heretofore primarily depended upon protection against fuel ignition and structural damage that can be produced by lightning.

There is increasing evidence of troublesome electromagnetic effects due to lightning, however. These have involved both permanent damage and temporary malfunction of equipment. In a few cases aircraft have been lost due to suspected lightning-induced effects; however, most of the effects have thus far resulted in curtailment of operations or reduced safety margins.

Earlier vacuum tube electronics were relatively immune to lightning-induced transient voltage surges; however, the newer generations of modern, solid state microcircuitry are increasingly vulnerable to upset or damage from such effects. Because these are electromagnetically induced surges, they are often referred to as the INDIRECT EFFECTS of lightning. Recently these effects have been receiving additional attention since the flight safety of modern flight vehicles is increasingly dependent on reliable operation of critical electronic systems. At present there are no standards or specifications applicable to the indirect effects of lightning.

With the advent of fly-by-wire systems, particularly those with digital computer and control electronics, the indirect effects of lightning very clearly have the potential of presenting a hazard to safety of flight. This hazard may be particularly acute for digital systems. While most practical digital fly-by-wire systems would include multiple redundant control circuits, it is possible to conceive of a situation in

which the high level electromagnetic interference produced by lightning could interfere with all of the channels of a fly-by-wire system at once, raising the possibility that there may in fact be no real redundance with respect to lightning effects.

The NASA Flight Research Center has developed and demonstrated a digital fly-by-wire flight control system in an F-8 aircraft. Recognizing the possibility of this hazard, an experimental program was implemented with General Electric to evaluate the possible electromagnetic effects of lightning on this aircraft and obtain data for use in minimizing these effects in future generations of fly-by-wire aircraft.

A recently developed simulated lightning test and measurement system known as the TRANSIENT ANALYSIS technique offers a means of investigating these electromagnetic effects of lightning without hazard to the aircraft being tested. This technique was utilized to study the NASA F-8 DFBW aircraft in this program. The experimental work was conducted during the period 26 November through 7 December 1973 at the NASA Flight Research Center, Edwards, California.

OBJECTIVES

The primary objective of this program was to determine the probable effects of lightning strikes on the flight control system of the NASA F-8 Digital Fly-by-Wire airplane and determine the need for protective measures to reduce harmful effects. A secondary objective of the program was to determine the basic mechanisms of lightning-induced interference or damage to digital fly-by-wire systems and the need for design modifications to minimize these effects in future systems.

The program was to be accomplished by an experimental investigation utilizing the TRANSIENT ANALYSIS technique for an in-the-field investigation of lightning-induced voltages in the electrical circuits of the aircraft and an analytical study of the effects of these voltages on the flight control system and the need for protective devices. The analytical study of the probable impact of these voltages on the DFCS was performed by Delco Electronics Division of General Motors Corporation, manufacturer of the DFCS. Delco personnel were present during the transient analysis tests at the Flight Research Center. The results of the Delco analysis are presented in Delco Report, "Lightning-Induced Voltage Impact on NASA F-8 Digital Flight Control System When Scaled to a 200,000 Ampere Stroke", No. R74-21, February, 1974, (Reference 1).

F-8 DIGITAL FLY-BY-WIRE AIRPLANE

The NASA F-8 Digital Fly-By-Wire (DFBW) airplane and Flight Control System (FCS) are fully described in other NASA publications, such as Ref. 2. Characteristics of the aircraft and DFBW system considered pertinent to this investigation are described in the following paragraphs.

Description

The NASA DFBW system has been installed in an F-8 airplane which has been modified by replacing the mechanical flight control system with the DFBW system which uses the Apollo Lunar Guidance Computer (AGC) and inertial measurement unit, an analog fly-by-wire backup system (BCS), and an electrohydraulic actuation system. The modified F-8 airplane has been flying since May 1972. Figure 1 shows the overall dimensions of this airplane, and Figure 2 shows the location of the Flight Control System and associated cabling inside.

The FCS components are shown in Figure 3. A single digital primary channel and triple redundant electrical analog backup channels replaced the F-8 mechanical control system. The primary and backup channels all provide three-axis control of the airplane. The digital channel consists of an Apollo Lunar Guidance Computer, inertial measurement unit, coupling data unit, and astronaut display and keyboard, all taken from the Apollo guidance and navigation system. A mode and power panel permits the pilot to request the AGC to make mode and gain changes. The three-channel backup control system consists only of surface position command electronics. Specially designed electrohydraulic secondary actuators interface the primary and backup electronic commands with the conventional F-8 control surface power actuators. Five secondary actuators are utilized, one for the rudder and one each for the two horizontal stabilizers and the two ailerons.

The AGC is the heart of the primary control system and performs all flight control computations. The computer performs all flight control functions in a 30-millisecond time frame.

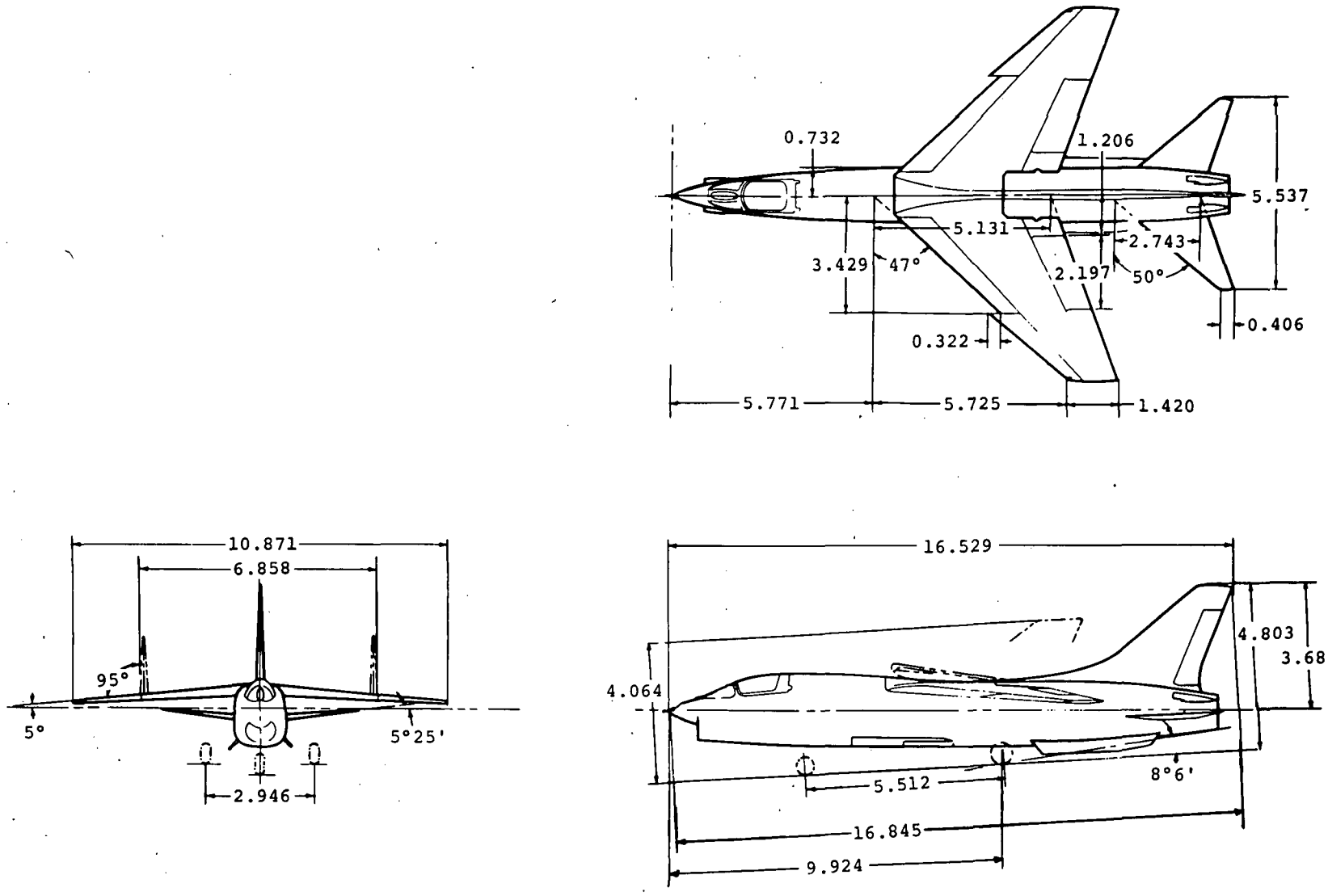

FIGURE 1 - GENERAL OVERALL DIMENSIONS OF
F-8 DIGITAL FLY-BY-WIRE AIRPLANE.
DIMENSIONS IN METERS.

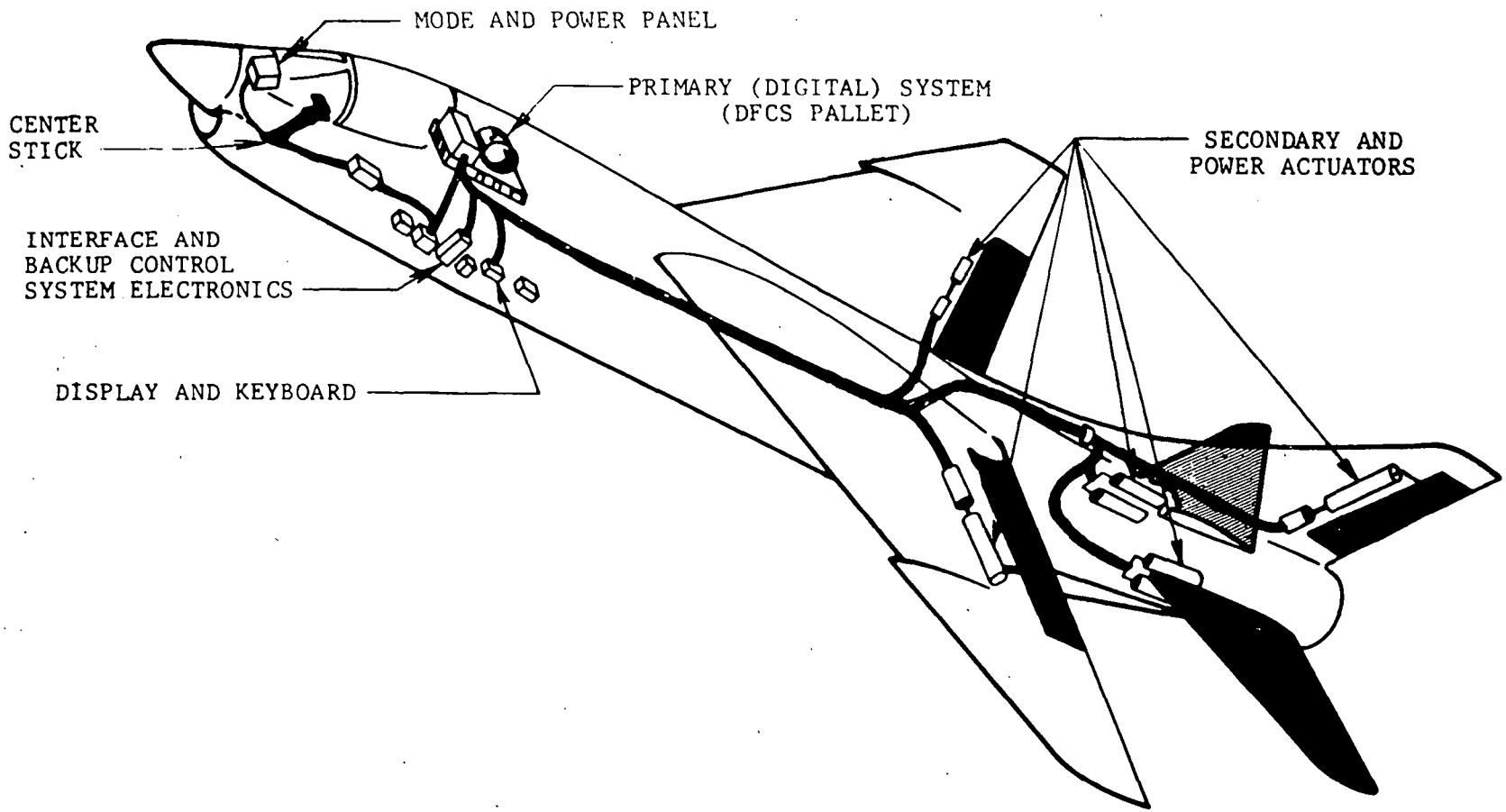

FIGURE 2 - LOCATION OF FLY-BY-WIRE CONTROL SYSTEM HARDWARE AND WIRING BUNDLES IN F-8 AIRPLANE.

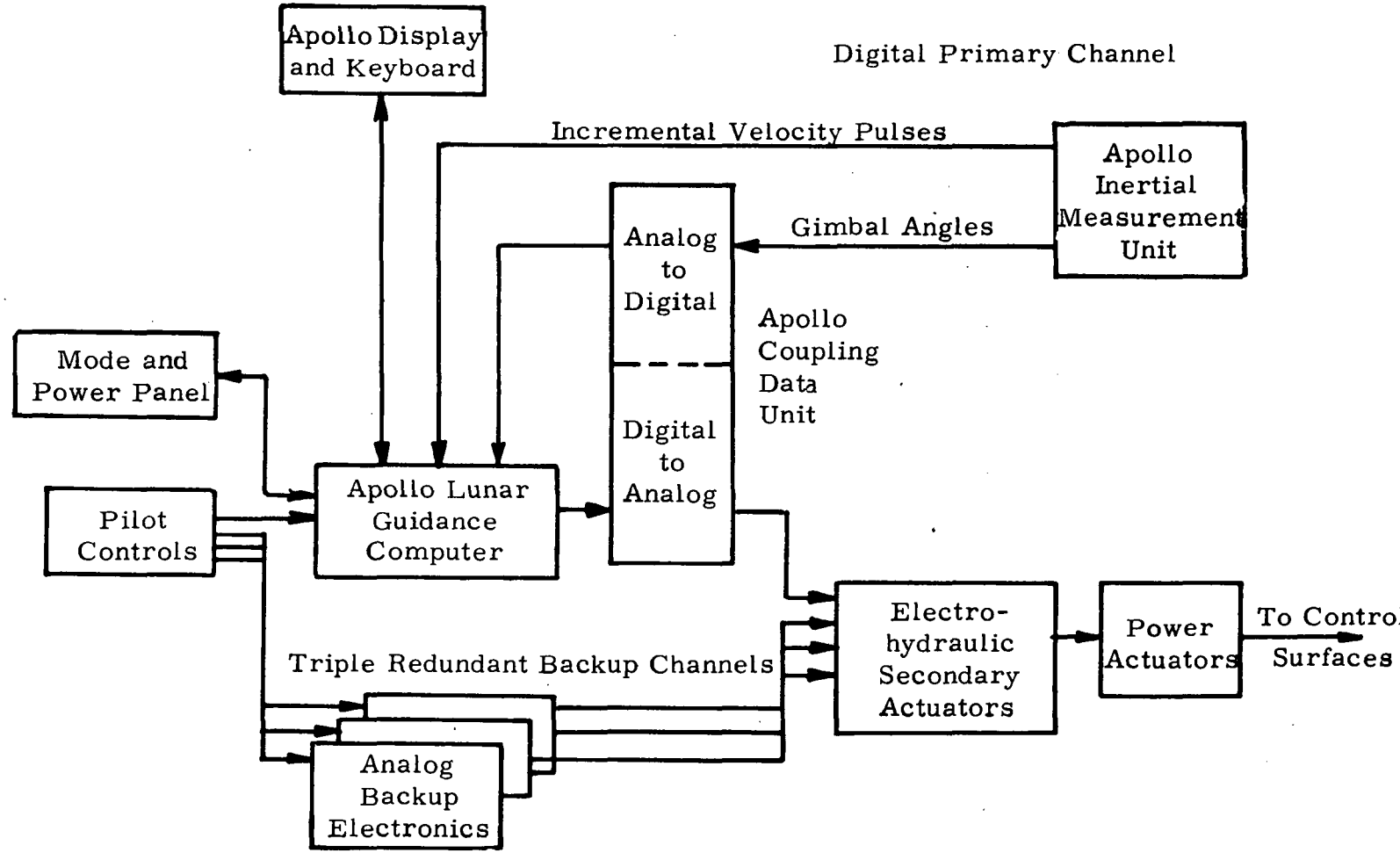

FIGURE 3 - F-8 DIGITAL FLY-BY-WIRE CONTROL SYSTEM COMPONENTS.

Other computer characteristics are as follows:

Read-only memory	36,864 words
Scratch pad memory	2,048 words
Word length	14 bits plus sign & parity
Number System	Fixed point, ones complement
Memory cycle time	11.7 microseconds
Computation time:	
Add	23.4 microseconds
Multiply	46.8 microseconds
Divide	81.9 microseconds

The executive software of the computer was retained, as were routines which serviced the inertial measurement unit and the display and keyboard. Flight control laws for the F-8 airplane are programmed for the computer's hardwired memory and cannot be changed. Feedback gains, logic flags, digital filter coefficients and other gain variables are placed in the computer's scratch pad memory where they can be changed. Approximately 150 such variables are associated with the flight control system.

Angular body rates and linear accelerations are determined by computing body rates and linear accelerations from the gimbal angles and the digital incremental velocity vector information which the inertial measurement unit provides to the computer.

Functional Operation

A functional diagram of the FCS system is shown in Figure 4. The AGC receives inputs from the pilot's stick, rudder pedal, and trim along with aircraft motion information from the inertial measurement unit. Surface commands are computed according to the programmed control laws. In order to protect against failures outside the computer, the analog portion of the primary channel was dualized.

The two drive signals for each surface represent commands to the secondary actuator position loop which is closed with analog stabilization electronics outside the digital computer. As is shown in Figure 4, there is an active and a monitor servo path. If a failure occurs in either the active or the monitor path, a hydraulic comparator senses a differential pressure between the active and monitor servovalve and transfers control to the backup control system. As long as the primary digital channel is operating normally, the backup electronics track the

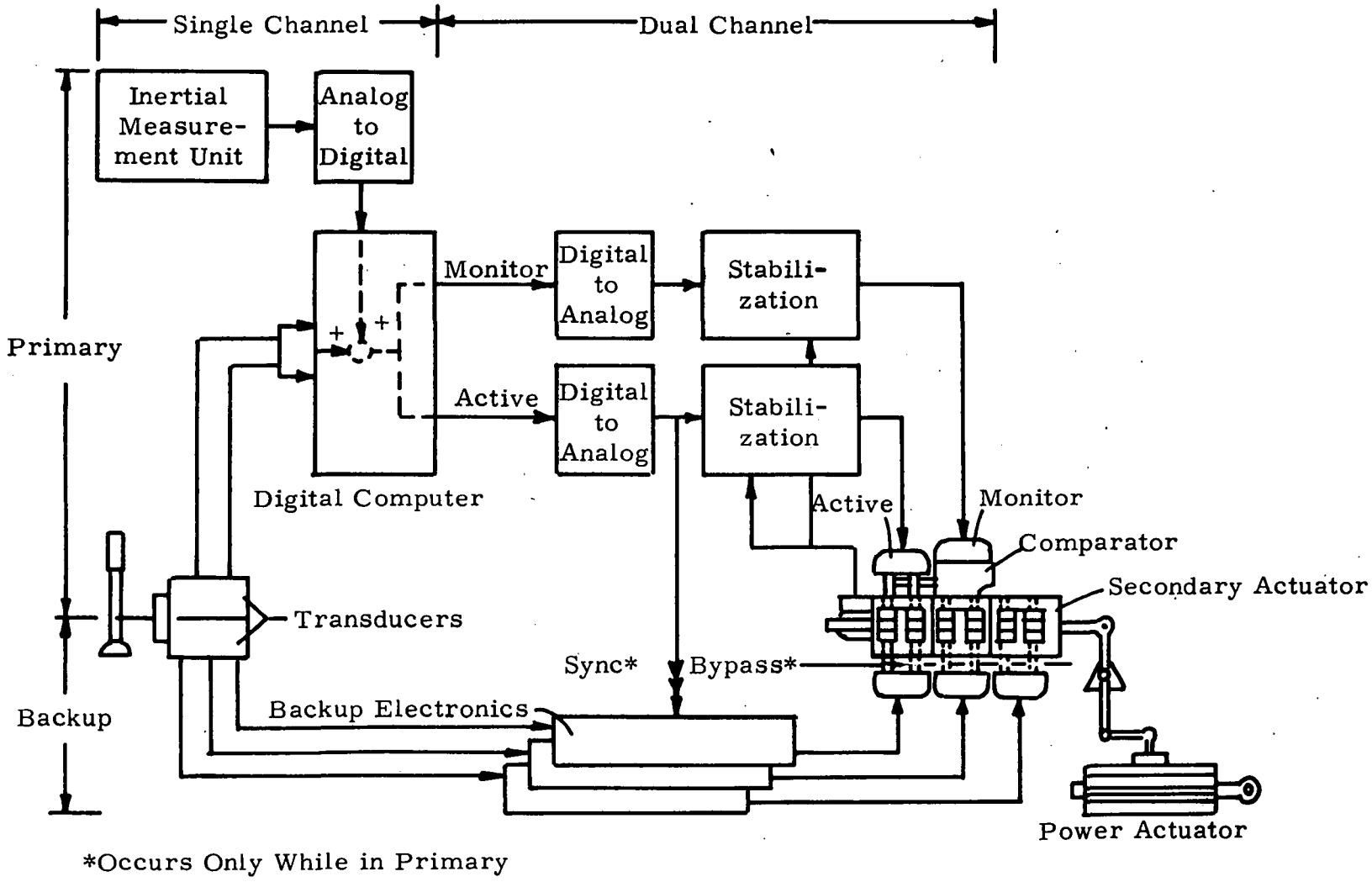

FIGURE 4 - FUNCTIONAL DIAGRAM OF F-8 DIGITAL FLY-BY-WIRE SYSTEM.

active channel by way of the synchronization network. Only the hydraulic pressure is bypassed at the secondary actuator, keeping the backup system ready to take over at any time. If a transfer to the backup system is requested, the bypass is removed and the synchronization network is disabled, resulting in immediate proportional control from the pilot's stick. While in the backup mode, the active servovalve is bypassed and the secondary actuator operates as a force summer for the three backup channels. The digital computer continues to operate, computing the control laws which give the best estimate of what the backup system commands. If a transfer to the primary channel is attempted, the transient would be small, assuming the computer was tracking the backup system. If an excessive error exists between the primary channel and the backup system, a cross-channel comparator (not shown in the figure) prevents transfer to the primary channel.

The lightning tests were performed with the FCS system powered by 28 volt batteries and operating in the primary (DFCS) Stability Augmentation System (SAS) mode on the Yaw, Pitch and Roll axes. At the beginning of each day of lightning testing an on-board system baseline was obtained by the systems turn-on sequence shown on the next page.

A block diagram of the complete FCS including primary digital and 3 analog backup channels is presented in the Appendix. This diagram shows all of the interfaces at which lightning-induced voltages were measured.

SYSTEMS TURN-ON SEQUENCE

1. Ground Cooling Cart ON
2. A/C Power On Batt. C. B.'s IN
3. Comp. ON IMU STBY.
4. If Prog. or restart on DSKY. interrogate.
5. Self test
   - V21N27E (Start self test)
     - 10 E
   - V15N01E (Monitor)
     - 1366 E
   - V21N1E (Terminates self test)
     - 1366 EE
6. IMU ON-GAI check
7. Program 00
   - V37E 00E
8. OPS Test
   - V93E Monitor V16 N 20E
   - Verify program 07 on DSKY
   - after @ 12 min Key Release flashes
     - Record R_1 _____
     - Record R_2 _____
     - depress PRO
     - Record R_1 _____
     - Record R_2 _____
     - terminate V 34
9. Initialize EMP 04 V25N26E
   - V31E or 00100 E
   - 01651 E
10. Hydraulics ON 10003 E
11. Engage Servos
12. Wing Down
13. BCS Self Test
14. Surface Throws
15. All Systems to SAS
16. Lightning Test

BASIC LIGHTNING EFFECTS ON AIRCRAFT ELECTRICAL CIRCUITS

Lightning currents flowing through aircraft skin and structure may produce voltages in electrical systems within by two different methods: Direct Coupled voltages and Induced voltages. Basically, the direct coupled voltages occur when lightning strikes an external electrical component such as an antenna or a position lamp. The induced voltages, which are actually a combination of magnetically induced, capacitively coupled and resistive voltage rises, occur as a result of lightning current flow through the aircraft skin and structure and comprise the INDIRECT EFFECTS of lightning on the system.

Direct Coupled Voltages

Direct coupled voltages occur via direct contact between lightning stroke currents and exposed (external) electrical components. These most commonly include antennas and navigation lights, particularly if located in areas such as wing tips and extremities where lightning is likely to strike the aircraft. In general, the magnitude of such voltages will be equal to the minimum dielectric breakdown voltage between the active element of the struck component and the airframe. In other words, if the struck component is a light bulb and the socket breakdown voltage is 3,000 volts, the lightning flash, which can deliver many times this voltage, will cause the socket to flash over and thereby "clip" voltage entering connected circuitry to 3,000 volts. Of course, if another component in this circuit, such as a terminal board, has a lower breakdown voltage, voltages traveling beyond this component will be limited accordingly. Direct coupled voltages are known to have caused damage to electrical systems and avionics.

Induced Voltages

The other mechanism by which lightning can affect aircraft electrical and avionics systems is in the generation of magnetically induced and resistive voltage rises with aircraft electrical circuitry. To describe the manner in which induced voltages occur, it is first necessary to consider the mechanisms by which magnetic fields may appear inside an aircraft.

If a long conductor is carrying a current, i, and the return path is far removed, the average field intensity at a distance, r, from the conductor is

$$H = \frac{i}{2\pi r} \qquad (1)$$

as shown in Figure 5a.

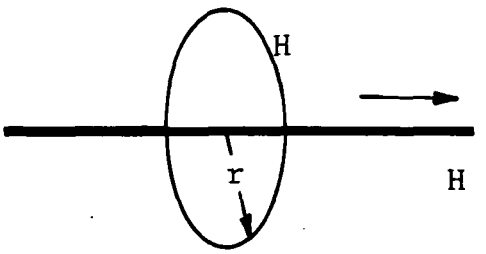

$$H = \frac{i}{2\pi r}$$

a) Current Carrying Filament

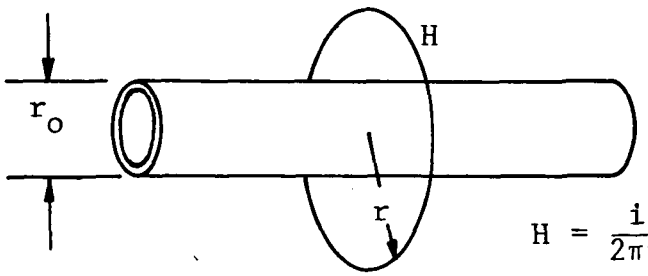

$$H = \frac{i}{2\pi r} \qquad (r \geq r_o)$$

$$H = \frac{i}{2\pi r_o} \qquad (r = r_o)$$

$$H = o \qquad (r \leq r_o)$$

b) Tubular Conductor

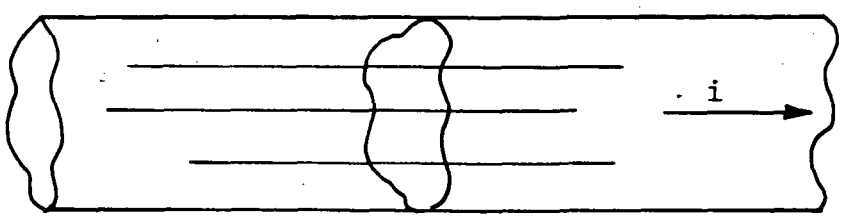

$$H = \frac{i}{C}$$

C = Circumference

c) Irregular Conductor

FIGURE 5 - MAGNETIC FIELDS AROUND CURRENT CARRYING CONDUCTORS.

If instead of a solid wire the current is carried on a hollow tube of radius of r_o, as shown in Figure 5b, the field intensity at radius $r < r_o$ is again

$$H = \frac{i}{2\pi r} \tag{2}$$

and, at the surface of the tube where r equals r_o, the field intensity is

$$H = \frac{i}{2\pi r_o} \tag{3}$$

Since the circumference of the tube is

$$C = 2\pi r_o \tag{4}$$

it follows that the field intensity at the surface of the tube is

$$H = \frac{i}{C} \tag{5}$$

The average current density at the surface of the tube is also equal to the total current divided by the circumference,

$$J_{ave} = \frac{i}{C} \tag{6}$$

If the conductor is not cylindrical, as shown in Figure 5c, the field intensity at different points on the surface will be different. Field intensity will still be equal to the total current divided by the circumference,

$$H_{ave} = \frac{i}{C} \tag{7}$$

The actual field intensity will be greater than average at points where the radius of curvature is less than average; and less than average at points where the radius of curvature is greater than average, as shown in Figure 6. For example, the circumference of the F-8 just forward of the wing is about 5.5 meters. The average field intensity, assuming a lightning stroke current flowing through the fuselage of 30,000 amperes (an average stroke amplitude), would be

$$\frac{30,000A}{5.5m} = 5455 \text{ A/m} \tag{8}$$

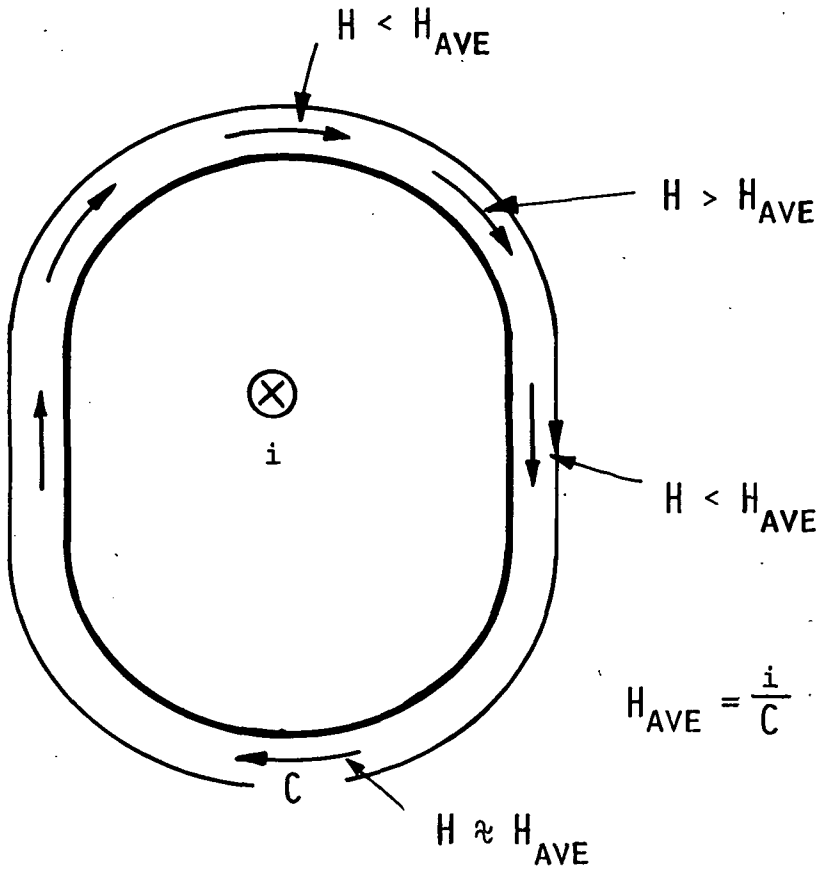

Typical cross section of aircraft fuselage

FIGURE 6 - FIELD INTENSITY VS. RADIUS OF CURVATURE.

Since there are no points of very sharp radius, the field intensity around the fuselage would probably not vary more than a factor of about 1.5 from the average value.

The situation along a wing carrying lightning current is considerably different in that the leading and trailing edges have radii of curvature much greater than the average. Field intensity along the leading and trailing edges should then be quite high compared to the field intensity along the top or bottom surfaces.

Since both the average current density, J_{ave}, and the average field intensity, H_{ave}, are equal to the total current divided by the circumference,

$$J_{ave} = H_{ave} = \frac{i}{C} \qquad (9)$$

it follows that the tangential field intensity at the surface of a conducting object is equal to the current density at that point. This is in fact true, at least for transient currents. The relation is not true for DC currents or transients sufficiently slow that appreciable magnetic fields penetrate the skin.

The orientation of the H-field vector is always at right angles to the direction of the current vector, as shown in Figure 7.

While small gaps in the structure direct the current around the gap, the magnetic field is virtually unaffected, except directly on the surface and on a length scale small compared to dimensions of the gap interrupting the current flow, as shown in Figure 8.

So far we have dealt only with the field external to the aircraft. Even if the aircraft has an electrically continuous metallic skin, some magnetic flux may appear within the aircraft as lightning current diffuses through its skin to the inside surface. Cancellation effects will eliminate this in perfectly symmetrical cases such as a cylinder with uniform skin current distribution, but in other cases some net DIFFUSION FLUX may exist inside. It is generally characterized by the interior field having a slower time to crest than the exterior field as well as having a lower amplitude, as illustrated in the cases of Figure 9.

If apertures (openings) exist in the aircraft skin, a portion of the external magnetic flux surrounding all of the current

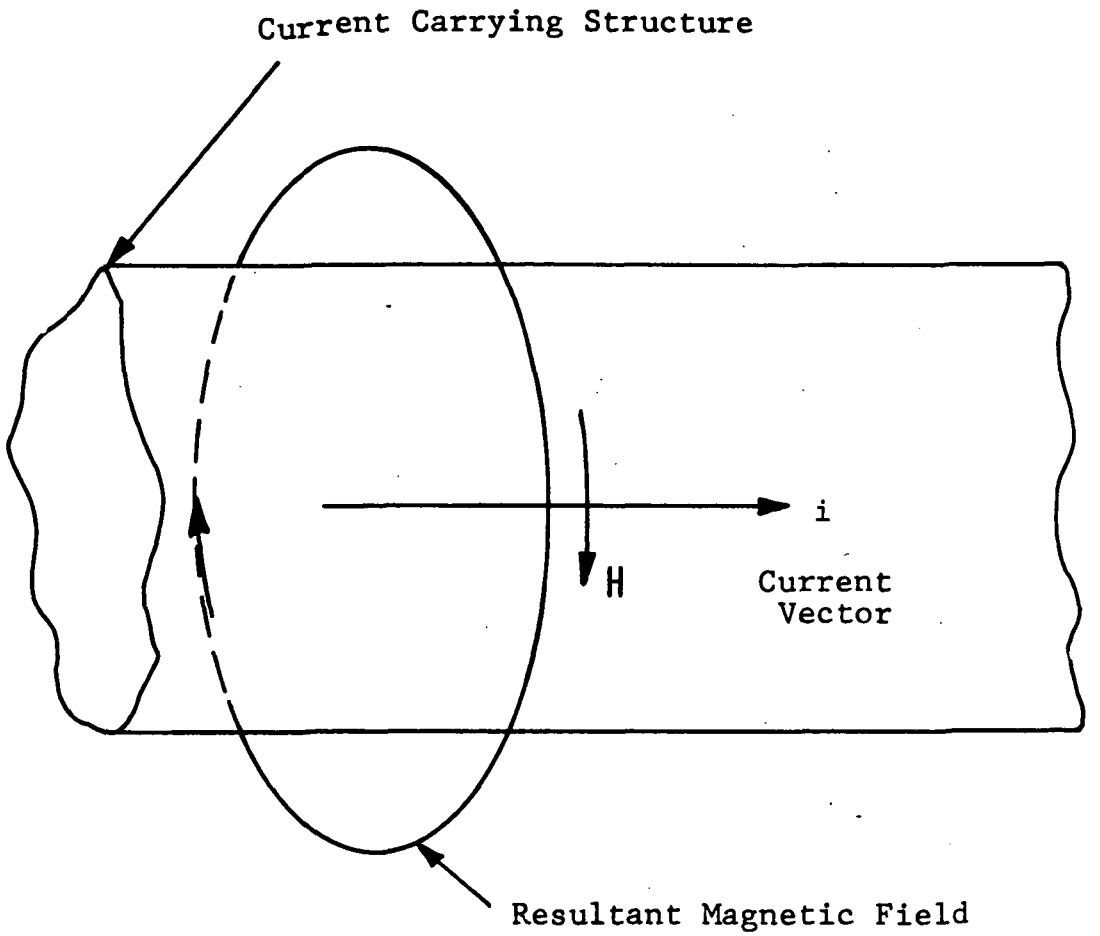

FIGURE 7 - ORIENTATION OF CURRENT AND MAGNETIC FIELD VECTORS.

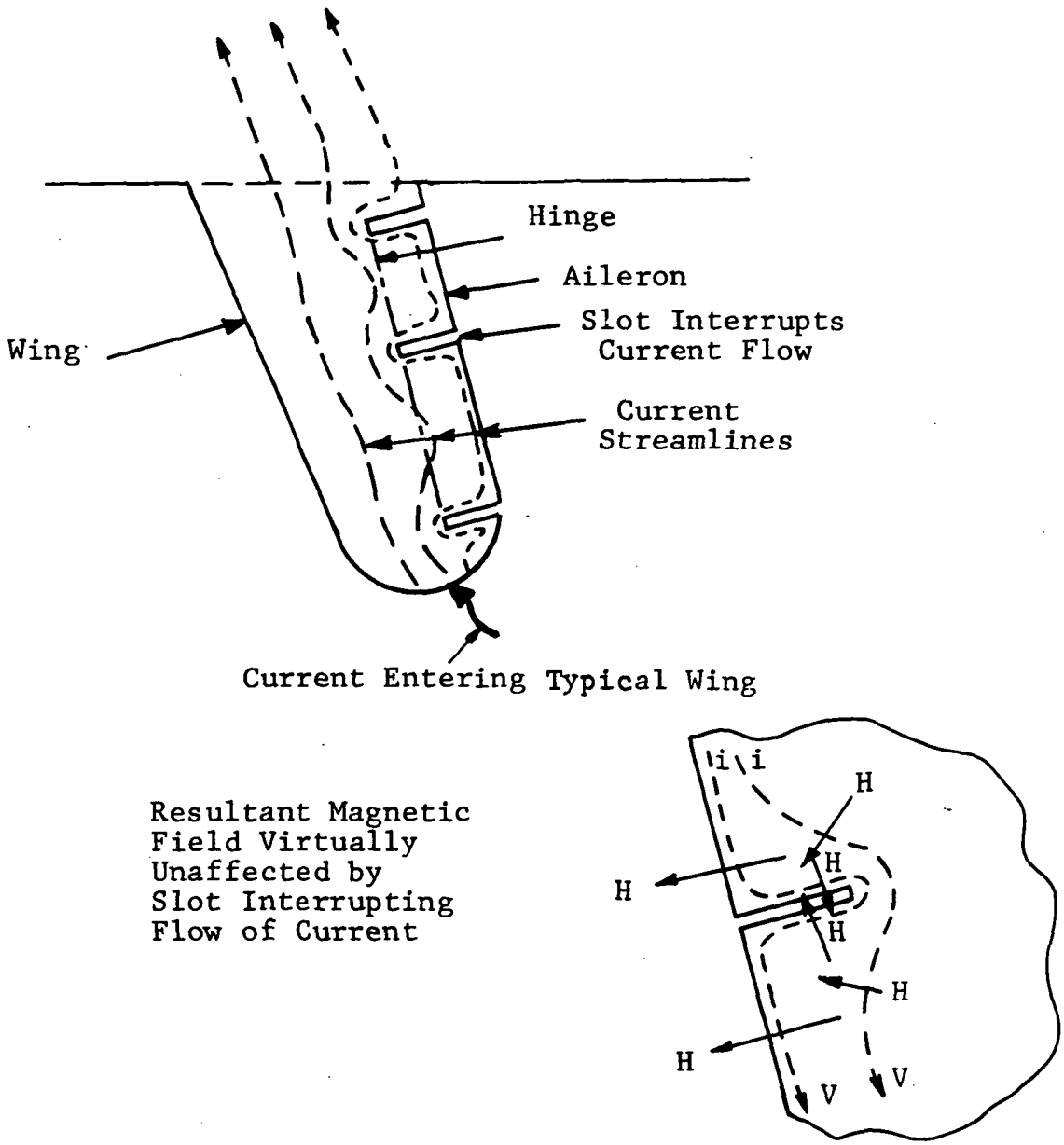

FIGURE 8 - CURRENT FLOW AND MAGNETIC FIELD AROUND STRUCTURAL GAPS.

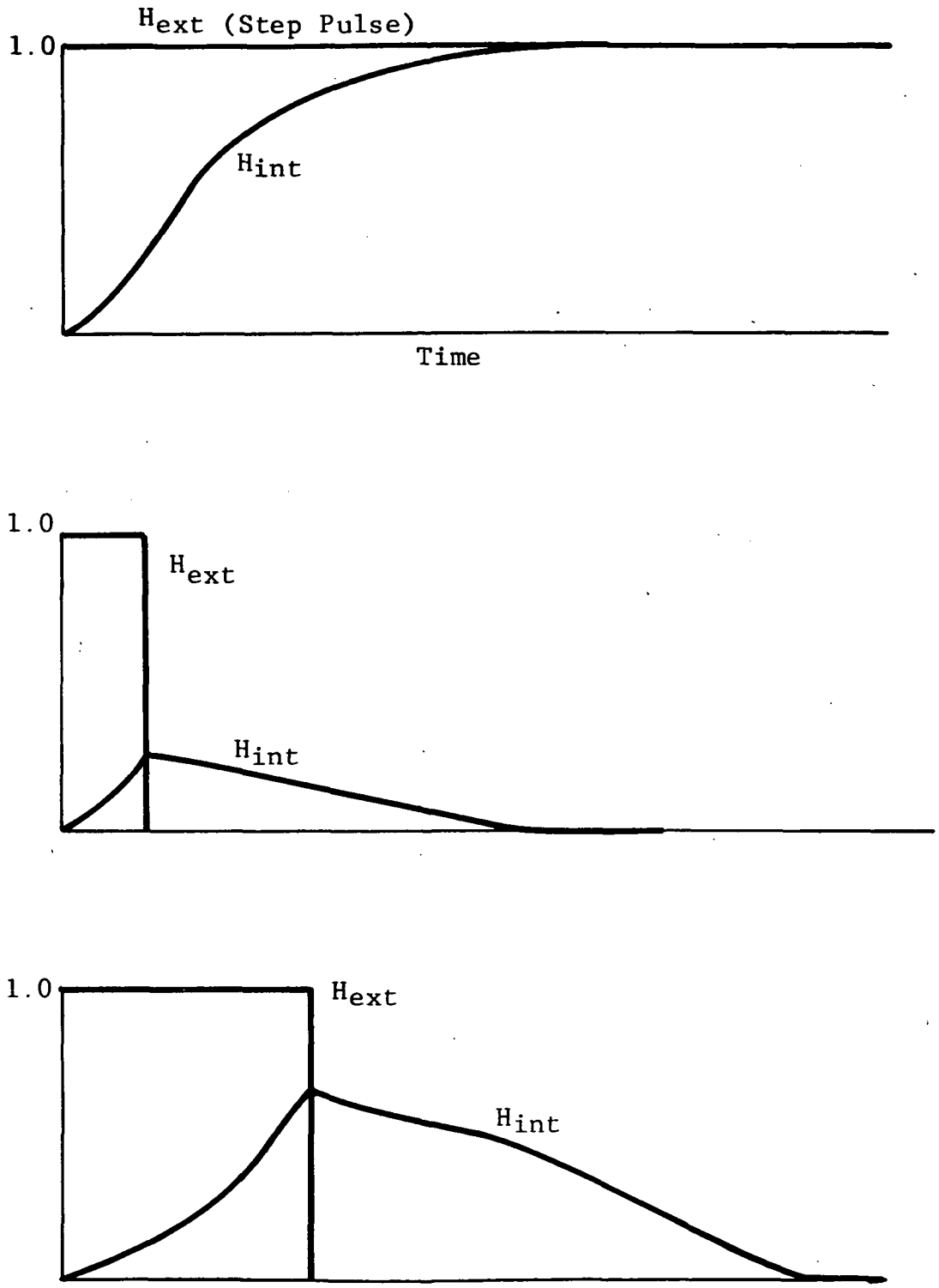

FIGURE 9 - INTERNAL DIFFUSION FIELDS AS A FUNCTION OF EXTERNAL FIELDS.

flowing through the aircraft will leak inside through these apertures as shown in Figure 10. This is known as APERTURE FLUX and, since there is no time required for it to accompany current diffusing through a skin, it appears inside much sooner than the diffusion flux and usually with a higher rate of change, similar to that of the total lightning current. Aperture flux is usually more localized than diffusion flux and in the vicinity of an aperture it may have a much higher amplitude than the diffusion flux.

An aperture can be described in terms of an equivalent magnetic dipole, as shown in Figure 11. In Figure 11a, current streamlines are seen being diverted around a hole in a current carrying sheet. A filamentary dipole producing the same magnetic effects as the diverted current flow would be as shown on Figure 11b. The magnetic field pattern produced by such a dipole would be as shown on Figure 12. This pattern is the same as the classic electric field produced in the near field zone by an electric dipole. The field intensity is less the farther one is away from the opening, falling off approximately as the third power of the distance for distances large compared to the size of the opening, as shown in Figure 13. Close to the opening, the field decreases more slowly.

These changing internal magnetic fields will link aircraft electrical circuits inside the aircraft, inducing voltages therein. These voltages can be related to the lightning current by inductive transfer functions in accordance with Faraday's Law. The transfer function for diffusion flux coupling is conveniently described by a constant inductance relating the portion of lightning current appearing at the inside surface of the skin to the voltage it induces in a circuit. The transfer function relating voltages induced into a circuit by the aperture flux is more complex due to less uniform field patterns and aperture geometries.

Because the induced voltages are dependent upon the lightning current, they vary considerably in amplitude and waveshape according to different lightning current waveshapes. Induced voltages are also dependent upon the characteristics of the particular aircraft circuit in which they are induced and the location at which the lightning stroke attaches to the aircraft.

In addition to the magnetically induced voltages, the resistance of the metallic skin will permit resistive voltage rises in the skin (or structure) along the path of lightning current flow.

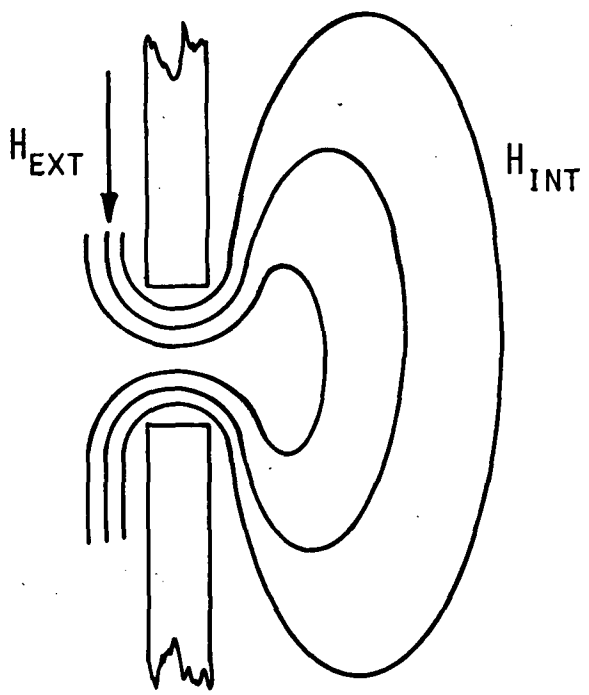

FIGURE 10 - APERTURE FIELDS.

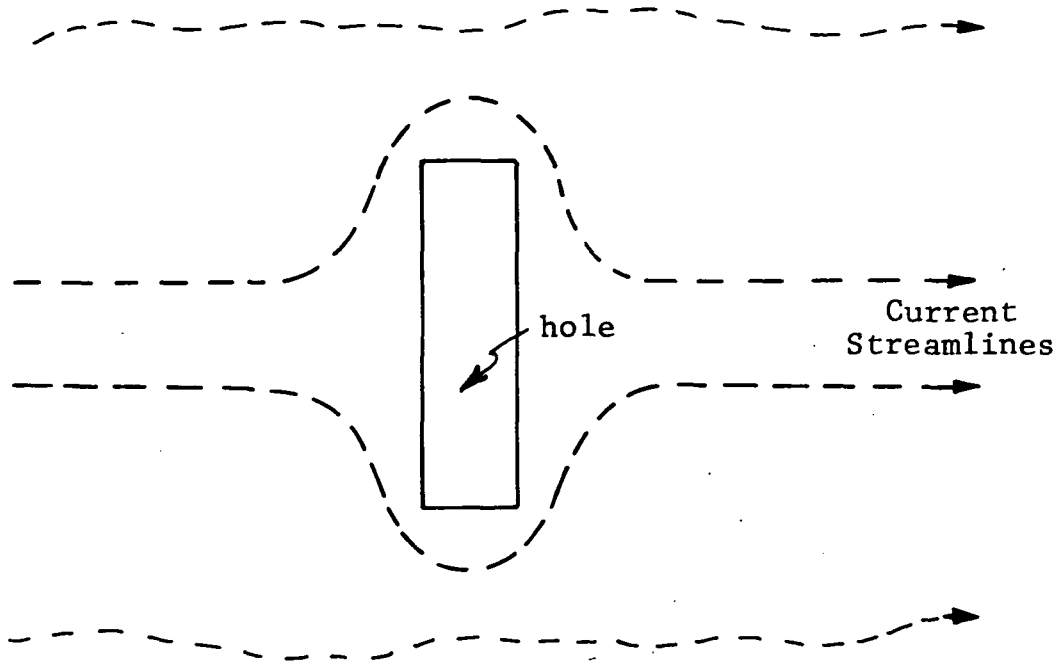

a) Actual Current Flow

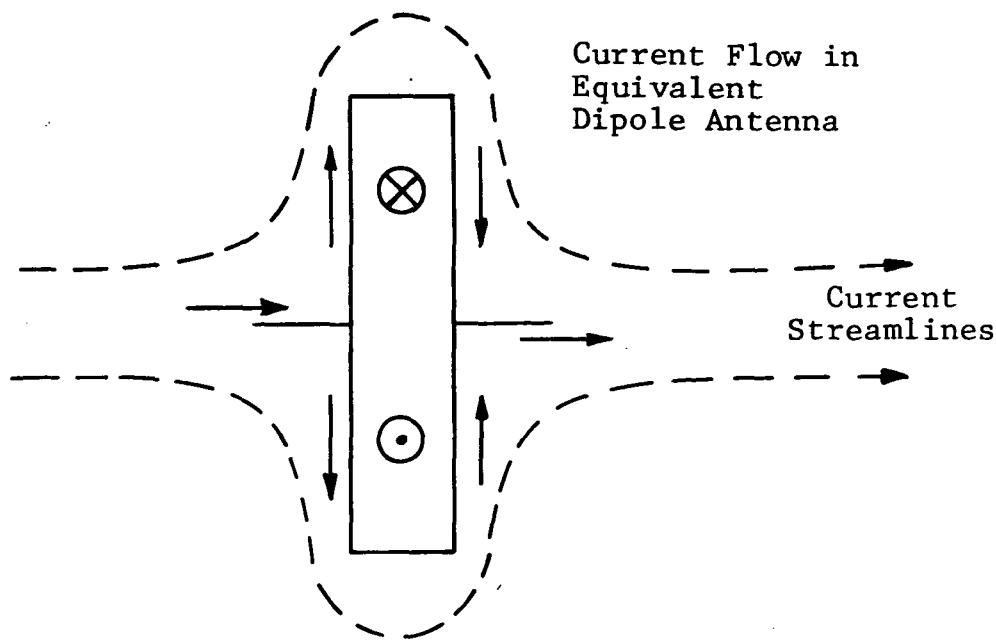

b) Equivalent Dipole.

FIGURE 11 - DEVELOPMENT OF THE EQUIVALENT MAGNETIC DIPOLE.

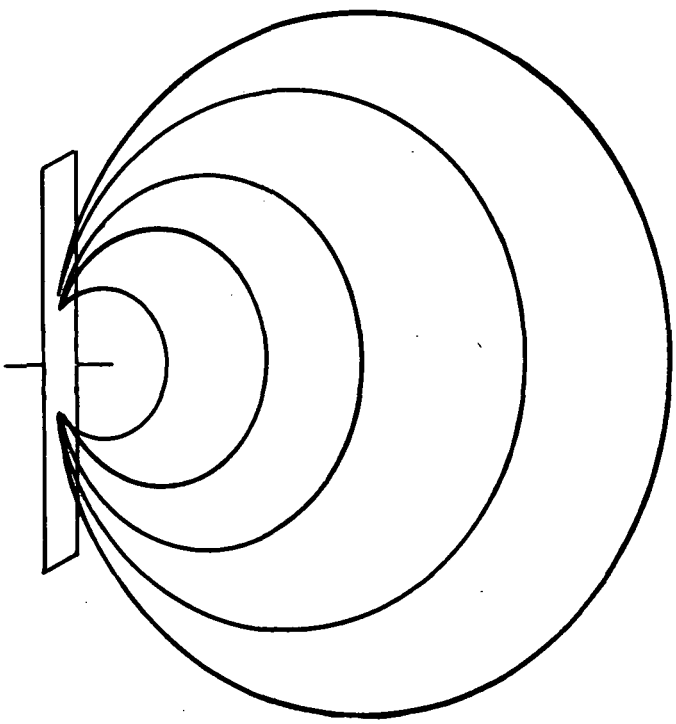

FIGURE 12 - FIELD PATTERN DUE TO AN APERTURE DIPOLE

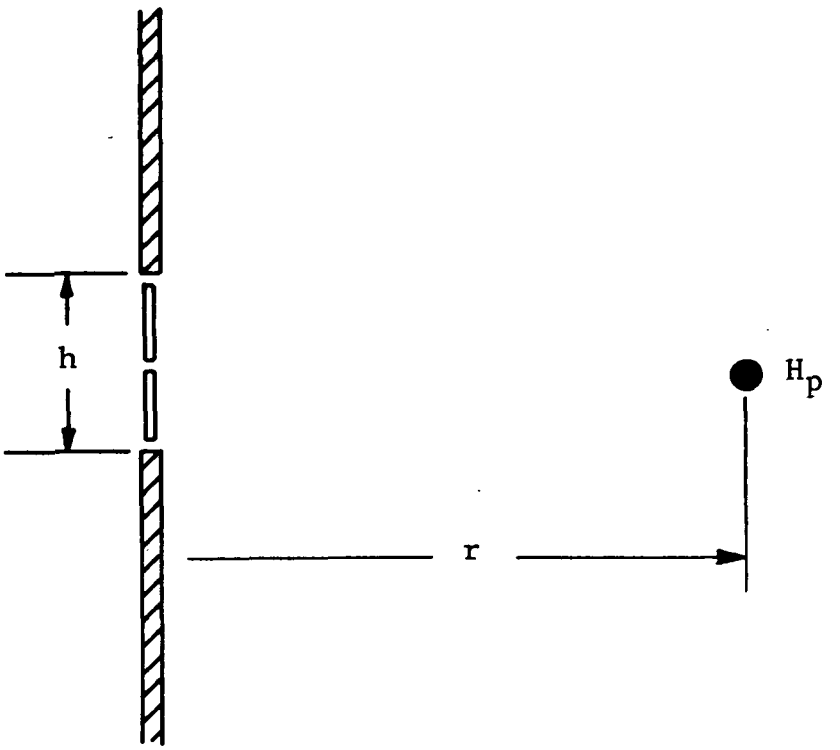

$r \gg h$	H_p varies as $\frac{1}{r^3}$
$r > h$	H_p varies as $\frac{1}{r^2}$
$r \sim h$	H_p varies as $\frac{1}{r}$
$r < h$	H_p varies as $\frac{1}{r^{\frac{1}{2}}}$

FIGURE 13 - APPROXIMATE MANNER IN WHICH FIELD STRENGTH VARIES WITH DISTANCE FROM APERTURE.

If an aircraft electrical circuit happens to employ the structure as return path, then this resistive voltage enters the circuit in series with the magnetically induced voltage in the same circuit and any other (normal) steady state voltages present. Capacitively coupled voltages may also be produced in these circuits; however, the essentially uniform conducting skin of metallic aircraft keeps potential differences among structural elements low, thereby limiting the voltages which can be electrostatically coupled to interior electrical circuits. In practice, experimental measurements have shown magnetic and resistive components to be the most predominant.

The combination of the resistive and magnetic components of induced voltage is expressible as a function of the lightning current itself, as follows (Ref. 3):

$$e_{oc} = R_s i_L(t) + M_1 \frac{d\left[(1-e^{-\alpha t}) i_L(t)\right]}{dt} + M_2 \frac{di_L}{dt} \qquad (10)$$

where:

e_{oc} = voltage induced in the circuit (using the airframe as return)

R_s = the effective structural resistance

M_1 = the diffusion transfer inductance between the lightning current flowing on the inside surface of the skin and the particular electrical circuit

M_2 = the aperture transfer inductance between the total lightning current flowing through the aircraft and the particular aircraft circuit

$i_L(t)$ = lightning current (a time varying function)

α = the reciprocal of the time constant of current penetration into the aircraft skin

Of course, circuit transmission line and termination impedance characteristics as well as secondary induced effects may change the induced voltage appearing at a particular point from that predicted by equation (10). In any event, analytical techniques are not yet available to permit accurate determination of the transfer inductances and calculation of induced voltages in a typical aircraft electrical circuit by equation (10). Therefore, experimental procedures were applied to determine the magnitude of possible lightning-induced voltages in the NASA F-8 DFBW system. The experimental techniques and results obtained are described in the following paragraphs.

EXPERIMENTAL TECHNIQUES

Test Procedures

This program utilized the transient analysis technique for lightning-induced voltage measurement. Development of this test method has been sponsored by the National Aeronautics and Space Administration, Aerospace Safety Research and Data Institute, Lewis Research Center, under Contract NAS3-14836 (Lightning Hazards to Aircraft Avionics) with the General Electric Company. Essentially, this technique involves the use of a low-energy impulse generator (transient analyzer) to inject impulse currents, similar in waveform to natural lightning strokes but greatly reduced in amplitude, into an aircraft in the same manner as lightning. Measurements are then made of resulting induced voltages in internal aircraft electrical circuits, and the amplitudes are scaled upward to correspond with full scale lightning current amplitudes. The basic technique is more fully described in Ref. 4.

Lightning Simulation.- The test setup is pictured in Figure 14 and the test circuit is shown in Figure 15. In this case, the airframe is grounded at the point nearest the terminals of the circuit being measured. A 0.914 m, 3 mil aluminum foil was utilized to connect the airframe to the instrument table and the hangar ground, about 6.096 m away. Use of the aluminum foil provides a very low impedance between the airframe and instrument table. The instrument cable was placed along this foil so that no air gap existed between it and the foil. As shown in Figure 15, the lightning current circuit is grounded once and only via this airframe ground foil. Consequently, no simulated lightning current could flow off of the airframe along this path or the instrument cable shield and return to the transient analyzer. This arrangement had the following significant advantages.

1. At all times the airframe was solidly grounded and personnel could touch the aircraft without danger of being shocked, even when simulated lightning current was flowing.

2. No simulated lightning current could flow off the aircraft via the ground foil. Currents entered and exited the aircraft only at the specifically chosen attachment points.

3. Differences of potential along the instrument cable shield or aluminum foil, and resulting common-mode instrument error voltages, were minimized.

FIGURE 14 - F-8 DFBW AIRPLANE AND SIMULATED LIGHTNING TEST SETUP.

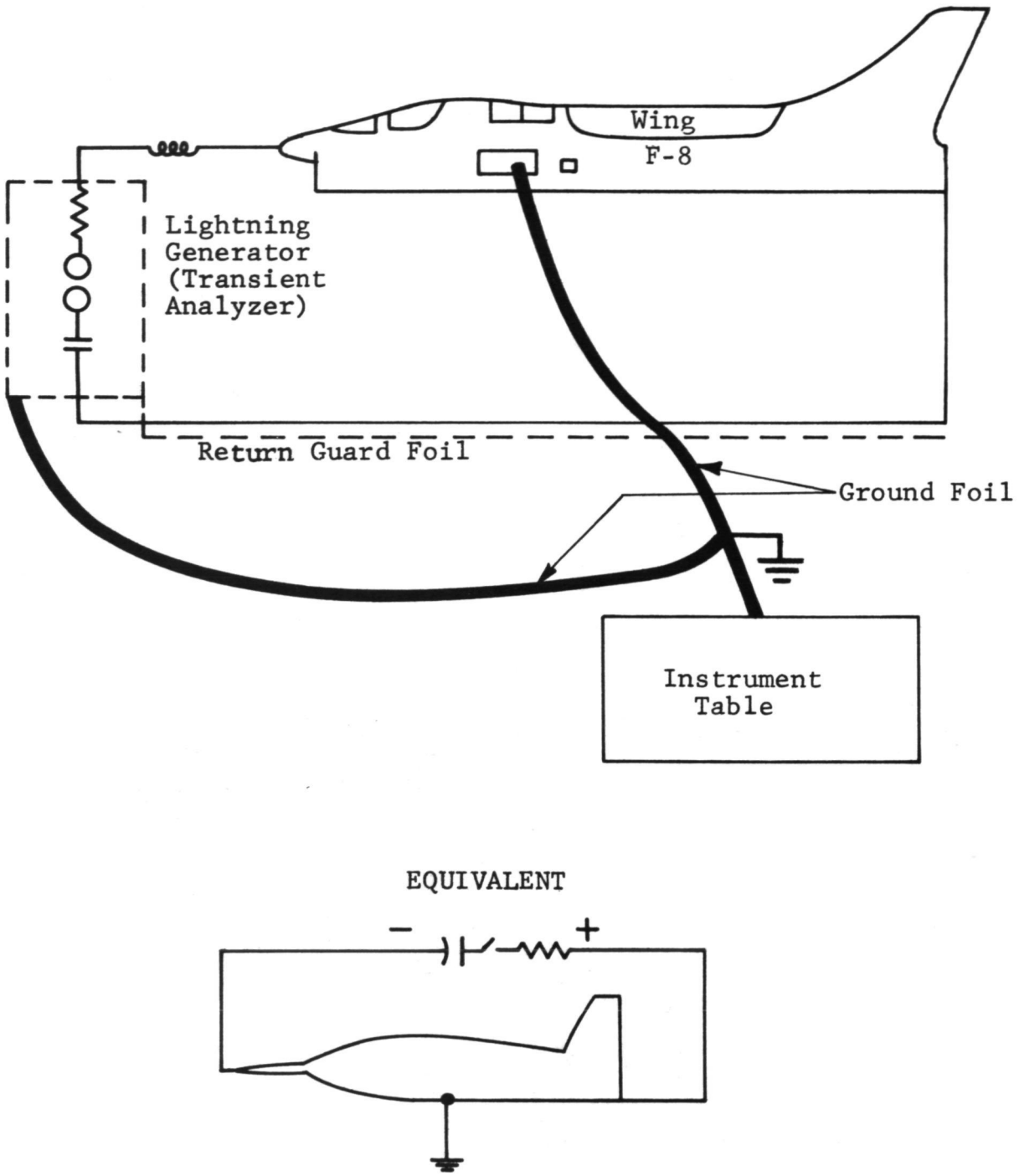

FIGURE 15 - SIMULATED LIGHTNING TEST CIRCUIT.

Description of the waveshape of the applied current is facilitated by use of the standard waveshape notation for current impulses. An impulse current simulating a high-amplitude, short-duration lightning stroke is ideally an aperiodic transient current which rises rapidly to a maximum value and falls less rapidly to zero. The waveshape of such an impulse is defined by:

(1) polarity

(2) front time (T_1)

(3) time to half value on the tail, T_2

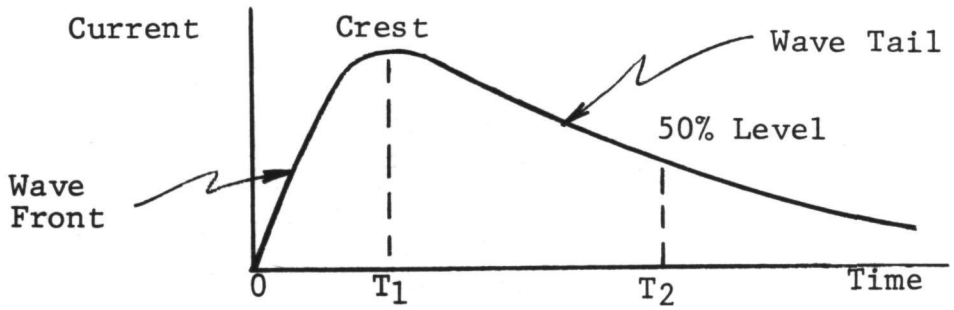

The waveshape is then described by the notation:

$$(T_1 \times T_2)$$

where T_1 and T_2 are usually expressed in terms of microseconds (μs). Thus, a wave rising to crest in 2.75 μs and decaying to 50% level in 60 μs is referred to as a 2.75 x 60 μs wave.

Since natural lightning strokes may vary considerably in waveshape, the effect of this variable upon the induced voltages was evaluated by making most of the measurements at each of two waveshapes, a "fast" waveshape, meeting the requirements of the Lightning Design Criteria recently established for the NASA Space Shuttle, and a "slow" waveshape, with a front time nearly 4 times as long. These two waveshapes are representative of natural lightning stroke waveshapes, and are shown in Figure 16. A few measurements were made with a "very fast" waveform of approximately 1 μs front time (T_1) and 40 μs tail time (T_2). This waveform has a somewhat faster rate of rise than is considered probable from lightning. The amplitude of each waveform was set at 300 amperes to minimize the possibility of interference or damage to any of the electronic systems or components aboard the aircraft. Natural lightning strokes exceed 200,000 amperes about 1% of the time but the peak amplitude of an average stroke is about 30,000 amperes.

SLOW WAVEFORM

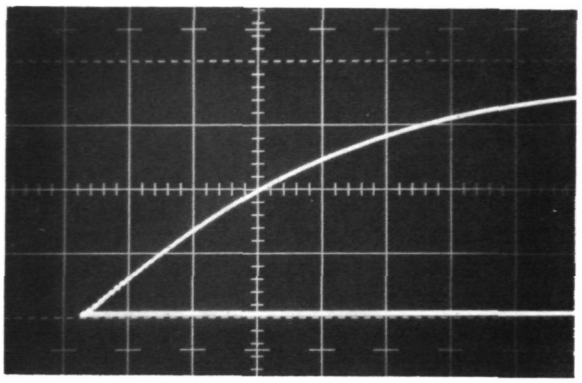

2 μs/Div. 83 A/Div.

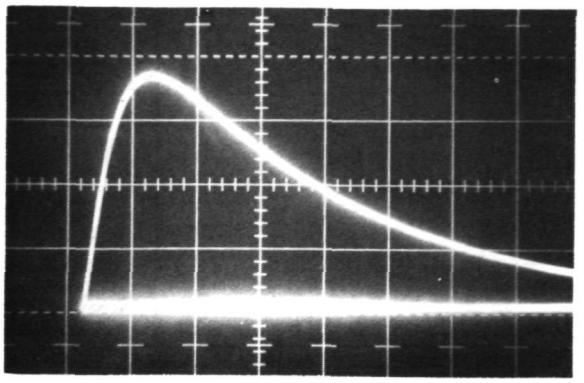

20 μs/Div. 83 A/Div.

FAST WAVEFORM

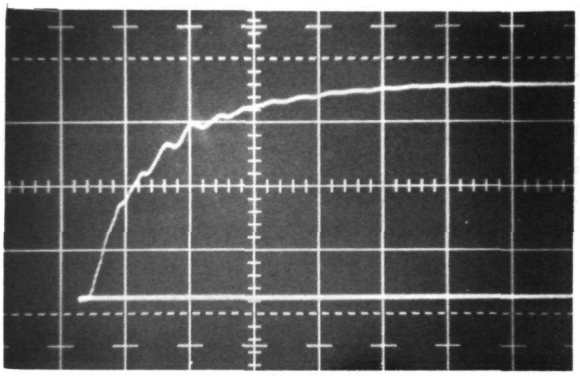

1 μs/Div. 83 A/Div.

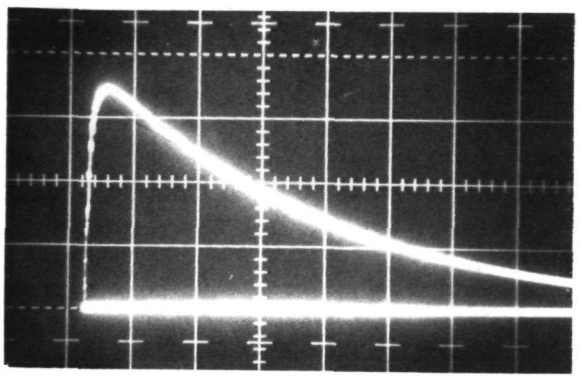

20 μs/Div. 83 A/Div.

VERY FAST WAVEFORM

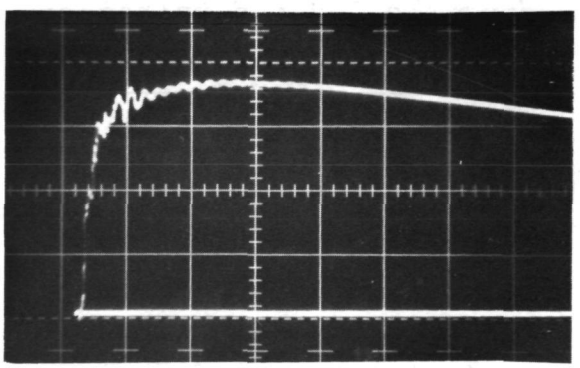

2 μs/Div. 83 A/Div.

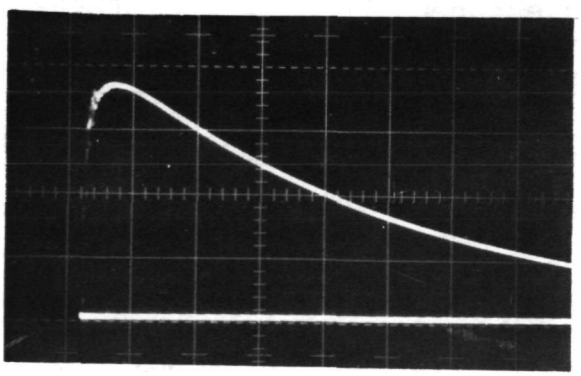

10 μs/Div. 83 A/Div.

FIGURE 16 - SIMULATED LIGHTNING TEST WAVEFORMS.

Note: "__μs/Div." is horizontal time scale and "__A/Div." is vertical amplitude scale.

It will be noted that damped oscillations appear on the wavefronts of the fast and very fast waveforms. These are believed to be the result of traveling wave reflections in the transmission line formed by the aircraft and return conductor beneath it. Measurements were made of the current entering as well as leaving the aircraft, verifying that the superimposed oscillations flowed through the aircraft along with the fundamental exponential current waveform. Attempts were made to minimize these oscillations since they complicate analysis of the relationships between induced voltages and the simulated lightning currents causing them. The waveforms shown in Figure 16 are the best that could be obtained and are the ones utilized for all of the tests reported herein. The extent to which oscillations or "jagged edges" occur in natural lightning current wavefronts is not well known, although available oscillographic data (Ref. 5) does show evidence of such occurrences in some strokes.

Measurement Techniques

Magnetic Field Measurements.- Two different types of magnetic field sensors were used for measurements. The first consisted of a coil of wire on a C-shaped ferrite core. When placed in a magnetic field the magnetic flux lines go in one end of the core, through the winding and out the other side, in the process inducing a voltage in the coil of wire. The magnetic core concentrates the magnetic lines of force existing in the surrounding area and thus the probe averages the H-field intensity over an area several times its cross-sectional area. The probe of course senses only changing magnetic fields.

The probe has a time constant of about 4 microseconds. If the time for which the field is changing is short compared to 4 microseconds, the voltage output of the probe will be proportional to the intensity of the magnetic field itself. For magnetic field changes which take place over times long compared to 4 microseconds, the output of the probe is proportional to the rate of change, dH/dt, of the magnetic field intensity.

Some measurements were also made with another probe built to respond almost completely to dH/dt. This consisted of a 3-turn coil of wire 15.24 cm in diameter and covered with an electric shield. The time constant of this probe was about 1 microsecond.

Measurements of the magnetic field intensity on the exterior of the aircraft were made by holding the probe against the aircraft as shown on Figure 17. For some measurements of the magnetic field intensity internal to the aircraft the measurements were made in the same way, the probe being held against the inside surface of the aircraft skin. In other cases the probe was suspended away from the wall of the aircraft and as far away from other conductive objects as possible. When making interior measurements the instrument cable from the probe was brought out through a door or panel remote from the position under measurement in order to avoid errors from magnetic field leakage around the hole through which the cable passed. Voltage outputs from both probes were measured with a Tektronix Type 545 oscilloscope with a Tektronix Type G pre-amplifier.

Induced Voltage Measurements.- Induced voltages were measured by a Tektronix Type 545 oscilloscope with a Tektronix Type G pre-amplifier. The differential measurement system described in Reference 3 was utilized, and signals were transmitted from the aircraft via an RG-22 twinaxial cable, as shown in Figure 18a. This cable had an additional copper braid shield. In the aircraft the "A" channel was normally connected to the circuit conductor (P1) being measured, and the "B" channel was connected to the FCS ground, airframe ground or circuit low side, P2, as required for the measurement being made. The inner and outer cable shields were also connected to each other and to the airframe at this point, as shown in Figure 18a.

The RG-22 cable was usually terminated at the oscilloscope end with resistors equal to the surge impedance of each channel, as shown in Figure 18b.

The type G differential pre-amplifier subtracted the line-to-shield signal on "B" from that on "A", so that common-mode errors induced in the instrument cable would not appear in the A-B measurement.

FIGURE 17 - MAGNETIC FIELD PROBE USED TO MEASURE EXTERNAL MAGNETIC FIELD INTENSITY.

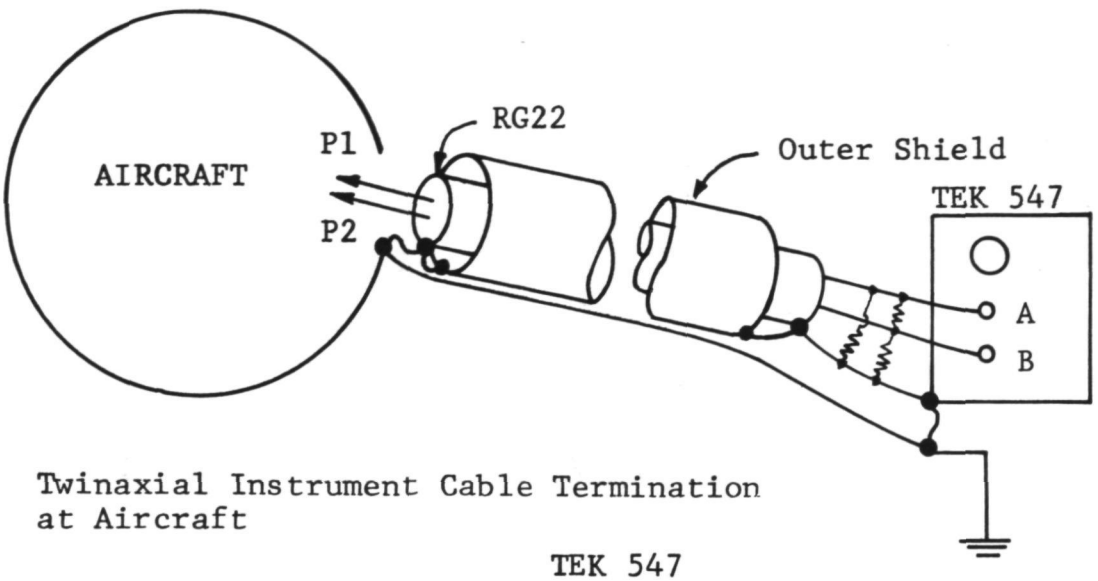

a) Twinaxial Instrument Cable Termination at Aircraft

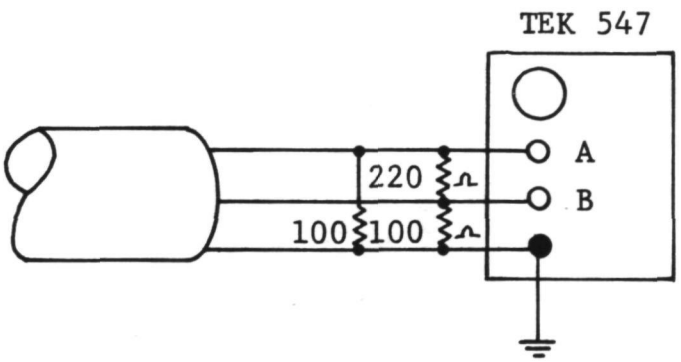

b) Twinaxial Instrument Cable Termination at Oscilloscope

FIGURE 18 - INSTRUMENT CABLE AND TERMINATIONS.

MAGNETIC FIELD MEASUREMENTS

External Fields

The first measurement made was of the way that magnetic field strength is distributed around the outside of the aircraft fuselage. The results of the measurements are shown on Figure 19. Measurements were made just forward of the wing while the simulated lightning current was being injected into the nose boom and drained from the tail of the aircraft. The path through which the current returned to the transient analyzer was along the insulated conductor underneath the aircraft, in the approximate position shown on Figure 19. These measurements show that the field strength is not uniformly distributed around the fuselage of the aircraft nor is it related directly to the fuselage radius of curvature of the aircraft. Instead, the field strength is the greatest near the current return path. This would indicate that the simulated lightning current injected into the aircraft does not distribute itself uniformly over the perimeter of the fuselage, but instead concentrates along the bottom of the fuselage near the current return path. The field strength on top of the fuselage is 20 amperes per meter while the field strength in the vicinity of the access doors to the gun bay and the battery compartment is 36 amperes per meter, for the simulated lightning current of 300 amperes. If an average lightning stroke of about 30,000 amperes is assumed, the values would all be multiplied by a factor of 100, giving a field strength on top of the fuselage of 2000 amperes per meter and 3600 amperes per meter outside the gun bay and battery compartments. In previous tests using the transient analysis technique (Ref. 4) however, the position of the return conductor with respect to the aircraft has had little discernible effect on the magnitude of induced voltages measured in aircraft circuits.

Next, measurements were made of the magnetic field distribution along the bottom surface of the left wing as lightning current was injected into the nose boom and drawn off of the left wing tip. Measurements were made along two paths as shown on Figure 20. One of the paths was inboard from the wing hinge and the other outboard from the wing hinge. Measurements were made at the middle of the chord and near the leading and trailing edges. The results of the measurements are shown on Figures 21 and 22 for the outboard and inboard paths, respectively.

On these figures, the curves marked "calculated" are the field intensities predicted by theoretical calculations of current distributions on an elliptical cylinder carrying the same current as was carried through the F-8 wing.

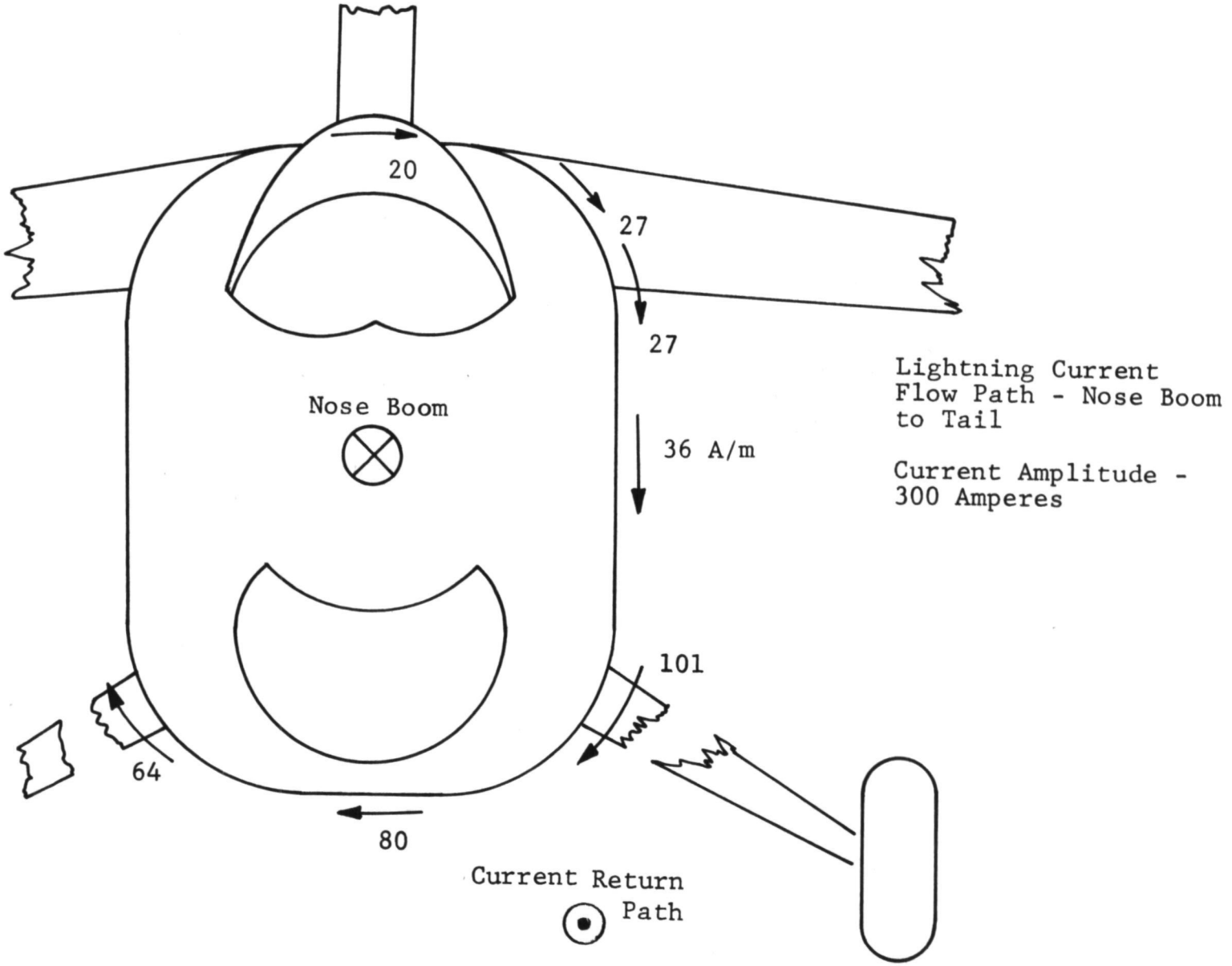

FIGURE 19 - FIELD DISTRIBUTION AROUND MID SECTION OF F-8 FUSELAGE.

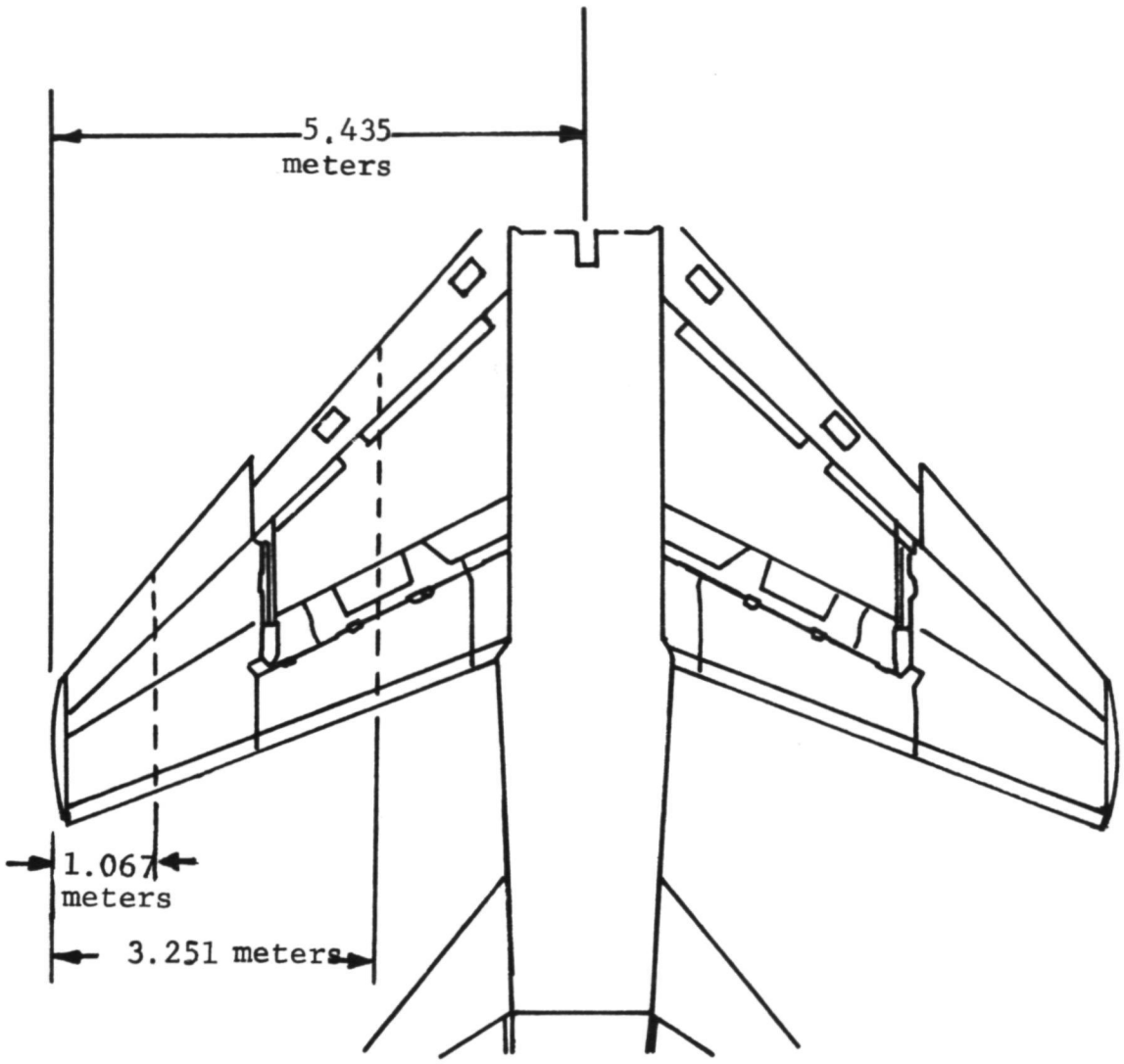

FIGURE 20 - LOCATION OF WING FLUX MEASUREMENTS
(INBOARD AND OUTBOARD PATHS).

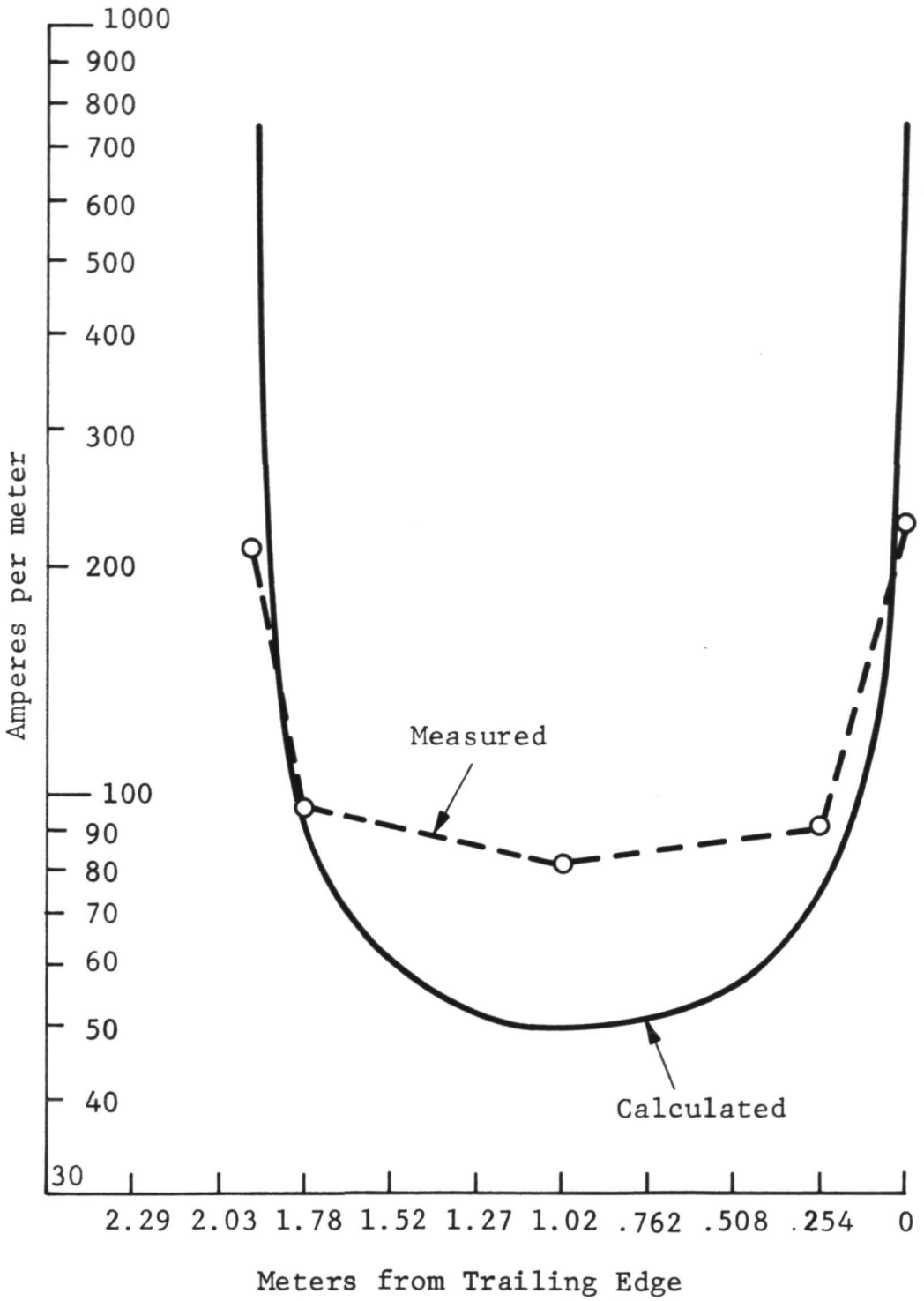

FIGURE 21 - MEASURED AND CALCULATED FIELD DISTRIBUTIONS AROUND F-8 WING (OUTBOARD PATH).

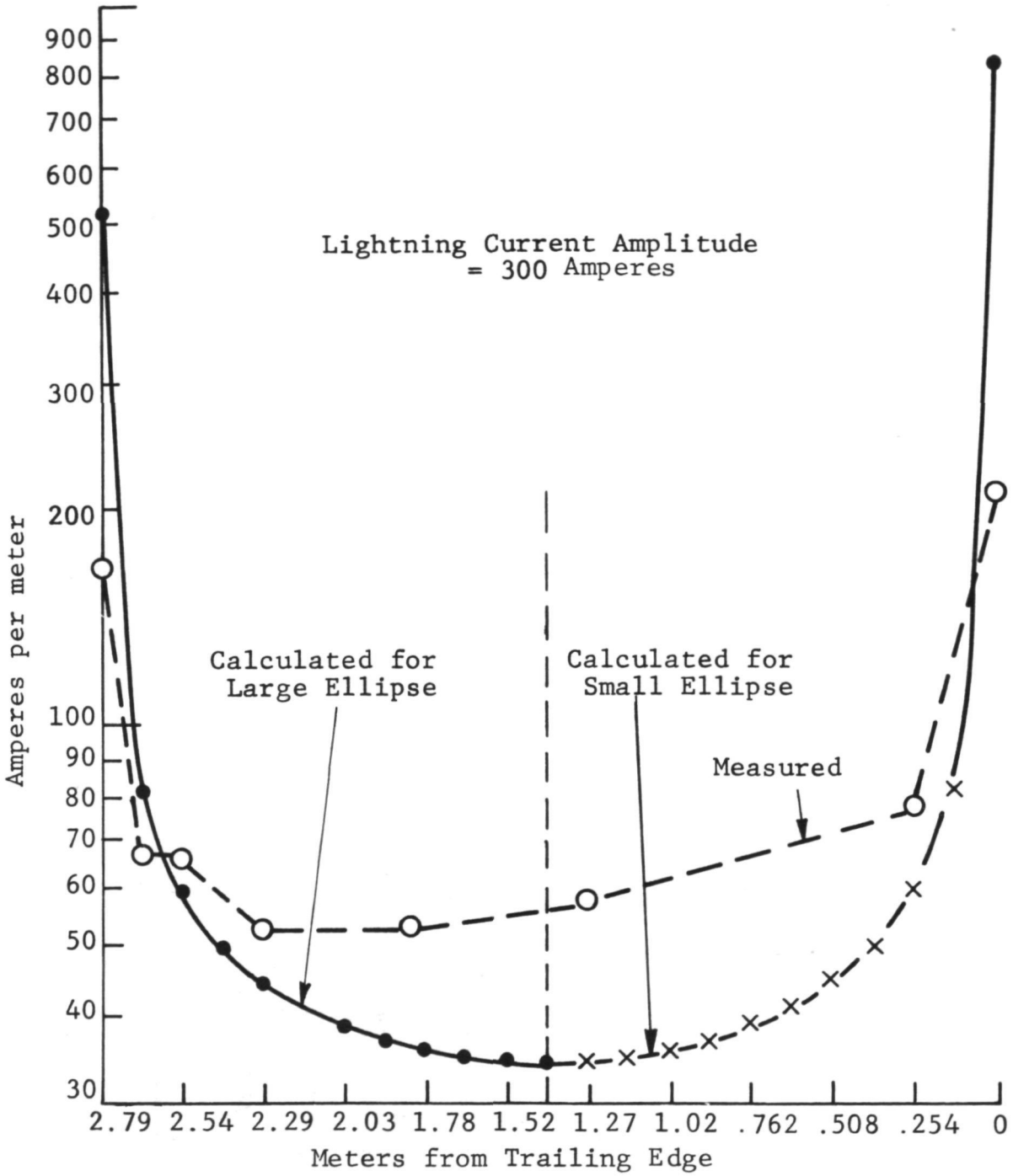

FIGURE 22 - MEASURED AND CALCULATED MAGNETIC FIELD INTENSITIES AROUND F-8 WING (INBOARD PATH).

It has been shown (Refs. 6 and 7) that the magnetic field intensity around an elliptical conductor (or the current density at the surface of the elliptical conductor) can be described by the following relationship:

$$H_{surface} = \frac{i}{\tau} \frac{1}{\sqrt{b^2 - (2x)^2 \left[1 - \frac{d^2}{b^2}\right]}} \qquad (11)$$

where:

b = width (meters)

d = thickness (meters)

τ = distance along horizontal axis measured from center (meters)

For this analysis the cross section of the wing along the inboard path was assumed to be that of Figure 23a. This is approximated by two thin ellipses, one for the leading edge of the wing and one for the trailing edge. The two ellipses are shown on Figure 23b. The large ellipse representing the leading edge of the wing has a minor axis of 0.184 m while the small ellipse representing the trailing edge of the wing has a minor axis of .114 m. The major axis of each ellipse was 2.794 meters.

It is more important to make the minor axes of the ellipses closely represent the actual leading and trailing edge radii of curvature of the wing than it is to have the major axes represent the wing thickness at the center, since current densities at the smaller radii of curvature are known to be the greatest.

The field distribution around these two ellipses representing the inboard cross section of the wing are shown on Figure 22 where they are compared to the measured field intensities. The calculated field intensities for an ellipse representing the outboard cross section of the wing are shown on Figure 21. For the outboard cross section only, one ellipse of minor axis .128 m and major axis 1.93 m was used. In either case the calculated field strengths follow roughly the same pattern as the field strengths measured. Discrepancies are that the field strength calculated along the center of the wing is lower than that measured, whereas that calculated along the forward and trailing edges is higher than measured.

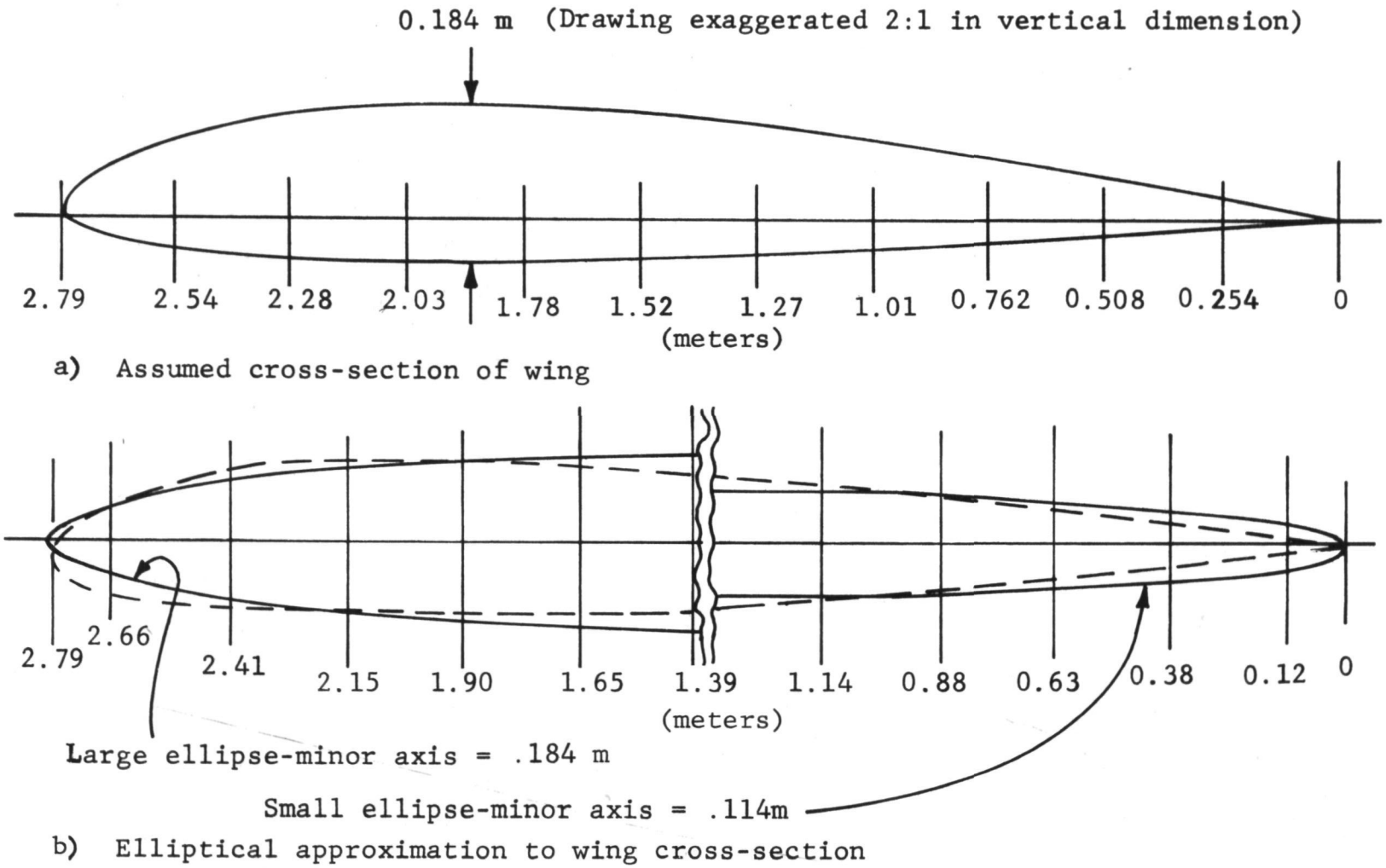

FIGURE 23 - F-8 WING CROSS-SECTION APPROXIMATED WITH ELLIPSES.

Part of the discrepancy may be that the return path for the current was again underneath the wing. In such a case the current in the wing would tend to flow in a path closest to the return path, thus along the center of the wing. Another important possible reason for the discrepancy is shown on Figure 24. Since the magnetic field probe used for this investigation was fairly large and averages the field strength over a volume of several centimeters, it could not measure the true field strength right at the sharp leading and trailing edges. Accordingly, the measured field strength, averaged near the leading and trailing edges of the wing would be lower than the actual field intensity at the edges. As might be expected, the discrepancy is greatest at the trailing edges, which are sharper than the leading edges.

Internal Fields

Measurements were then made at several locations inside the aircraft. Figure 25 shows where the magnetic field measurements were made in and around the cockpit. The figure shows a circled number corresponding to the measurement location and the amplitude at that point. These measurement locations were as follows:

1 - along the windshield above the instrument panel

2 - about 7.62 cm in front of the instrument panel

3 - on the pilot's seat

4 - above the seat and in the same plane as the side rails of the cockpit

5 - along the lower left instrument panel

6 - along the top of the center stick grip

7 - along the front end of the right console

8 - near the middle of the left console

The waveshape of the fields measured near the pilot's seat are shown on Figure 26. The probe was positioned to measure the major axis component of the field expected to have the greatest amplitude, which in this case was the component of the field oriented along the pitch axis of the aircraft, with respect to the direction of lightning current flow from nose to tail. In some cases measurements were made with the probe oriented along all three orthogonal (pitch, roll and yaw) axes.

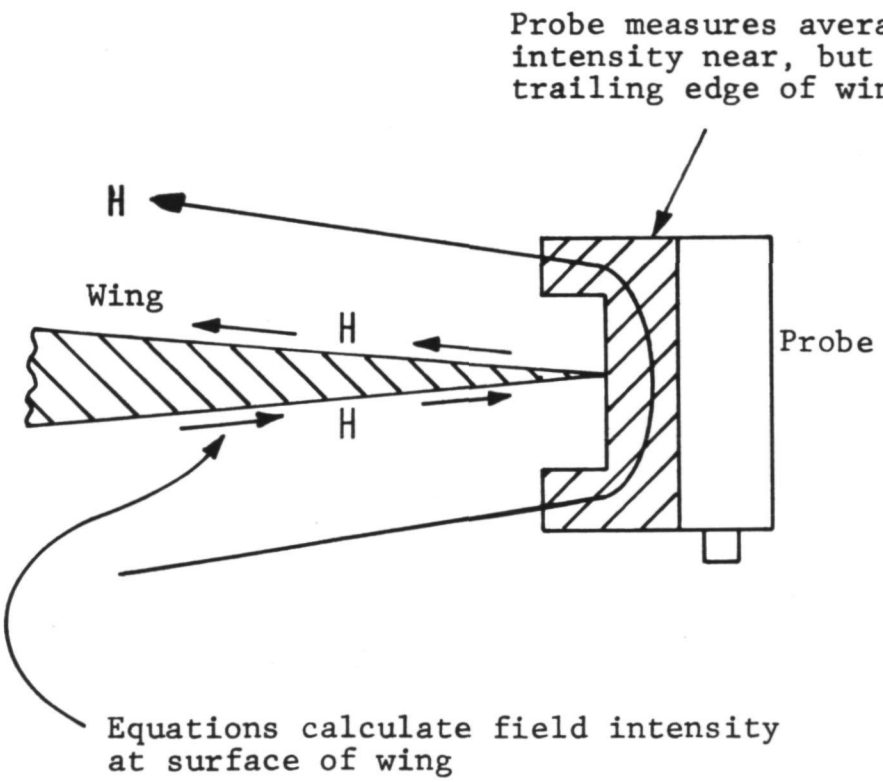

FIGURE 24 - WHY PROBE WILL NOT MEASURE TRUE FIELD INTENSITY NEAR A SHARP EDGE.

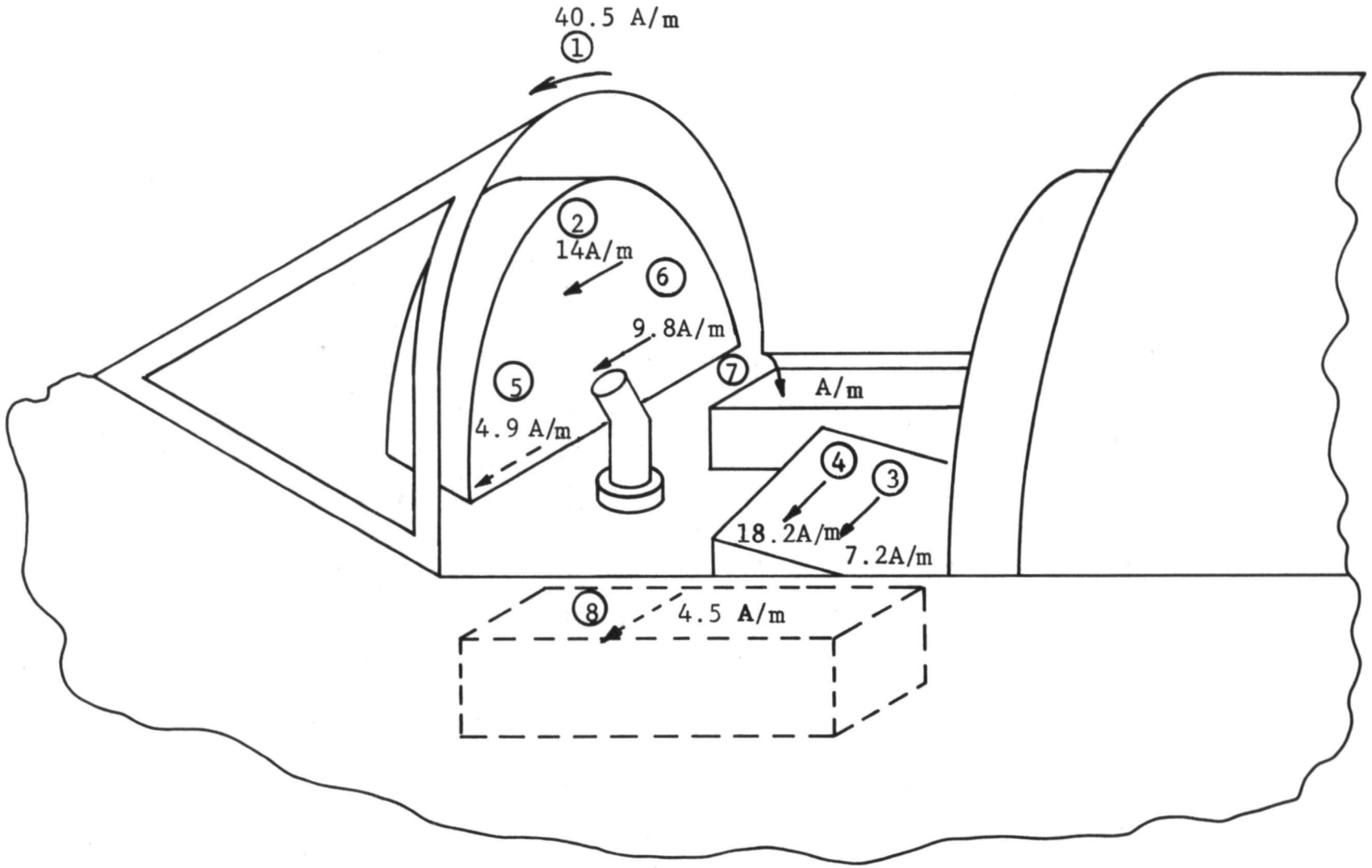

FIGURE 25 - MAGNETIC FIELD MEASUREMENTS IN THE COCKPIT.

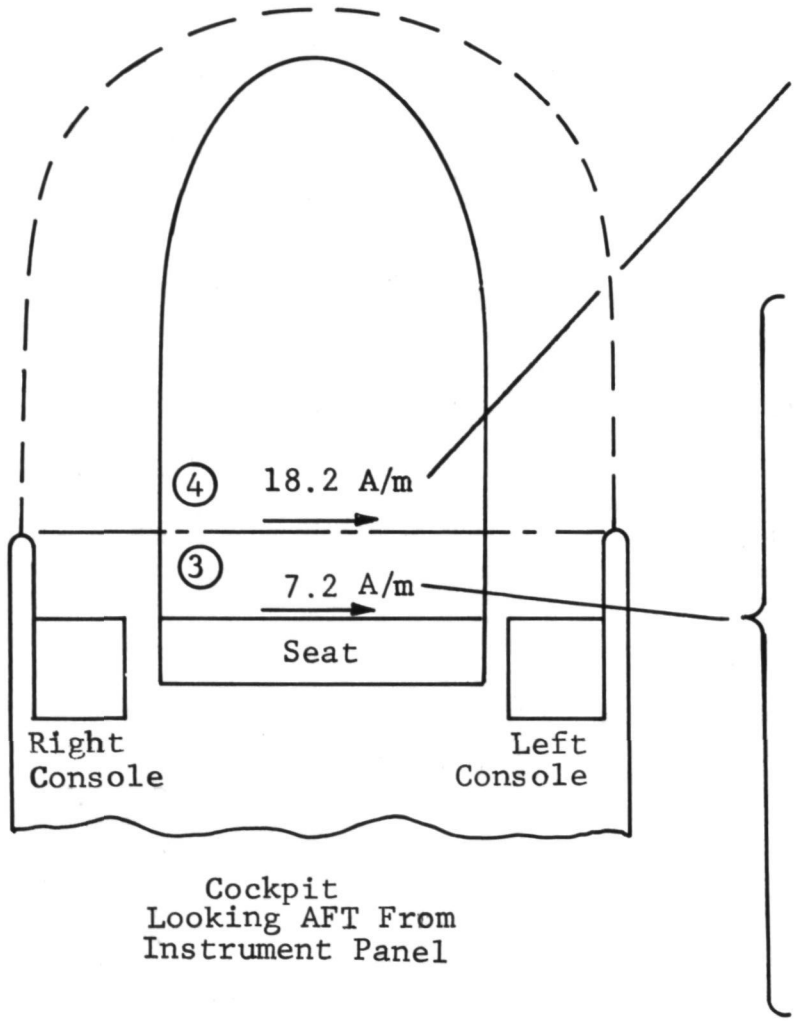

Field Above Seat - Position 4

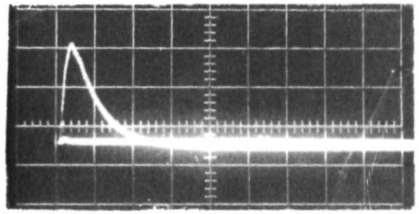

No.363
PITCH
7.5 A/m/Div.

Field on Seat - Position 3

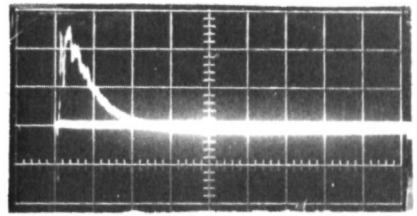

No.325
PITCH
3 A/m/Div.

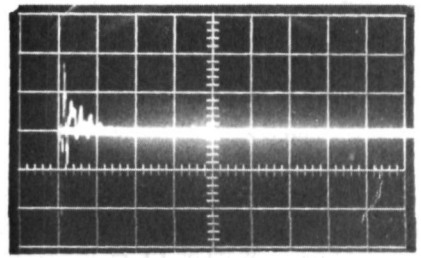

No.327
ROLL
3 A/m/Div.

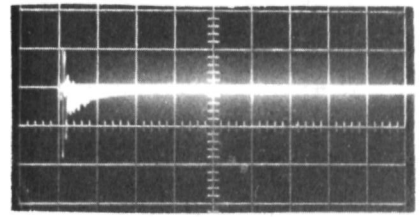

No.328
YAW
3 A/m/Div.

All pictures 5μs/Div.

FIGURE 26 - MAGNETIC FIELDS NEAR PILOT'S SEAT.

Where appropriate, oscillograms are shown at the probe output for each of these three axes. One such case is the field along the surface of the pilot seat. As would be expected, the major component of the field is oriented along the pitch axis. Observe, however, that there is some high frequency component of the field superimposed on the pitch axis oscillogram at the seat that was not present on the corresponding field several centimeters above the seat. There is also a good deal of high frequency field components in the roll and yaw axes. Since the field at any point is the sum of the incremental fields produced by all of the incremental currents in the aircraft (with those currents nearest the point in question of course being the most important) the resultant high frequency field in the other axes farther within the cockpit area would seem to indicate current flow momentarily along all of the different structural members or current carrying paths in the cockpit area. The currents do not flow continuously along any one element however. They may circulate in structural elements and change with time. The result indicates that in future aircraft designs one cannot count on orienting electrical conductors or electrical apparatus along an axis that will eliminate all magnetic field coupling. While it may be possible to predict the axis along which the major component of the magnetic field will appear, there is little likelihood that the axes of all of the high frequency components of the field can be predicted, or that there exists an axis along which the magnetic flux vector is zero.

Magnetic fields measured near the right and left consoles are shown on Figure 27. Each of these oscillograms also show the evidence of high frequency variations of current. In particular, the field along the right console shows a major component of the field oriented along the yaw axis. This results because the field was measured in a corner near the vertical front of the right console. A magnetic field will always flow parallel to a metallic surface and indeed none of the components, whether high or low frequency, at a metallic surface will be oriented at right angles into that surface.

All of the measurements presented thus far have been made with the probe that responded to the magnetic field intensity for times short compared to 4 microseconds and to the derivative of the magnetic field for times long compared to 4 microseconds. A few measurements were also made at the pilot seat with the probe that responded to rate of change of magnetic field intensity, dH/dt. Measurements of this nature are shown on Fig. 28.

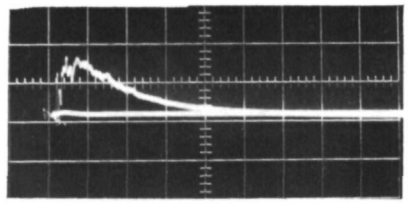

No. 393
PITCH
3 A/m/Div.

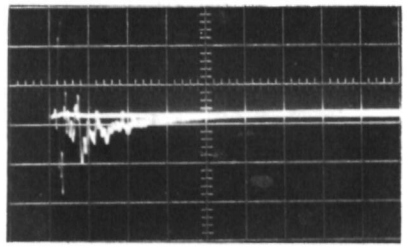

No. 394
ROLL
3 A/m/Div.

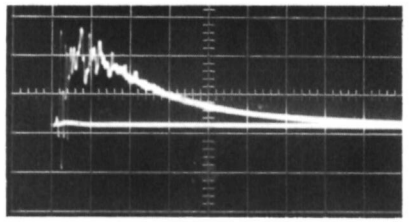

No. 395
YAW
3 A/m/Div.

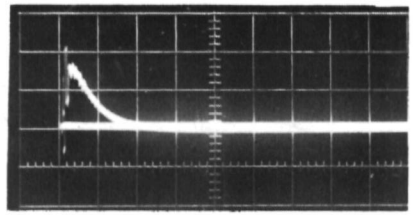

No. 330
PITCH
3 A/m/Div.

5μs/Div.

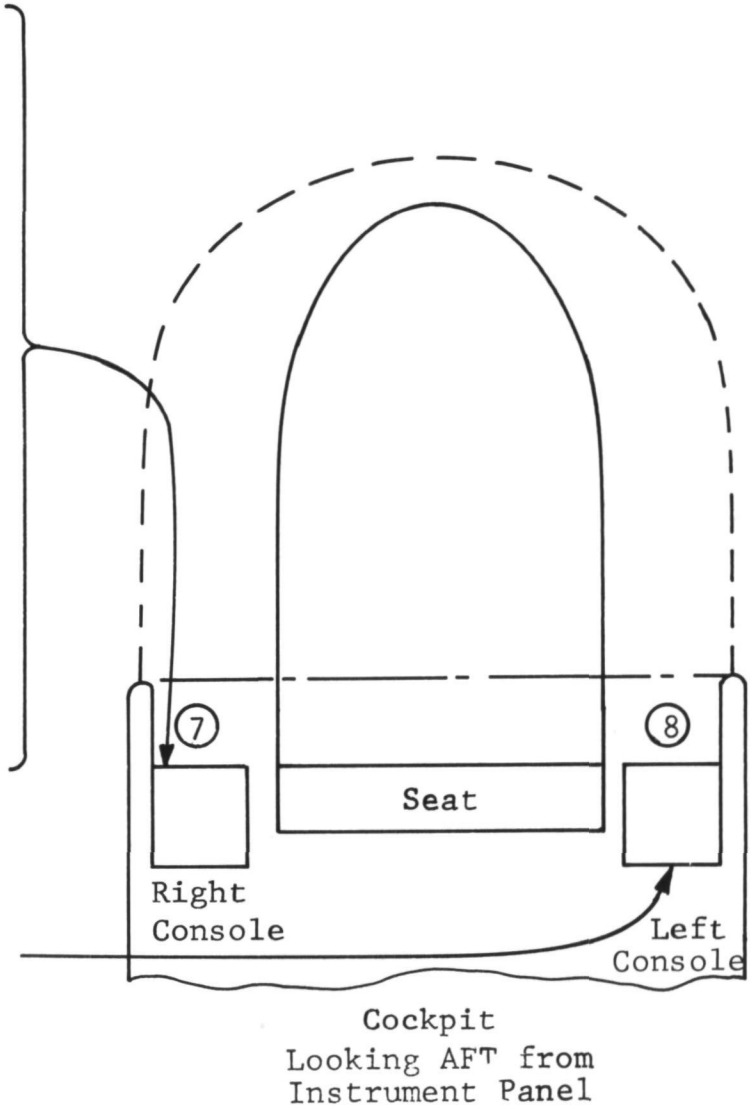

FIGURE 27 - MAGNETIC FIELDS NEAR RIGHT AND LEFT CONSOLES.

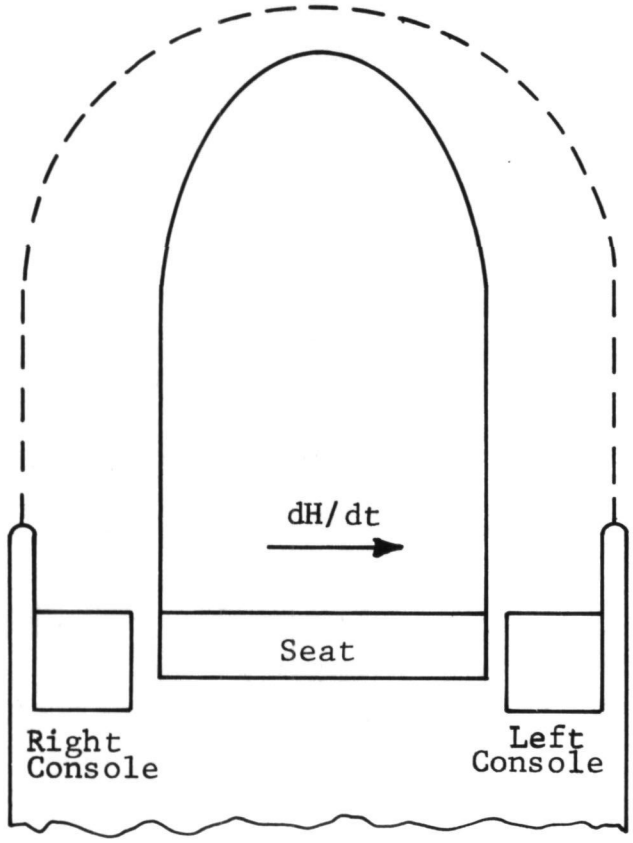

FAST Lightning Current

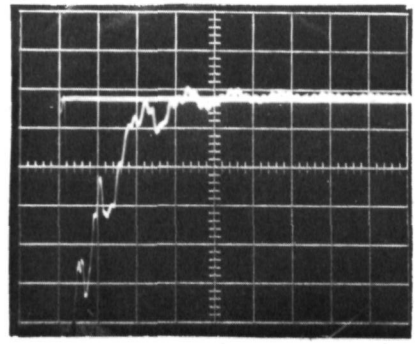

No. 375

0.1 V/Div. 1 μs/Div.

SLOW Lightning Current

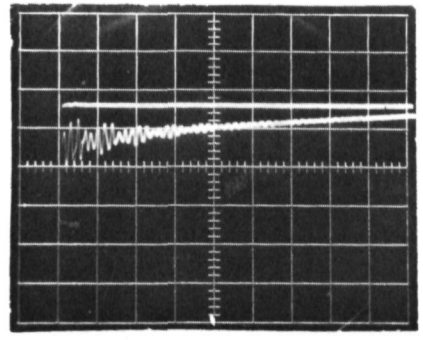

No. 379

.05 V/Div. 1 μs/Div.

FIGURE 28 - dH/dt NEAR THE PILOT'S SEAT.

Measurements were made for both the fast (3 x 60 μs) and the slow (12 x 76 μs) simulated lightning current waveforms. As expected, the amplitude of the rate of change waveform produced by the slow lightning current was considerably lower than that produced by the fast lightning current. Both measurements show a substantial amount of high frequency oscillation superimposed upon the fundamental waveform. Some of these are thought to be the result of the damped oscillation superimposed on the test current waveforms, though there is some question as to whether it is all due to this stimulus or to secondary effects such as circulating currents in portions of the airframe.

The results of magnetic field measurements inside the gun bay are shown on Figure 29. This is where the BCS and interface electronics packages are located, along with much of the interconnecting wire bundles. Since the aircraft electrical equipment was operating during these measurements, the currents flowing on all of the wires within the left gun bay produced magnetic fields of their own, to which the probe also responded. These fields made the traces on the oscillograms difficult to readily interpret so pictorial waveforms of the correct traces are presented on the figures instead. Significant indications from these measurements are:

1. The field intensity on the inside of the left gun bay is reduced by a factor of 100 or 200 (40-46 db) from the field existing outside the gun bay.

2. The field intensity inside the left gun bay rises to its maximum amplitude about as fast as the field intensity outside the gun bay but decays more slowly. It must be remembered that the probe is responding only to the rate of change of the field for times greater than about 4 microseconds. Accordingly, the actual field intensity inside the gun bay has a longer duration than does the field outside the gun bay.

No attempt was made to measure the three orthogonal field components inside the gun bay, but the absence of significant high frequency oscillations on the front of the oscillogram shown on Figure 29 indicates that there are few high frequency components along the other axes.

No. 388

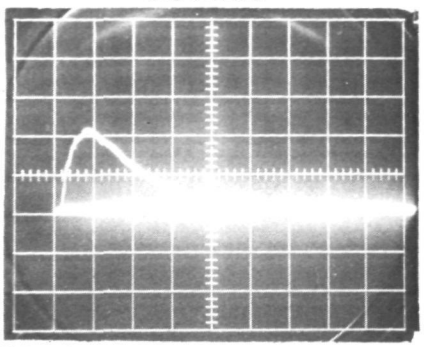

30A/m/Div. 2μs/Div.

External Field

View Looking Forward
Current Flow Fwd to Aft

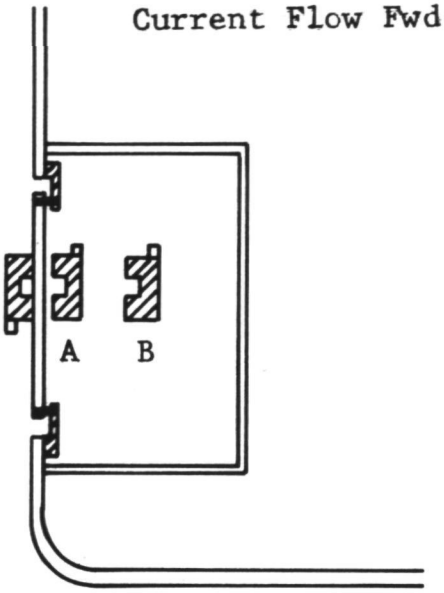

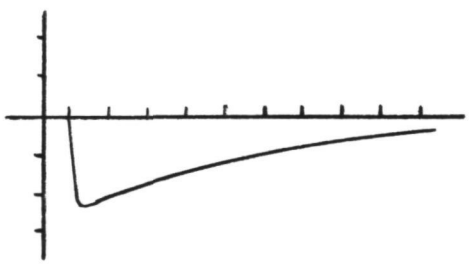

0.15A/m/Div. No.432 5μs/Div.

Probe Against Inside of Door-Pos.A

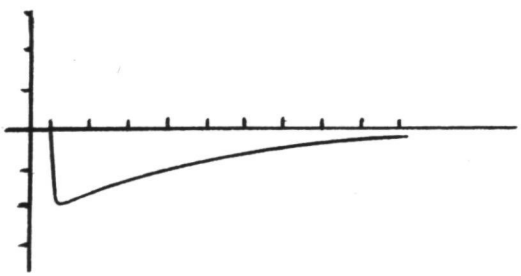

0.30A/m/Div. No.440 10μs/Div.

Probe in Middle of Left Gun Bay-Pos. B.

Internal Field

FIGURE 29 - MAGNETIC FIELDS INSIDE GUN BAY.

Figure 30 presents some measurements made with the dH/dt probe inside the gun bay. The measurements were made with the sensor located in one place, but with the gun bay hatch cover first removed from the aircraft and then placed back in position. These measurements thus give an indication of the shielding provided directly by the hatch cover, whereas those of Figure 29 gave an indication of the total shielding produced by the hatch cover plus the rest of the surrounding aircraft structure.

Figure 31 presents some measurements made along the external surface of the aircraft adjacent to the cover over the battery compartment. Oscillogram No. 387 shows the field intensity at the surface of the hatch cover with the hatch cover in place. Most of the oscillations superimposed on this oscillogram should be ignored since later inspection showed the instrument cable from the probe touching the ground return path, a condition known to produce spurious oscillations such as this. Oscillogram No. 447 shows the corresponding measurement with the door removed. Removing the hatch cover therefore allows the field at the surface of the hole thus produced to drop to about half the value that it would have been if the hatch cover were in place. These measurements indicate that the field along an aperture is about one half of what the field would be were the aperture closed by a conductive sheet that would carry current.

Magnetic field measurements were also made inside the battery compartment, as shown on Figure 32. Primary and back-up FCS power supply batteries and associated circuitry are located in this compartment. All measurements were made with the probe sitting on top of one of the batteries. Oscillogram No. 449 shows the field intensity measured with the hatch cover of the battery compartment removed. If oscillogram No. 449 is compared with oscillogram No. 447 on Figure 31, the shielding produced by placing the probe inside the cavity is evident. The field intensity at different distances from an aperture was discussed on Figures 12 and 13.

Oscillograms 450, 451 and 452 of Figure 32 show, on three different time scales, the field produced inside when the cover is in place. The major significance of these oscillograms is that the field inside the battery compartment rises to its crest much more slowly than does the field external to the aircraft and lasts for a much longer time. This is the pattern characteristic of diffusion coupling through a conductive surface. The reason that the field inside the battery compartment displays this diffusion characteristic, whereas the

View Looking
Forward

Current Flow
Fwd to Aft

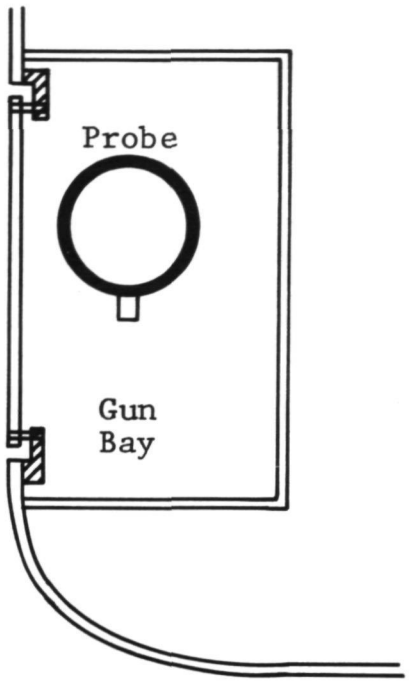

No.435

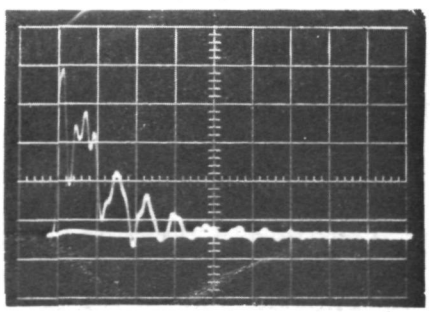

0.5V/div. 1μs/div.
(Cover Removed)

No.436

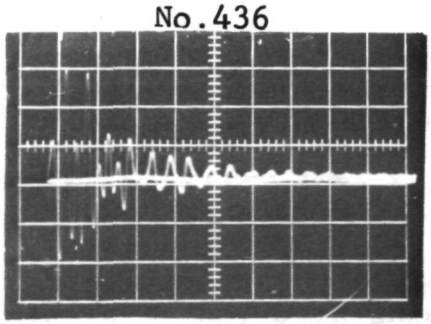

0.1V/div. 1μs/div.
(Cover in Place)

FIGURE 30 - dH/dt INSIDE LEFT GUN BAY.

Views Looking Forward
Current Flow Fwd to Aft

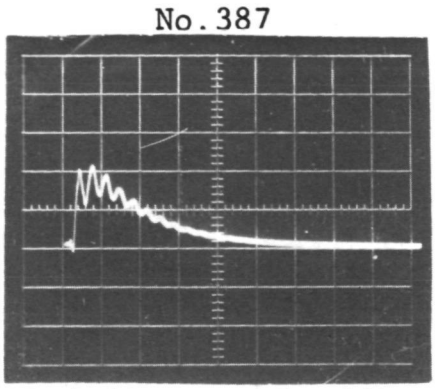

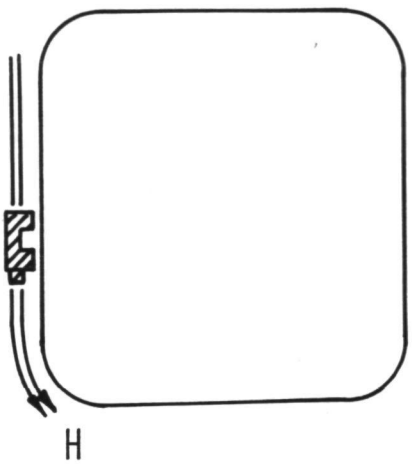

a) Cover Closed

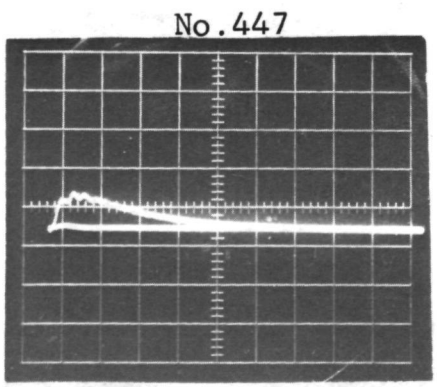

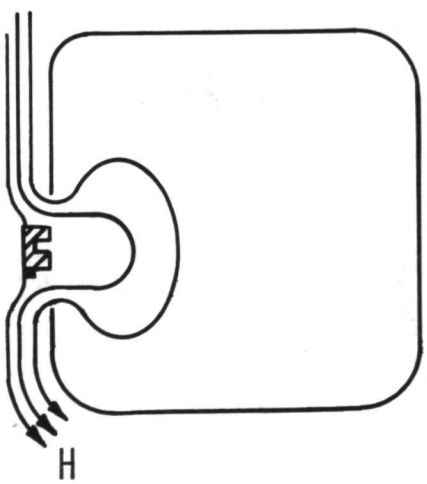

b) Cover Open

FIGURE 31 - MAGNETIC FIELDS AT SURFACE OF BATTERY COMPARTMENT (PROBE TIME CONSTANT = 4μs).

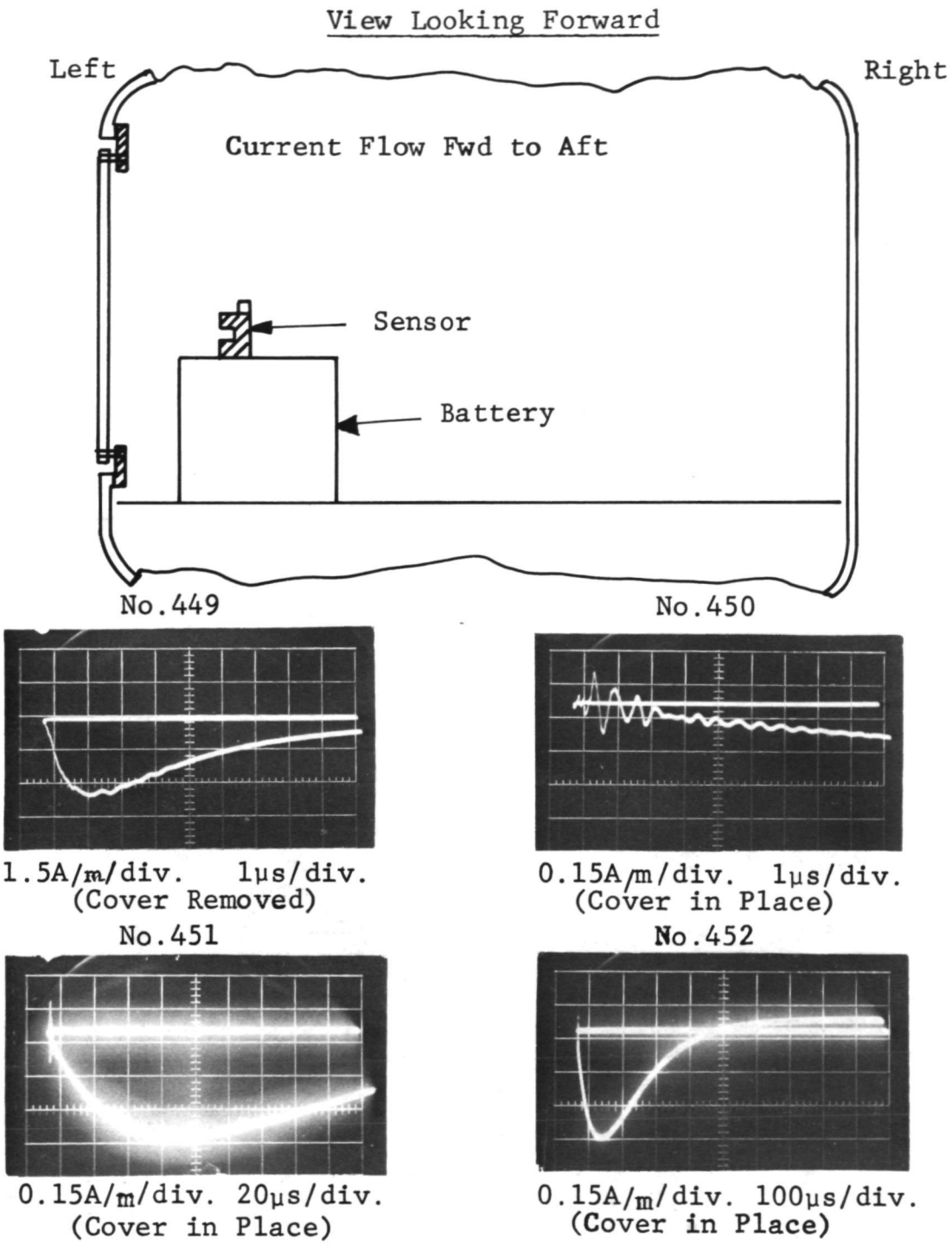

FIGURE 32 - MAGNETIC FIELDS INSIDE THE BATTERY COMPARTMENT. (PROBE TIME CONSTANT = 4μs).

field inside the gun bay does not, is that the hatch cover of the battery compartment was held in place with fasteners spaced about every 3.81 cm, whereas the hatch cover for the gun bay was held in place by fasteners spaced about every 30.48 cm.

Figure 33 shows measurements of dH/dt inside the battery compartment with the cover removed, and in place. Oscillogram Nos. 446 and 448 are evidently the derivatives of Nos. 449 and 450, as expected. The amplitudes of magnetic field and derivative are greatly attenuated when the cover is in place, and with it in place the high frequency oscillations become the predominant cause of the dH/dt signal, as is evident from oscillogram Nos. 450 and 448. The magnetic field inside the enclosed battery compartment oscillates at a frequency of 1.54 megacycles during the first 3 microseconds, as shown on oscillogram No. 450 of Figure 32. The frequency of the oscillations superimposed on the fast lightning current waveform is 2.2 megacycles, indicating that the magnetic field oscillation inside the battery compartment is not entirely due to aperture flux originating outside the aircraft. Secondary oscillatory current flow in structural members or aircraft cabling may account for some of this.

Summary of Field Measurements

Table I summarizes the magnetic flux density, H, at the various locations where measurements were made outside and inside the aircraft. The data are presented as measured at a simulated lightning current of 300 amperes and scaled up to correspond with full scale lightning strokes of 30 and 200 kiloamperes.

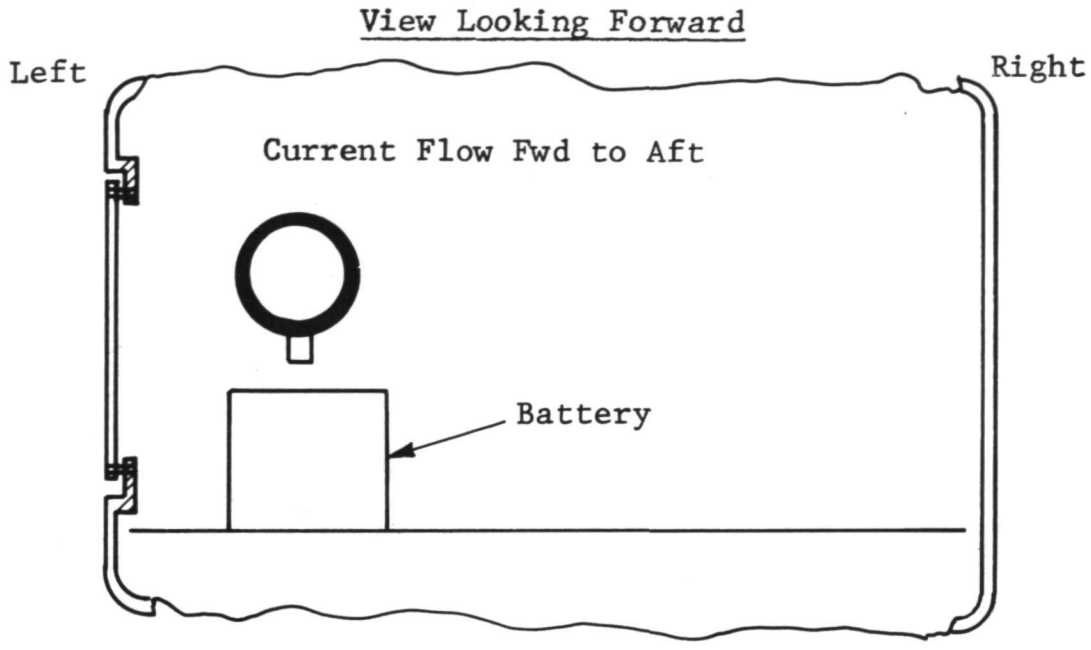

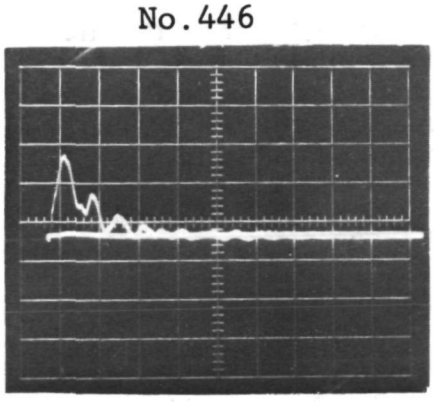

No.446

0.2V/div. 1 μs/div.
(Cover Removed)
(Probe Reversed)

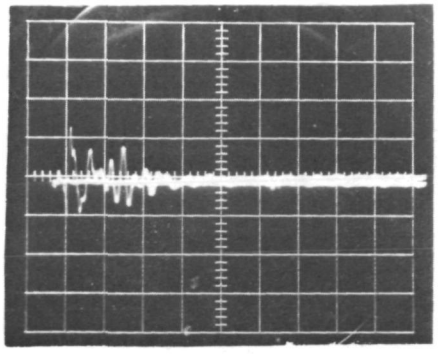

No.448

0.01V/div. 1 μs/div.
(Cover in Place)

FIGURE 33 - dH/dt INSIDE THE BATTERY COMPARTMENT.

Table I - Summary of Magnetic Field Measurements

Location	Magnetic Field, H (amperes/meter) at i_L=300A	at i_L = 30kA	at i_L=200kA
	OUTSIDE		
Side of fuselage, beneath wing leading edge	36	3,600	24,000
Wing leading edge (outboard path)	210	21,000	140,000
Wing leading edge (inboard path)	180	18,000	120,000
Wing trailing edge (outboard path)	220	22,000	146,740
Wing trailing edge (inboard path)	210	21,000	140,000
Wing mid-chord (inboard path)	55	5,500	36,680
Wing mid-chord (outboard path)	80	8,000	53,360
	INSIDE		
Inside left gun bay-near door, with door closed	0.33	33	220
Inside left gun bay-at center of volume, with door closed	0.60	60	400
Inside battery compartment on top of battery, with door closed	0.47	47	313
	WITHIN COCKPIT		
Position 1 along top of windshield	40.5	4,050	27,000
Position 2 8.89 cm in front of instrument panel	14	1,400	9,300

Table I (Cont'd.) - Summary of Magnetic Field Measurements

Location	Magnetic Field, H (amperes/meter) at i_L=300A	at i_L=30kA	at i_L=200kA
	WITHIN COCKPIT		
Position 3 on seat	7.2	720	4,800
Position 4 above the seat and on a level with the rail of the cockpit	18.2	1,820	12,140
Position 5 lower left instrument panel	4.9	490	3,270
Position 6 on top of center stick grip	9.8	980	6,540
Position 7 at right console	7.3	730	4,870
Position 8 at left console	4.5	450	3,000

INDUCED VOLTAGE AND CURRENT MEASUREMENTS

Induced voltage and cable current measurements were made at interfaces and cables located in each major DFBW system component location in the aircraft. These included the gun bay, DFCS pallet area, actuator locations and cockpit. All of the induced voltage oscillograms have been studied and their maximum voltage peak tabulated in Table II. Since all voltages were induced by a test current of 300 amperes, each of the tabulated peaks have been linearly extrapolated to correspond with an average lightning stroke amplitude of 30 kA and also a severe stroke of 200 kA. Scaling factors utilized were 100 for the average stroke and 667 for the severe stroke. The extrapolated values are also presented in Table II.

For possible use in analysis of their impact on FCS components, each voltage has also been approximated by an exponentially damped oscillatory waveform. The parameters E (amplitude coefficient), β (radial frequency) and α (damping coefficient) of each approximation have been determined from amplitude, period and decrement information taken from each oscillogram and are tabulated in Table II. The mathematical relationships utilized for these calculations are presented in the appendix. The oscillograms of each induced voltage waveform are presented in the figures which accompany the following paragraphs. The test number of each oscillogram is included in Table II for cross reference. Table II appears at the end of this Section.

Measurements of bulk cable currents are described in the appropriate paragraphs.

Prior to making induced voltage or current measurements at each location, measurement system integrity was verified by making a measurement of the extraneous noise induced in the instrument cable itself. This was done with the instrument cable drawn into the aircraft adjacent to the interface to be measured. Both instrument cable channels were shorted together and to the airframe or FCS ground, whichever was to be the induced voltage measurement reference point. This forced any noise induced in the instrument cable to appear at the oscilloscope end. The equipment bay was then closed up and the aircraft subjected to a simulated lightning current. Instrument noise was measured on the oscilloscope. Figure 34 shows one of these short circuit noise checks with the instrument probe in the gun bay near 28 VDC bus terminals where induced voltages were to be measured. About 50 mV (zero to peak) of noise was measured with the channels shorted

BATTERIES ONLY
SHORT CIRCUIT NOISE CHECKS
(PROBE IN LEFT GUN BAY NEAR BUSSES)

FAST

E_{A-B}
A,B Shorted
to FCS Grd.

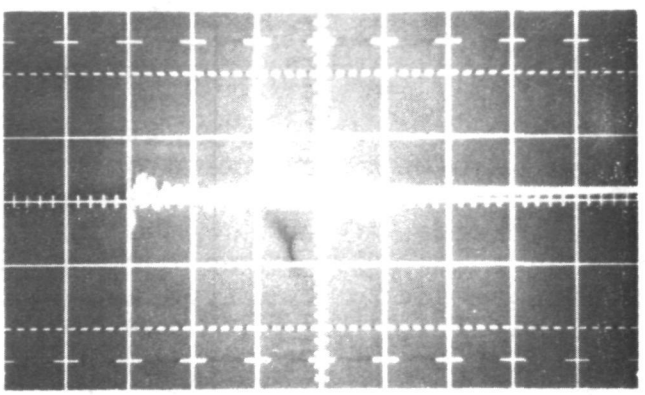

0.2 V/div. No.144 2 μs/div.

FAST

E_{A-B}
A-B Shorted
to A/C Grd.

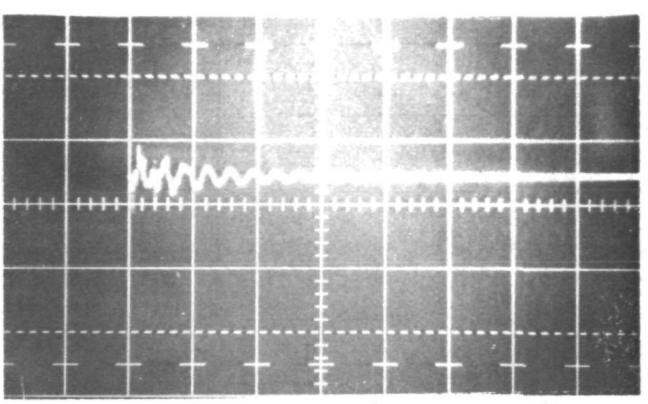

0.1 V/div. No.145 2 μs/div.

FIGURE 34 - SHORT CIRCUIT NOISE CHECK ON MEASUREMENT CIRCUIT
(PRI-SAS OPERATIONAL)

either to FCS ground or the airframe (note the difference in voltage scales). This was typical of instrument noise measured at all other locations. It is considerably less than any induced voltage or current measured in the DFBW system. It may be considered background noise and legitimately deducted from any other measurements, but for practical purposes, it has been neglected in the analysis of results.

Measurements are described in the following paragraphs according to the location where they were made.

Left Gun Bay Measurements

BCS and interface electronics, a display and keyboard unit and various power supply items are located inside the gun bay. Figure 35 shows the instrument cable drawn into the gun bay via a small snap-open access door. The main gun bay access door is removed in the photograph. It was replaced during all measurements.

FCS Power Bus Measurements.- Measurements were first made of induced voltages appearing on the 28 volt DC busses de-energized and disconnected from the FCS system. Thus, only power system circuitry itself was involved. Figure 36 shows these measurements, made under four lightning strike flow path and waveform combinations. Voltages induced in all four busses were similar, with the 300 ampere fast lightning waveform inducing about 1.5 volts (peak) and the slow waveform inducing about half as much. This is to be expected since the fast waveform creates a faster changing magnetic flux than the slow waveform. Each lightning waveform induces a damped oscillatory voltage on the busses. The fast waveform induced a somewhat lower frequency voltage on the busses than did the slower waveform. The reason for this is not entirely clear, but the higher frequency oscillation created by the slow lightning waveform may be due to natural traveling wave reflections (ringing) in the power circuits, while the fast lightning waveform might be driving the circuit at a more predominant component of the fast waveform itself. Lightning current flow path makes only a slight difference in the results, since the power system circuitry is located forward of the wing in a portion of the airframe common to both of the flow paths utilized.

Measurements of voltages induced on the de-energized busses are of course not representative of an in-flight situation and were made only to determine the susceptibility of the power system itself. Therefore, measurements were made next with the FCS system powered up using batteries. Figure 37 shows the induced

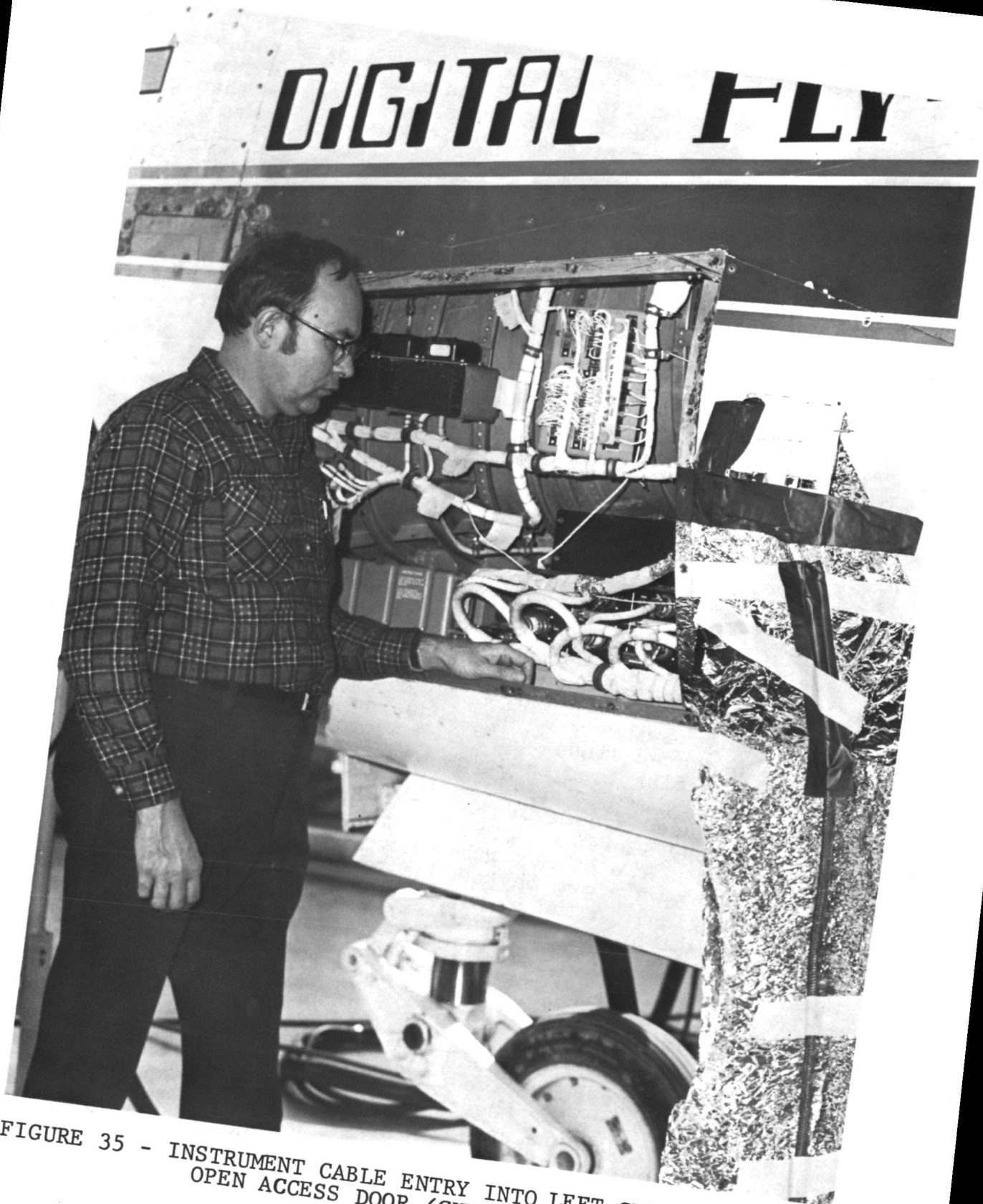

FIGURE 35 - INSTRUMENT CABLE ENTRY INTO LEFT GUN BAY VIA SNAP-OPEN ACCESS DOOR (GUN BAY DOOR REMOVED).

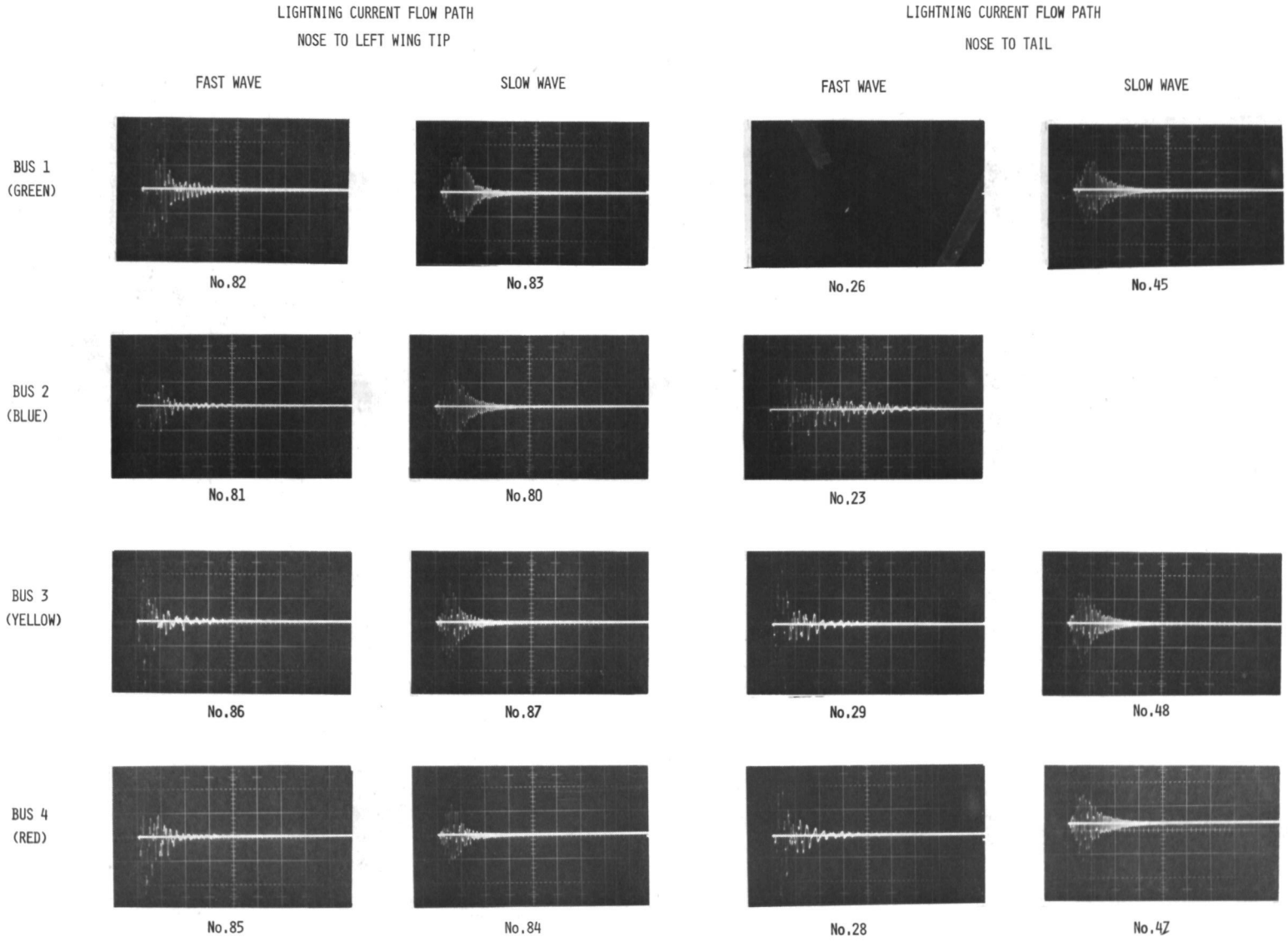

ALL OSCILLOGRAMS 0.5VOLTS/DIV, 2μSEC/DIV.

FIGURE 36 - OPEN CIRCUIT VOLTAGES INDUCED ON THE DC BUS POWER SYSTEM, WITH SYSTEM DE-ENERGIZED.

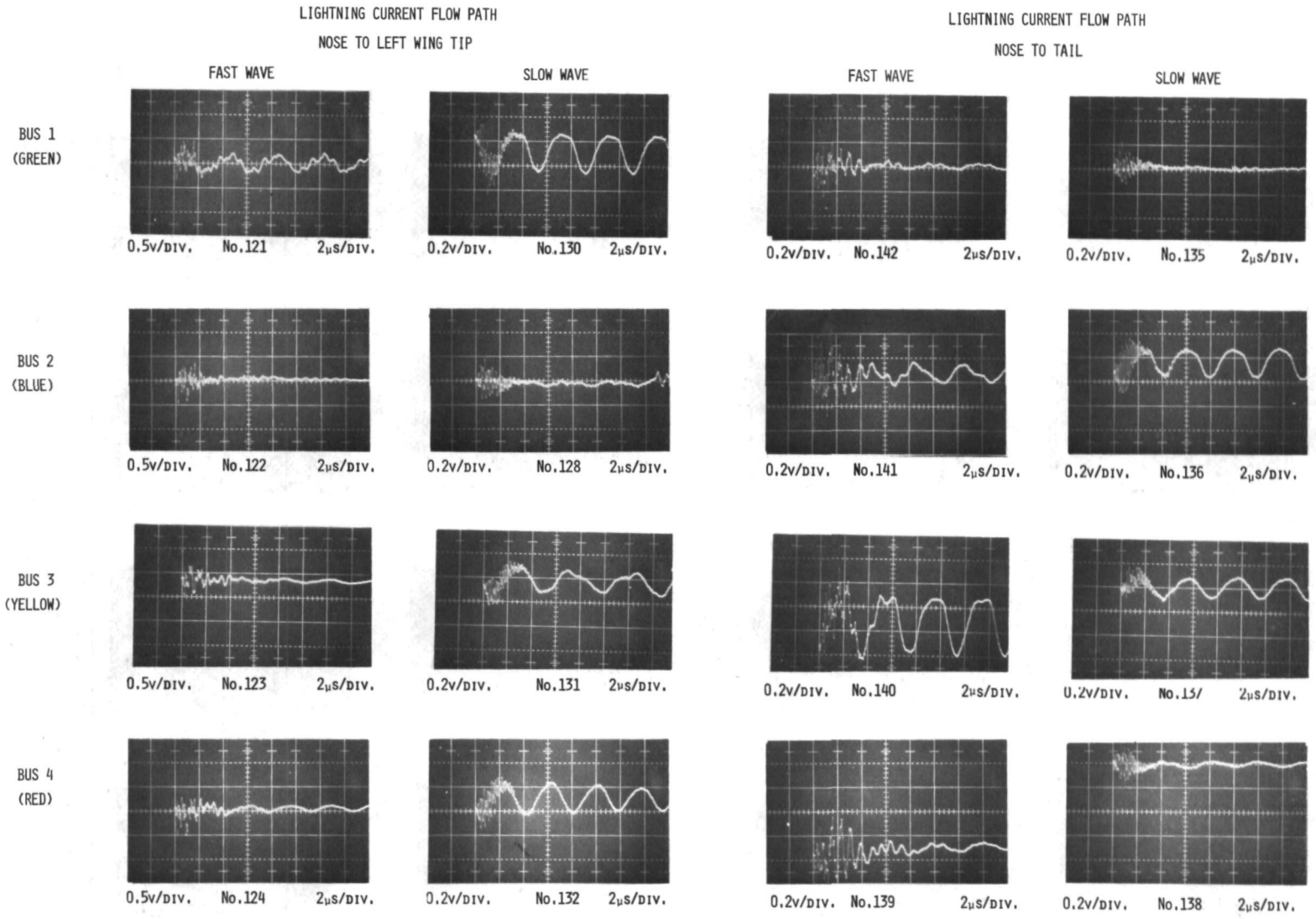

FIGURE 37- VOLTAGES INDUCED ON THE FCS DC POWER SYSTEM WITH BATTERIES ON

voltages appearing on the four battery-powered busses with the system operating. In this case, of course, the induced voltages appearing on the busses may have originated in the FCS system circuits as well as the power system circuitry. Also, application of system loads and batteries to the busses may suppress some of the induced voltages otherwise appearing there. Both of these factors are evident in the measurements of Figure 37. Universally, the induced voltages are lower than corresponding voltages measured on the de-energized busses of Figure 36. Also, note that voltages induced by a nose-to-tail strike are greater than those induced by a stroke entering the nose and leaving the left wing tip. This is probably because more FCS system circuitry is located in the fuselage aft of the wings than is located in the wings themselves.

When studying Figure 37, note that an occasional AC ripple appears on the oscillograms. This is a steady-state ripple imposed on the busses by the FCS system and has no relationship to the induced voltages, which appear superimposed on the first cycle or so of the ripple. The ripple occurs intermittently as the FCS system proceeds through its standard operational sequences. Some oscillograms show the ripple while others do not, since the lightning tests were made at random with respect to the FCS system operation. While the induced voltages shown on Figure 37 appear little greater in amplitude than the AC ripple itself, it must be remembered that full scale lightning would induce proportionately higher voltages. For example, oscillogram No. 142 for a fast waveform nose-to-tail strike induced 0.3 volts (zero to peak) on the primary bus. When extrapolated to correspond to an average lightning stroke of 30 kA, this would be 30 volts.

Sperry Interface Electronics Test Receptacle.- A test receptacle exists on the Sperry interface electronics package to provide access to various points in the FCS system for system test purposes. With the system powered up with batteries, measurements were made of induced voltages appearing between some of these points and an FCS ground point also available at the test receptacle. These measurements are shown on Figure 38. The pin number and corresponding circuit test point identification are shown above each oscillogram. Between each point and the test receptacle is an isolating buffer amplifier. Thus, induced voltages appearing at the test receptacle may not necessarily be representative of those at the identified point in the electronics package. Nonetheless, these measurements provide an indication of what some of the induced voltages appearing in the electronics package may be like.

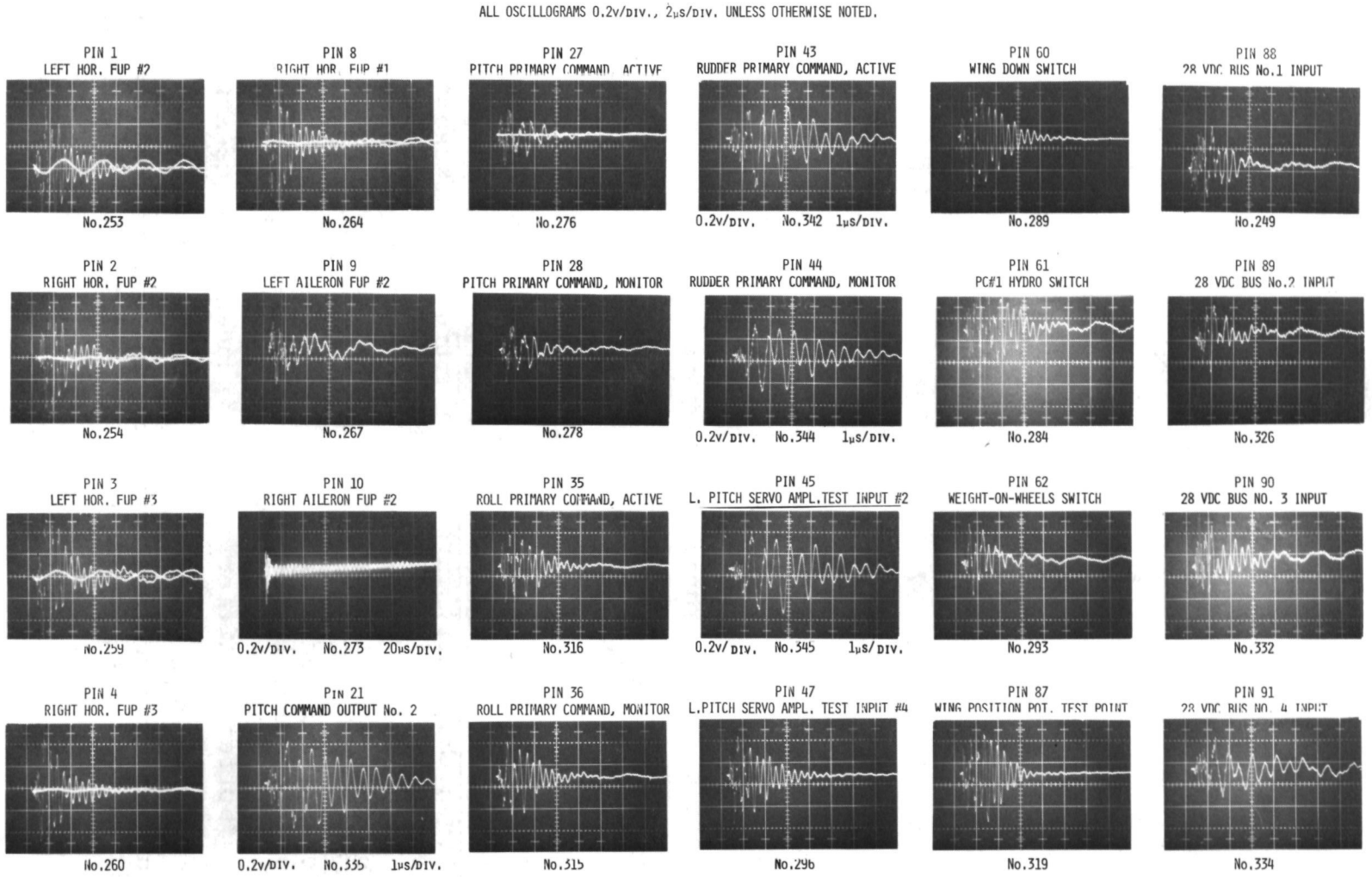

FIGURE 38 - INDUCED VOLTAGES AT TEST RECEPTACLE OF SPERRY INTERFACE ELECTRONICS PACKAGE IN LEFT GUN BAY (FAST I_L WAVEFORM DATA ONLY).

The induced voltages shown on Figure 38 are damped oscillatory waveforms of either of four different predominant frequencies. The predominant frequency of induced voltage measured at each pin is shown on Table III at the end of this Section.

The induced voltage attributed to 28 volt DC busses Nos. 1, 2 and 3 oscillated at 1.82 megahertz, which is the same frequency as the induced voltage measured earlier on the busses themselves, as shown on Figure 37. However, pin No. 91 attributed to bus No. 4 experienced a voltage oscillating at 0.82 megahertz, which is different from the 1.82 megahertz experienced on bus No. 4 itself in Figure 37. The Pitch Primary Command Active and Monitor test points experienced voltages oscillating at 1.0 megahertz, as did the left aileron FUP No. 2. The Rudder Primary Command Active and Monitor test points experienced voltages oscillating at 1.5 megahertz. All other test points shown on Figure 38 had voltages oscillating at 1.82 megahertz.

Further study of the oscillograms of Figure 38 shows evidence of higher frequency, lower amplitude oscillations superimposed on the fundamental waveforms during the first 2 microseconds or so. Oscillogram No. 332 (pin No. 90) is a good illustration. These appear to oscillate at about 5 megahertz.

Incoming Circuit Measurements.- Voltages were measured in several typical two-wire circuits coming into the gun bay from remote locations. These voltages were measured at open plug P22 which is an interface between actuator circuits and the BCS electronics package for channel 2. Voltages were measured at the open plug terminals so that all of the voltage induced in the incoming circuits would appear at the measurement point.

Figure 39 shows the voltage induced by a nose-to-left-wingtip strike in the Left Pitch Valve Drive Output circuit at plug P22. This circuit runs aft to the left pitch actuator as shown in Figure 39. The voltage induced in this circuit has peaks of about 0.1 volt and a predominant frequency of about 1.82 megahertz, the same frequency as many of the voltages measured at the test receptacle. The voltage induced in this incoming circuit, however, is much "cleaner" than those measured at the test receptacle. Apparently, the 1.82 megahertz voltage is characteristic of the voltage induced in extended circuits such as this. Voltages measured at the test receptacle, of course, are a combination of those induced in many circuits interconnected in the electronics package, and predominant frequencies are less evident.

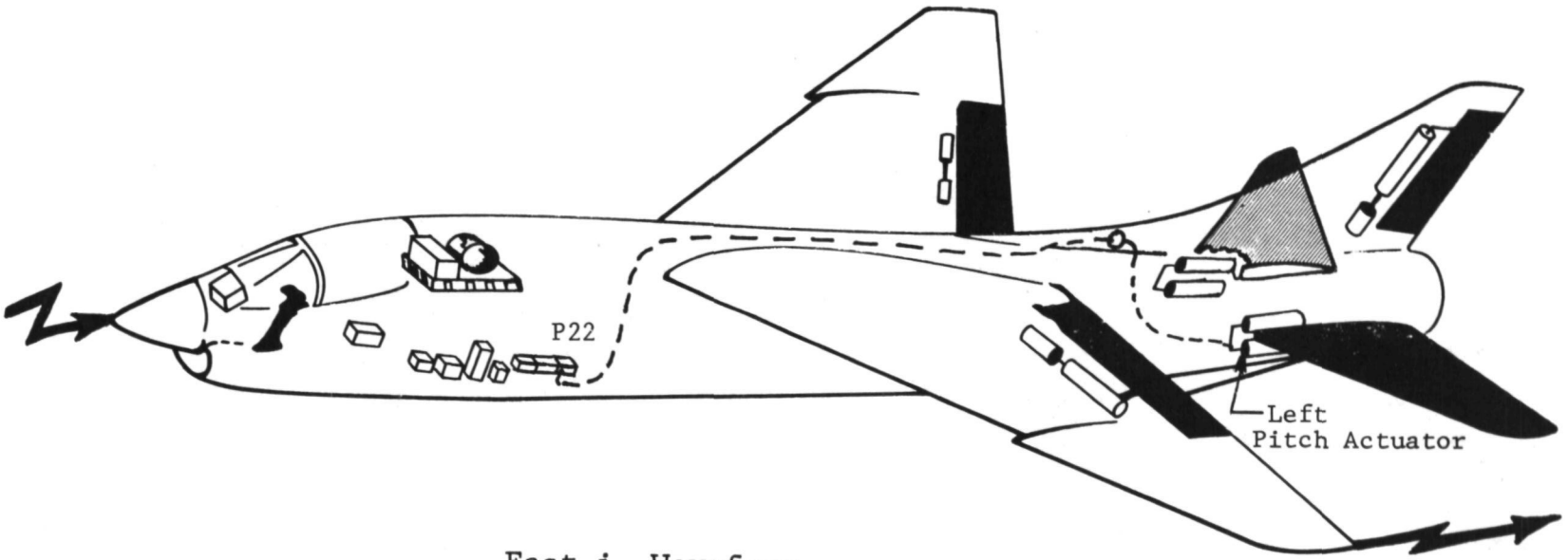

Fast i_L Waveform

Left Pitch Valve Drive Output
(High to Low) Pins 15-16

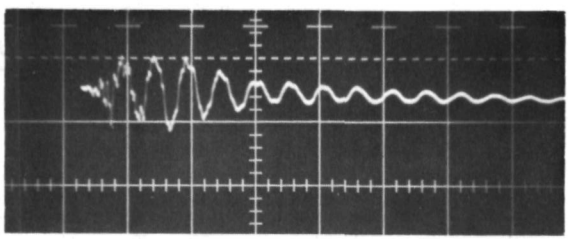

0.2V/div. No.355 1μs/div.

FIGURE 39 - LEFT PITCH VALVE DRIVE OUTPUT (HIGH TO LOW) AT PLUG P22 (SYSTEM BATTERY POWERED).

Figure 40 shows voltages induced by nose-to-left-wing-tip and nose-to-tail strikes in the Left Roll Valve Drive Output circuits at plug P22. As might be expected, there is more voltage induced in this circuit when lightning current leaves the aircraft through the left wing than is induced when it leaves through the tail. The predominant frequency of these voltages is 2.08 megahertz, slightly higher than the frequency measured in the Left Pitch Valve Drive Output circuit going to the left pitch actuator in the tail, as shown in Figure 39. If these oscillations are a function of circuit length, the shorter circuit to the roll actuator in the wing may be expected to produce the higher frequency.

A wing position indicator switch is located beneath the leading edge of the wing to provide information to the FCS system on wing up or down status. As for other circuits in the FCS system, the circuit to this switch has an independent return and is isolated from the airframe at the switch. Measurements were made with the switch closed although the wing was elevated. In this condition the switch is normally open, but it was manually closed for this test to assure that all of the induced voltage in the circuit would appear at P22 where it was to be measured. Figure 41 shows the line-to-line voltages induced in this circuit (oscillogram No. 361) and between one line and the airframe at plug P22 (oscillogram No. 364). The line-to-line voltage is greater in this circuit than in either of the actuator circuits of Figures 39 and 40. This is probably because the switch is located in a relatively exposed position in a structural region where lightning current is concentrated and the wing was raised. Lowering the wing would reduce the switch exposure, but there is still an open crack between the lowered wing and fuselage near the switch location, and the wing can be in either position when in flight. The voltage between one line and the airframe at P22 is greater than the line-to-line voltage, as might be expected since there is greater area between either wire of the circuit and airframe than there is between the two wires. Again, the induced voltage is oscillatory, this time at a fundamental frequency of about 2 megahertz.

Induced Voltages Between FCS Ground and Airframe Ground.- Since much of the FCS system electronics is located in the left gun bay and DFCS pallet which are relatively near the point (beneath the DFCS pallet) where the single point FCS ground is connected to the airframe, common-mode induced voltages between the FCS ground circuit in any electronic package and the airframe should be relatively low. To determine the magnitude of a typical

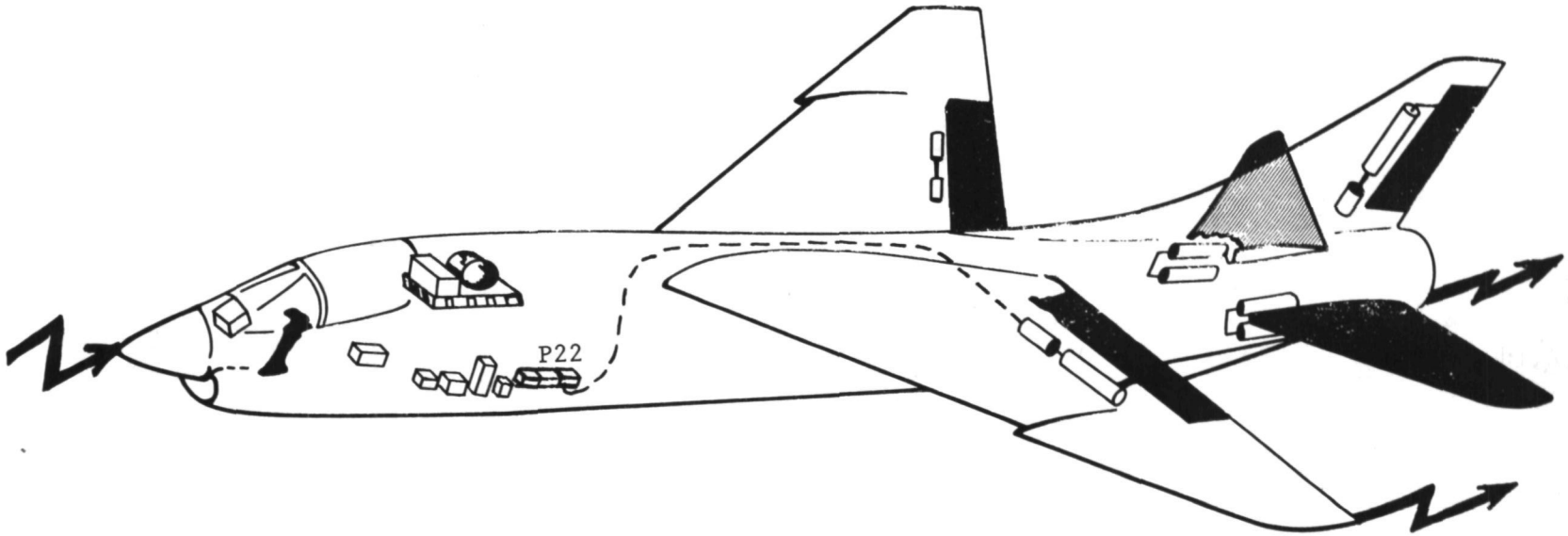

Fast i_L Waveform

i_L N - LWT

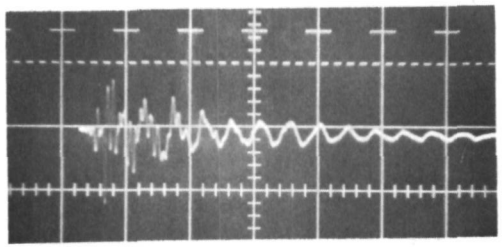

0.2V/div. No.359 1μs/div.

i_L N - T

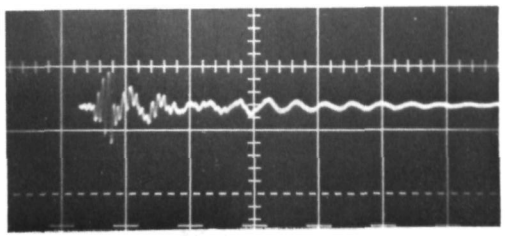

0.2V/div. No.360 1μs/div.

FIGURE 40 - VOLTAGES INDUCED IN LEFT ROLL VALVE DRIVE OUTPUT CIRCUIT (PINS 44-45) AT OPEN PLUG P22.

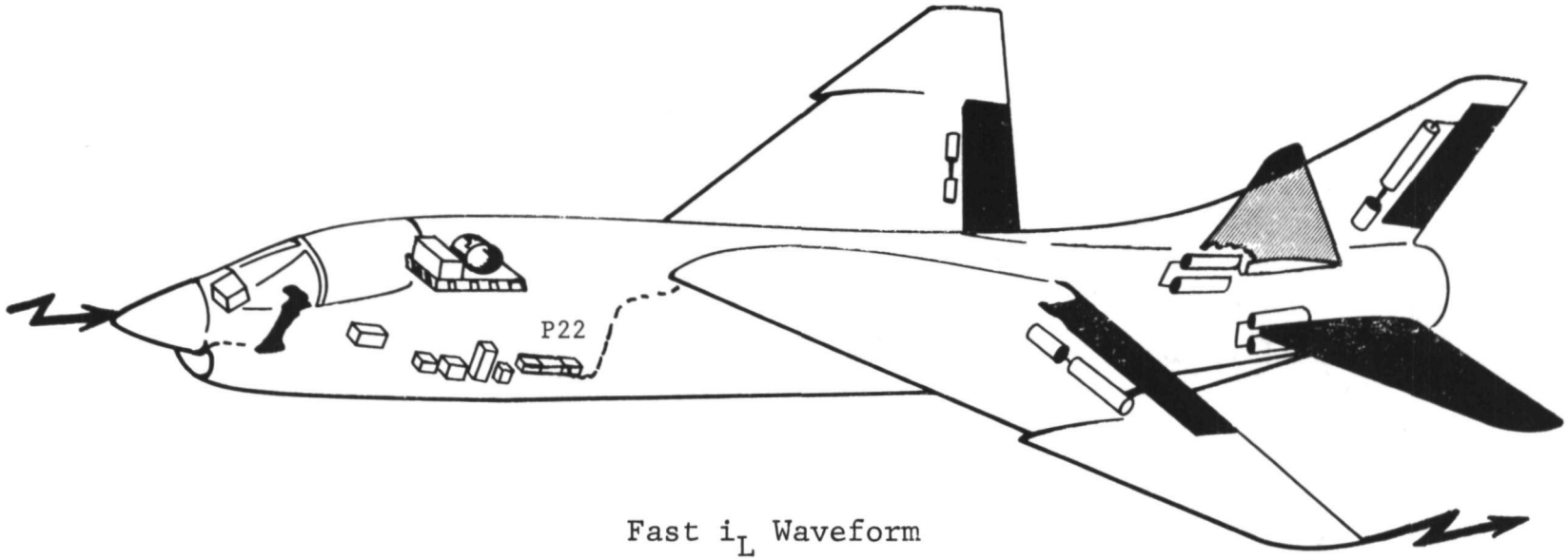

Fast i_L Waveform

i_L N - LWT

(Switch Closed
Wing Up)

Line-to-Line

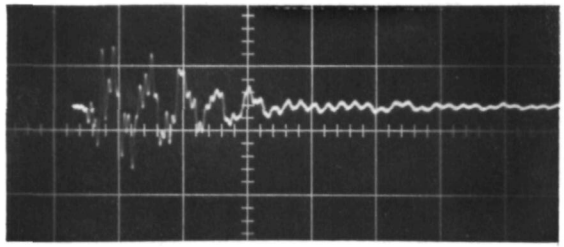

0.2V/div. No.361 1μs/div.

One Line to Airframe

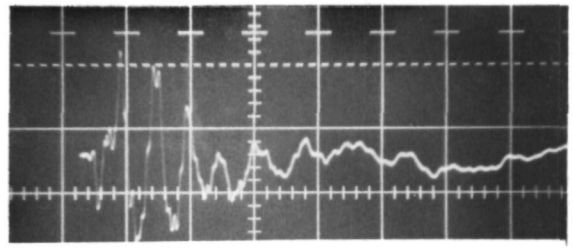

0.2V/div. No.364 1μs/div.

FIGURE 41 - VOLTAGES INDUCED IN WING POSITION INDICATOR SWITCH CIRCUIT AT OPEN PLUG P22.

common-mode voltage, a measurement was made between the FCS ground and the airframe at the FCS ground terminal strip in the gun bay. FCS grounds in the gun bay electronics packages are connected to this terminal strip. The measurement was made between the terminal strip and the airframe immediately beneath it. The results are shown for de-energized and powered-up conditions on Figure 42. With the system de-energized, measurements were made of the induced voltage between grounds. This is termed the open circuit voltage. Next, a jumper was connected from the FCS ground terminal to the airframe, thus forming a short circuited ground loop. Short circuit currents induced in this loop were then measured. Since such a ground loop might have adversely affected normal system operation, the jumper was not attached when measurements were made with the system powered up.

Open circuit induced voltages measured with the system de-energized include a high amplitude damped oscillatory component and a much lower amplitude DC component, as might be expected since the circuit includes the small portion of airframe between gun bay FCS ground terminal strip and the single-point ground connection to the airframe in the DFCS pallet area. Peak voltage is about 0.26 volts. Short circuit currents flowing in the jumpered ground loop have a smooth, unidirectional waveform. This indicates they are probably caused by a combination of diffusion magnetically induced and structural resistive voltages. The waveform of the short circuit currents also indicates they are not being driven by the high frequency voltages appearing in the open circuit. The high frequency voltages must therefore be secondary oscillations in the open-ended circuit, governed by this circuit's distributed inductance and capacitances.

Induced voltages measured between FCS ground and the airframe with the system powered up are about five times as great as the de-energized measurements, as shown on Figure 42, especially for the nose-to-tail test condition. This is probably because more elements of the system, such as the power supply, are connected in when operating and bring more common-mode voltage to the FCS ground. Since much of the system circuitry is in the fuselage and extends to the tail area, it is understandable that a nose-to-tail lightning flow path induces more voltage than does the nose-to-left-wing-tip path. The fast waveform induces an oscillatory voltage with a fundamental frequency of 1.28 megahertz in this ground circuit. This frequency is not identical with that of any other induced voltage measured in the system.

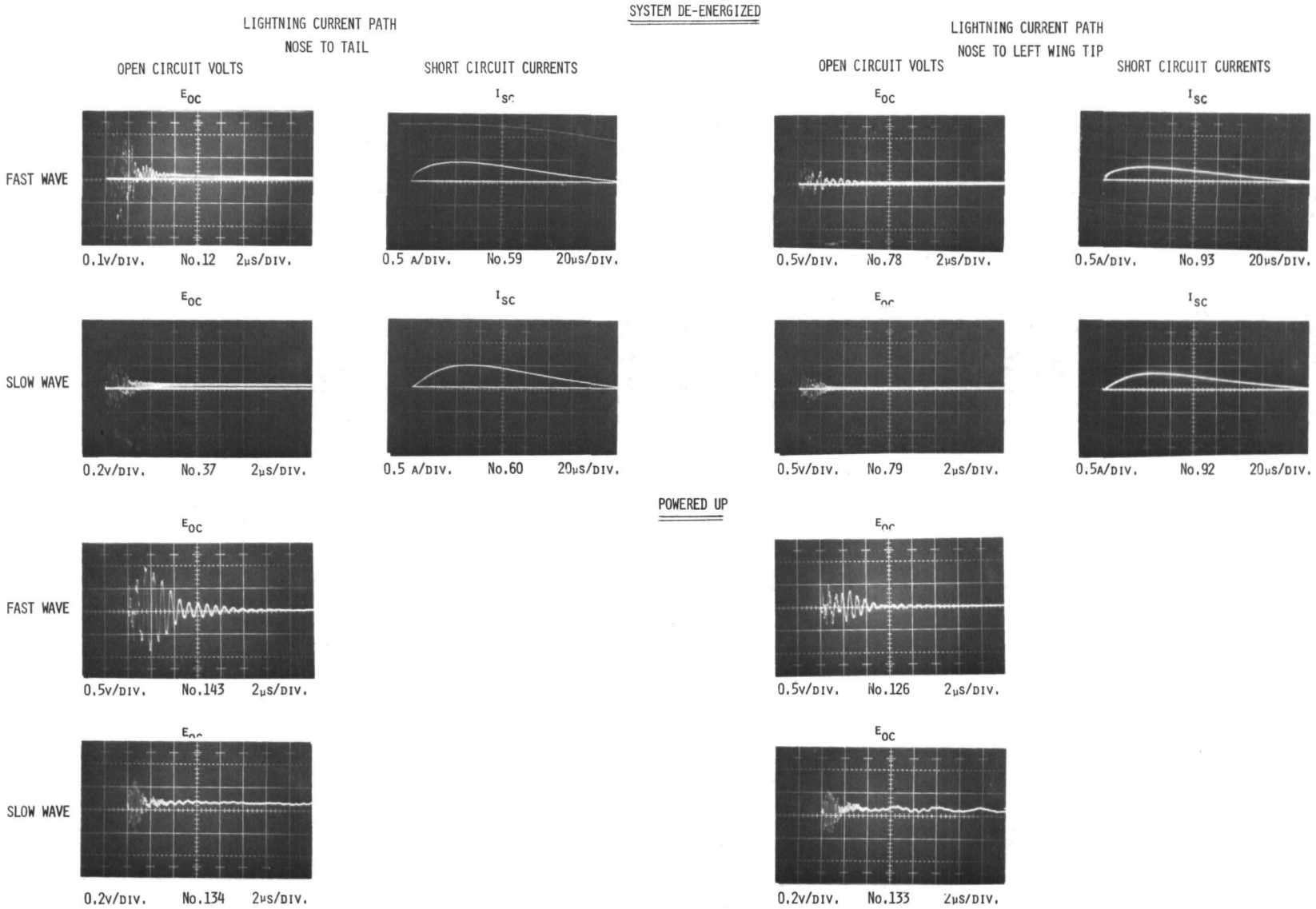

FIGURE 42 - OPEN CIRCUIT VOLTAGES AND SHORT CIRCUIT CURRENTS INDUCED BETWEEN DFCS GROUND AND AIRCRAFT GROUND, UNDER DE-ENERGIZED AND POWERED UP CONDITIONS.

Fast vs. Slow Lightning Waveform Comparison.- Up to this point in the program, most measurements had been made using both the fast and slow lightning test waveforms. In all cases, the fast waveform induced more voltage than the slow waveform. The duration of voltages induced by the fast waveform was also greater than the duration of those induced by the slow waveform. A typical comparison is shown on Figure 43 for a measurement made at the Sperry interface electronics test receptacle. Accordingly, for most of the remaining tests, it was decided to apply only the fast lightning test waveform.

Gun Bay Cable Current Measurements.- Measurements were also made of the total current induced in each of the cable bundles entering the gun bay. These measurements were made with the cable interfaces intact and the system powered up. A photograph of the gun bay showing the cable bundles and electronics packages is shown in Figure 44. Figure 45 is a sketch traced from this photograph and gives the key to the current measurements that were made. Shown are the measurement oscillogram numbers. Also shown on Figure 45 are the peak-to-peak amplitudes of the induced current measured in each cable. Peak-to-peak values are given since the steady state currents also flowing on the cables precluded easy identification of the appropriate zero trace on the oscillograms. They are shown with double arrows to indicate their oscillatory nature. The designations FAST and SLOW refer to the waveform of the simulated lightning current applied for the particular measurement. All of the current amplitudes shown in Figure 45, however, are for the fast waveform only. It should be noted that the currents measured are the sum of the currents induced in all conductors of the cable. Since each cable contains conductors from different parts of the system, it is not possible to directly associate these measurements with any particular part of the flight control system.

Figures 46, 47 and 48 present the oscillograms of induced currents measured in cables in the gun bay. Shown are currents induced by both the fast and slow simulated lightning current waveforms. As with the induced voltages, the induced currents are of an oscillatory nature. Occasionally these oscillations are superimposed upon longer duration currents similar to those measured on the short circuited FCS ground circuit of Figure 42. This indicates that one or more conductors in the cable are connected to the airframe through relatively low impedances at each end, since a long duration unidirectional current cannot, of course, flow in a conductor that has only a single point reference to airframe ground. High frequency oscillatory currents, however, can easily flow because the conductors have capacitance to the airframe, providing a sufficiently adequate path for high

frequency currents to flow. The type or location of any low impedance terminations to the airframe at remote locations was not determined.

SPERRY INTERFACE ELECTRONICS TEST RECEPTACLE IN GUN BAY
Pin 3 - LEFT HOR. FUP No. 3

INDUCED BY
FAST WAVEFORM

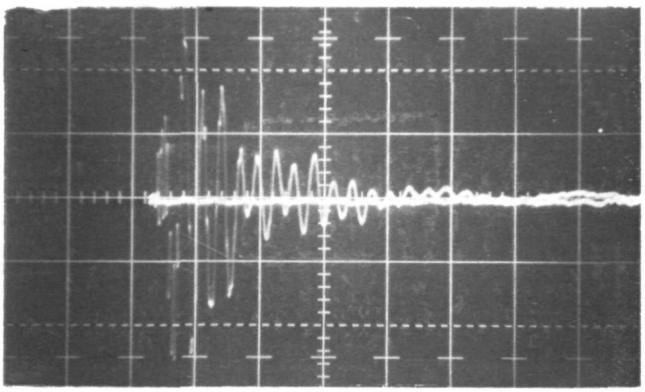

0.2 V/div. No.257 2 μs/div.

INDUCED BY
SLOW WAVEFORM

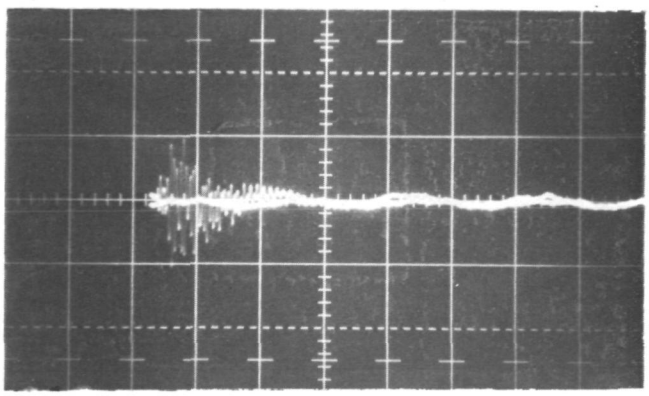

0.2 V/div. No.256 2 μs/div.

FIGURE 43 - COMPARISON BETWEEN VOLTAGES INDUCED BY FAST AND SLOW LIGHTNING STROKE WAVEFORMS.

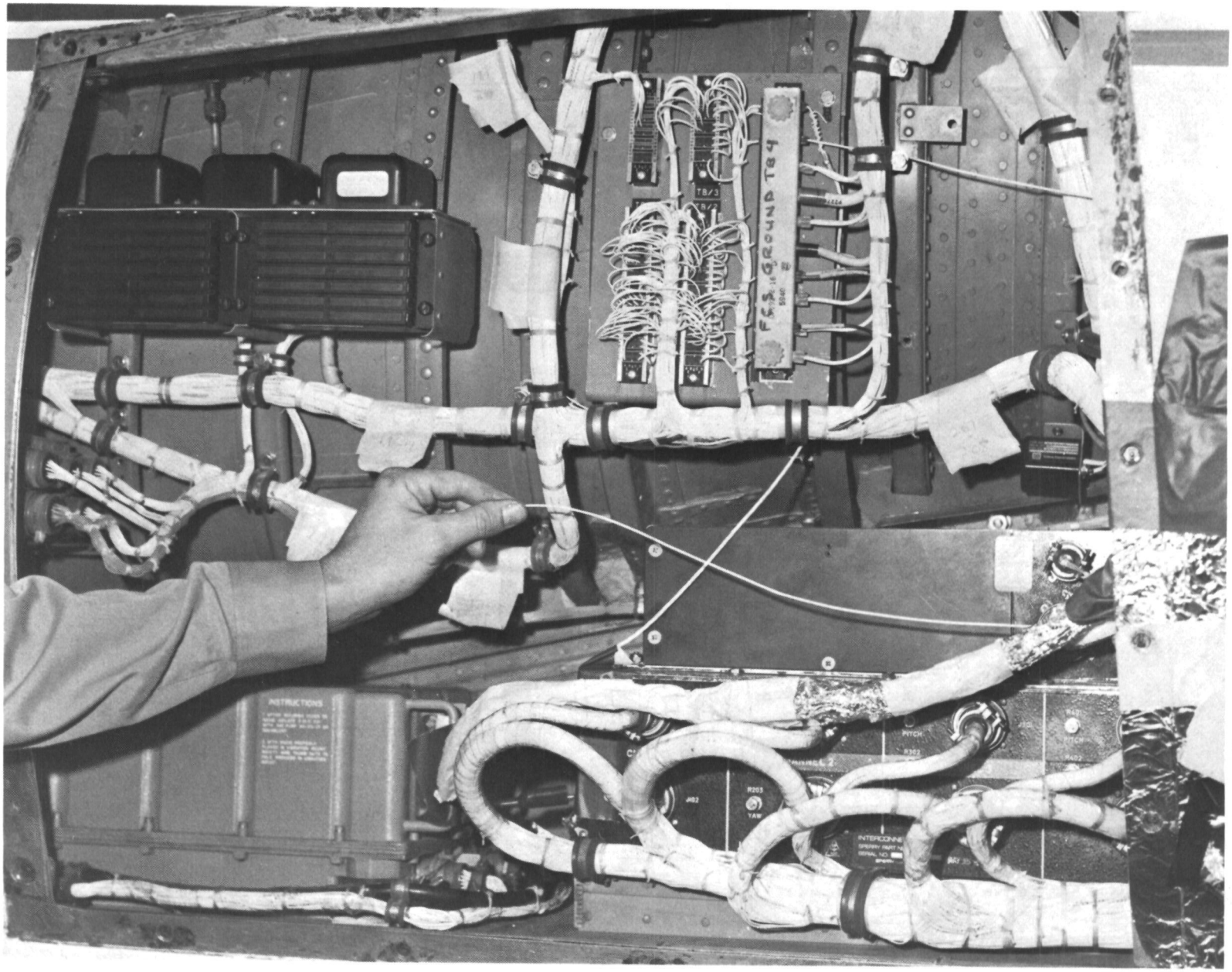

FIGURE 44 - WIRING BUNDLES AND ELECTRONIC PACKAGES IN THE LEFT GUN BAY.

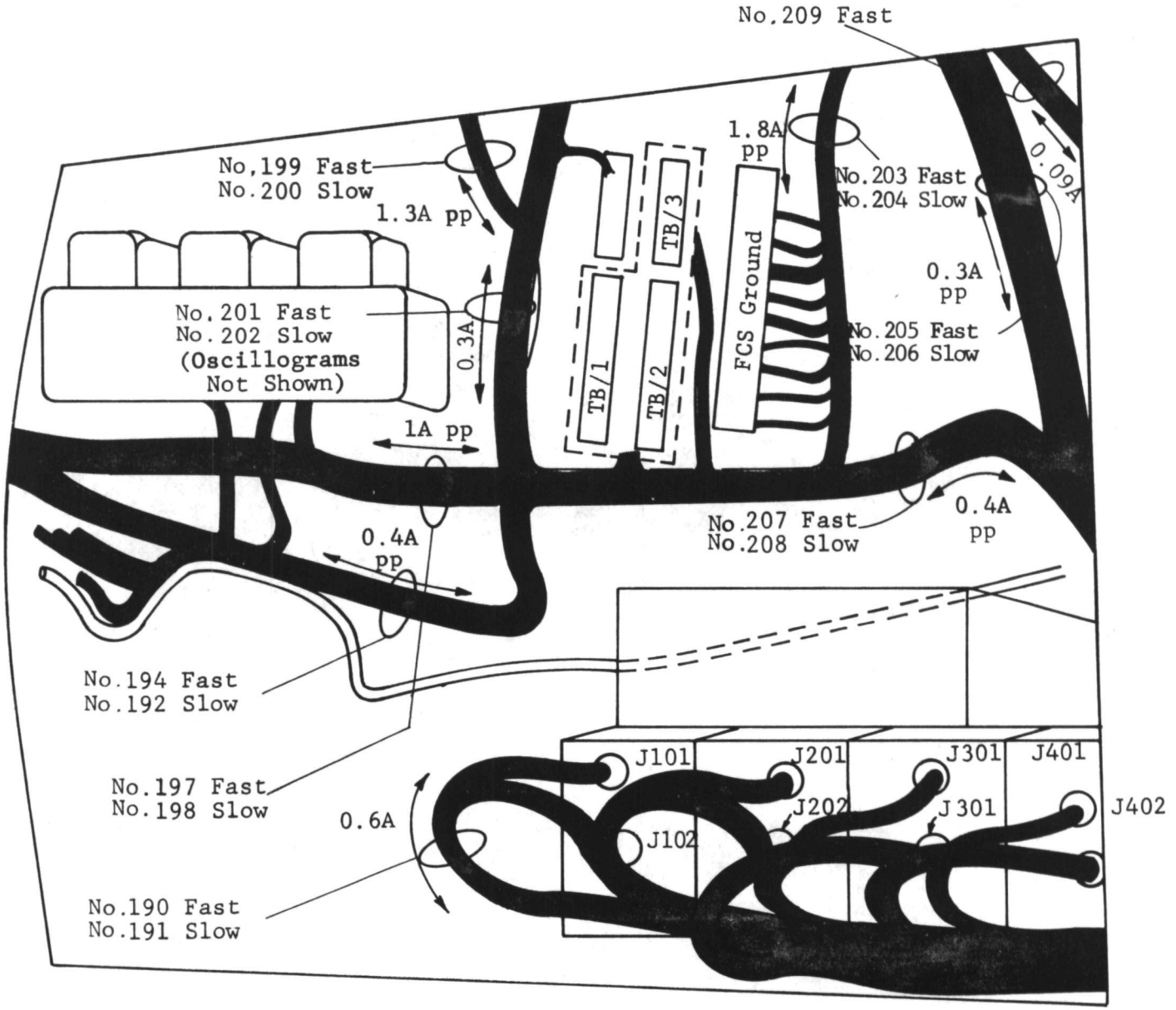

FIGURE 45 - KEY TO MEASUREMENT OF CURRENTS IN LEFT GUN BAY.

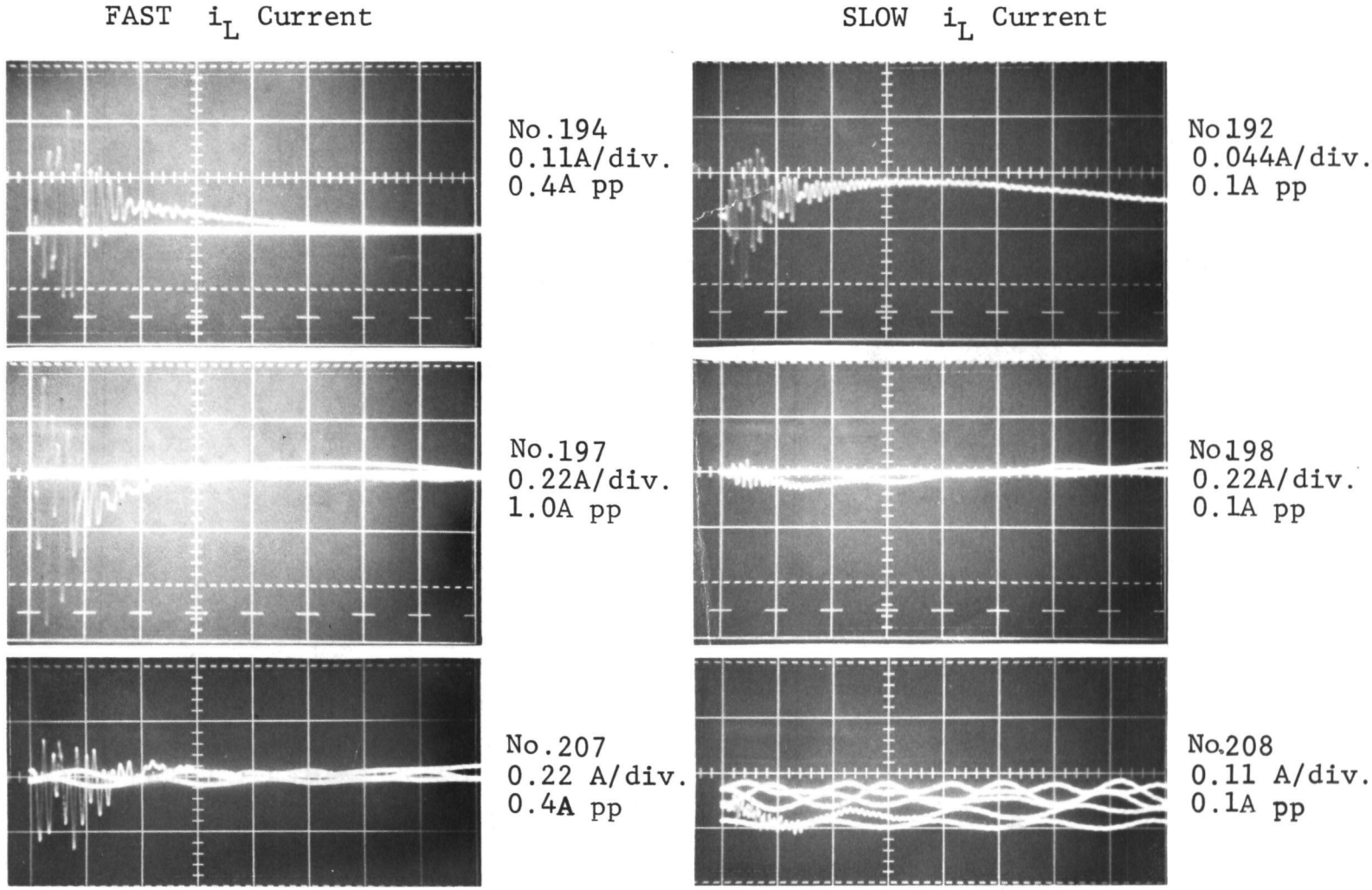

FIGURE 46 - CURRENTS ON CABLE BUNDLES LEADING TOWARD COCKPIT AND LH INSTRUMENT PANEL.

FAST i_L Current

SLOW i_L Current

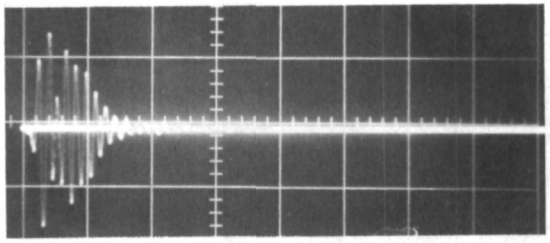

No.199
0.44A/div.
1.3A pp

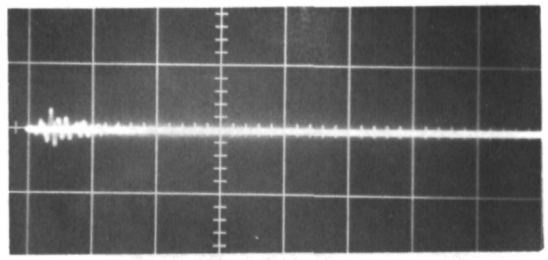

No.200
.22A/div.
0.1A pp

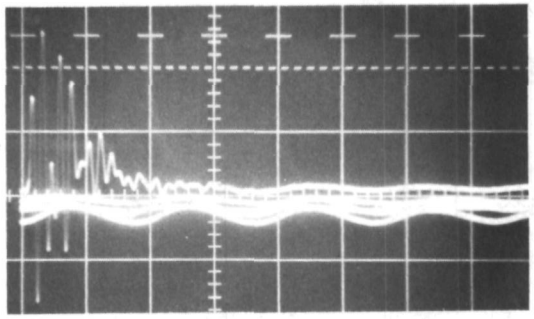

No.203
0.44A/div.
1.8A pp

Not Shown Because
Signal is Obscured
by Background Noise

No. 204

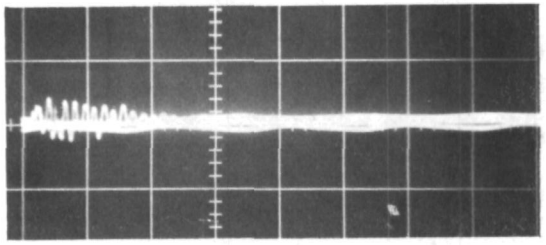

No.205
0.44A/div.
0.3A pp

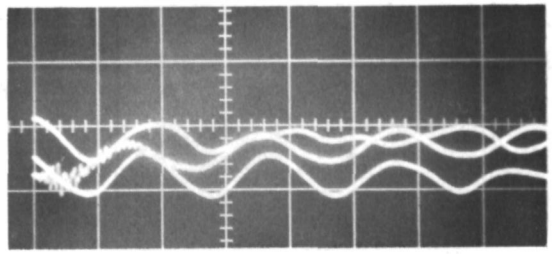

No.206
0.11A/div.
0.06A pp

All 2μs/div.

FIGURE 47 - CURRENTS ON CABLE BUNDLES LEADING TOWARD THE DFCS PALLET.

FAST i_L Current

SLOW i_L Current

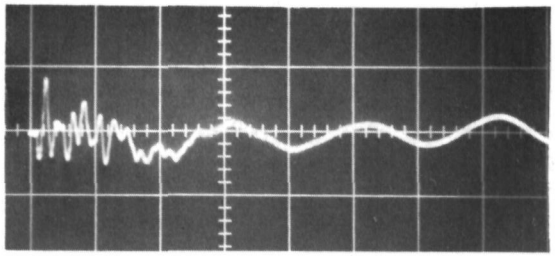

No.201
0.22A/div.
0.3A pp

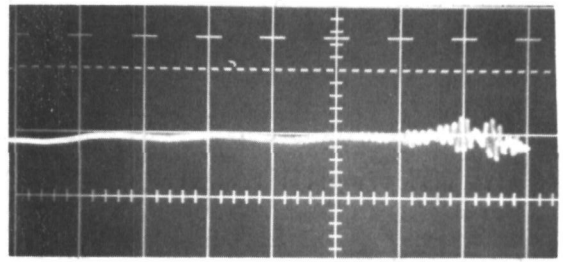

No.202
0.22A/div.
0.05A pp
0.5 MHz Signal is background noise on wire bundle.

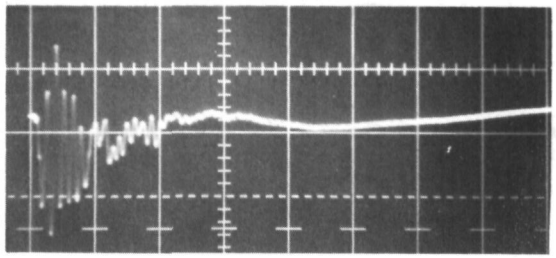

No.190
0.044A/div.
0.1A pp

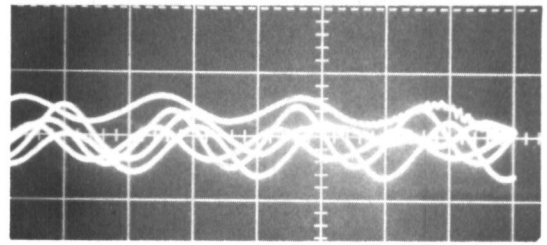

No.191
0.044A/div.
0.03A pp

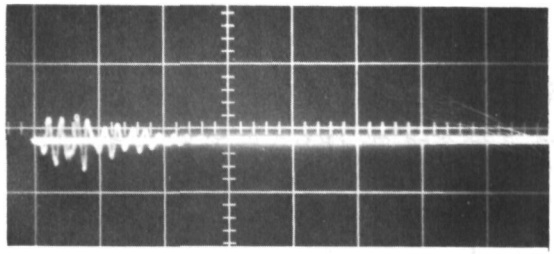

No.209
0.11A/div.
0.1A pp

All 2μs/div.

FIGURE 48 - MISCELLANEOUS CURRENTS ON CABLE BUNDLES IN THE LEFT GUN BAY.

DFCS Pallet Measurements

Of considerable interest are the induced voltages appearing at the wiring interfaces with the primary Digital Flight Control System (DFCS) which includes the Apollo Lunar Guidance Computer (AGC) and Inertial Measurement Unit (IMU). It was possible to utilize break-out boxes to provide access to circuits at several of the DFCS and AGC interfaces without breaking circuit continuity.

Figures 49, 50 and 51 show these measurements. For all of these tests the simulated lightning current entered the nose and exited from the tail of the aircraft. Measurements made at the AGC and Digital-to-Analog Converter packages on the DFCS pallet are described in the following paragraphs.

Apollo Guidance Computer Interface.- Figure 49 shows measurements made at the J25 interface to the AGC on circuits coming from the Mode and Power Control (MPC) panel and Stick, Back-up Control System (BCS) and yaw trim transducers in the cockpit area. These appear as damped oscillations at a fundamental frequency of about 1 megahertz. Most of the voltage subsides after about 6 microseconds has elapsed. Each voltage shown on Figure 49 is a damped oscillation at the same fundamental frequency of about 1 megahertz since all conductors follow the same bundle to the cockpit. The waveforms have slight variations which are probably due to differences in load impedances at each end. Peak induced voltage amplitudes ranged between 0.5 volts and 1.35 volts.

Digital to Analog Converter Interface.- Figure 50 shows voltages induced in the Pitch, Roll and Yaw control sensor circuits coming to the DFCS interface box containing digital-to-analog conversion circuitry. The measurements were made at plug P4 with this plug disconnected at the interface since no break-out box was available. These, therefore, are open circuit voltages and are not necessarily the same as the voltages which might appear at the closed interface, since input impedances would affect the voltages impressed across them. The characteristic frequencies of the open-circuit voltages measured in circuit pairs at pins D-E (osc. 528), G-H (osc. 525), W-X (osc. 523) and Y-Z (osc. 526) have a fundamental frequency of about 1.7 megahertz with lower amplitude oscillations at several higher frequencies superimposed. These are induced in circuits coming from the DFCS stick transducer in the cockpit. The fundamental frequency of voltages measured at pins A-B (osc. 524) and U-V (osc. 527) in circuits coming from the DFCS rudder pedal transducer in the tail area is also 1.7 megahertz but without as much

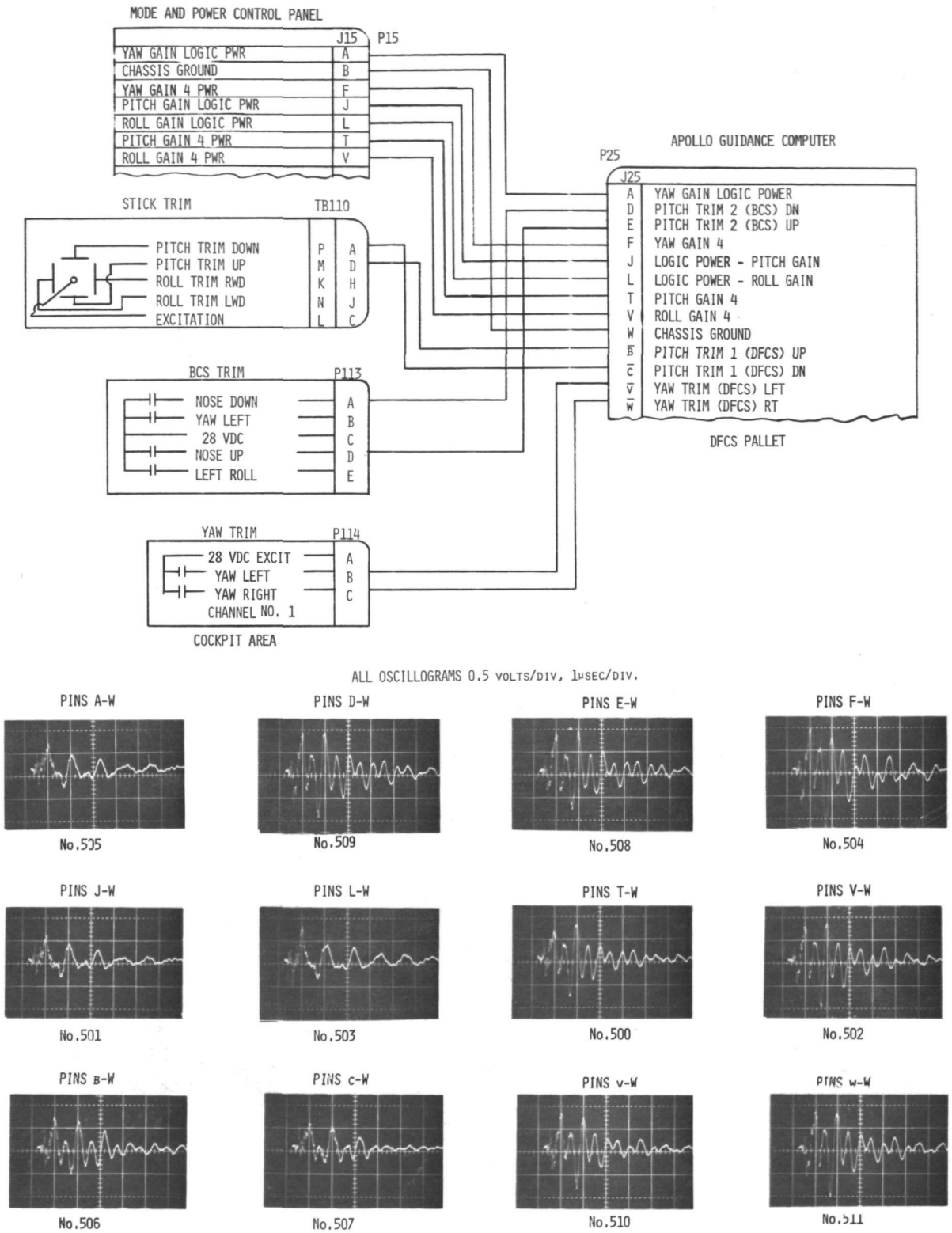

ALL OSCILLOGRAMS 0.5 VOLTS/DIV, 1μSEC/DIV.

PINS A-W

No.505

PINS D-W

No.509

PINS E-W

No.508

PINS F-W

No.504

PINS J-W

No.501

PINS L-W

No.503

PINS T-W

No.500

PINS V-W

No.502

PINS B-W

No.506

PINS C-W

No.507

PINS V-W

No.510

PINS W-W

No.511

FIGURE 49- INDUCED VOLTAGES ON J25 IN DFCS PALLET UTILIZING J25 BREAK-OUT BOX (LIGHTNING CURRENT PATH, NOSE TO TAIL).

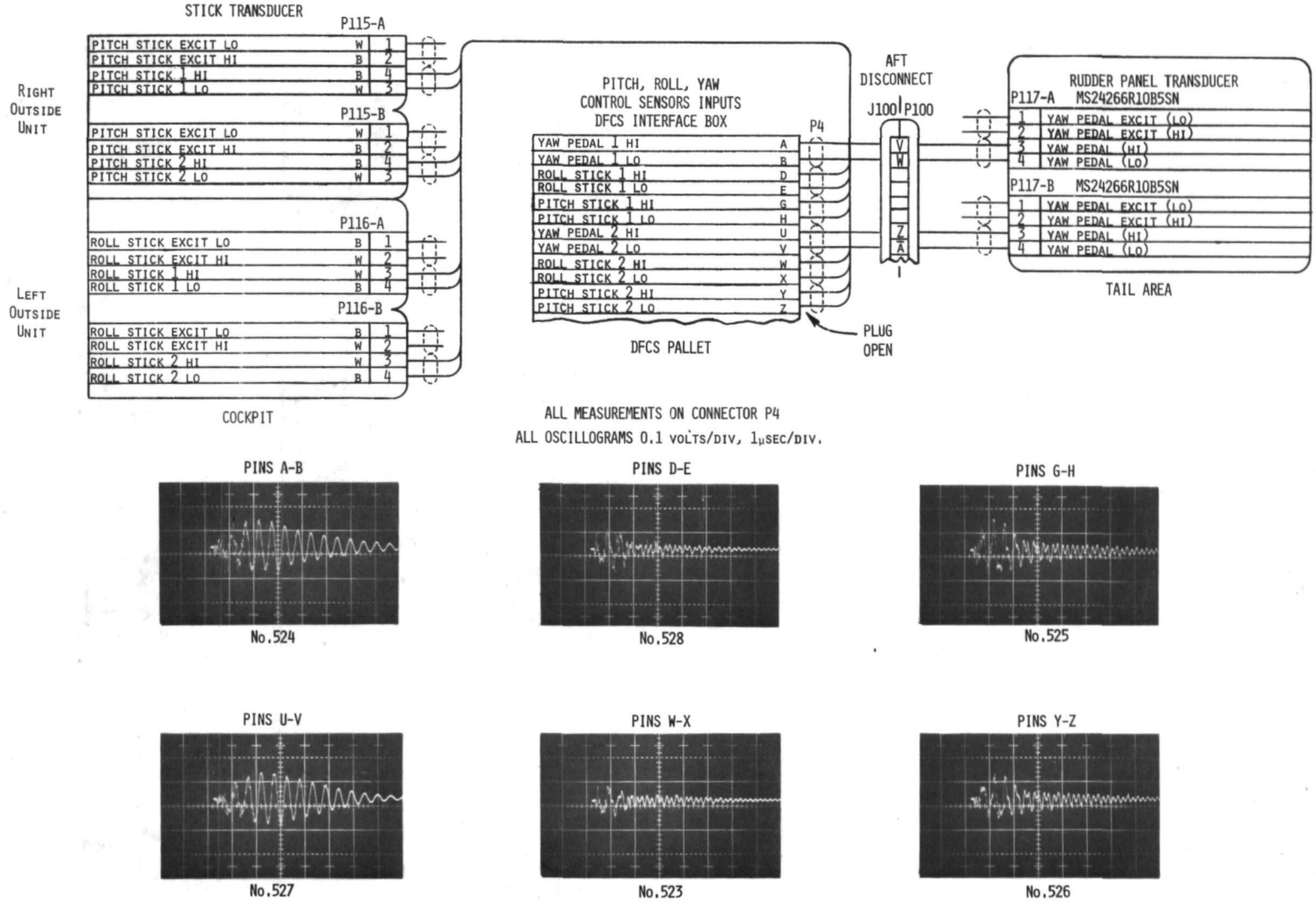

FIGURE 50 - OPEN CIRCUIT VOLTAGES ON P4, PITCH, ROLL, YAW CONTROL SENSORS INPUTS IN DFCS PALLET AREA (LIGHTNING CURRENT PATH, NOSE TO TAIL).

of the superimposed higher frequency component. Neither fundamental frequency is the same as that measured at the closed J25 interface in circuits also coming from the cockpit area, shown on Figure 50.

The peak amplitudes of voltages measured at this interface ranged from 0.06 volts to 0.13 volts.

Figure 51 shows the induced voltages measured at a break-out box at the J2 interface with the digital-to-analog converter. Analog control signals pass through this interface to the Primary Control Electronics in the gun bay, and from thence to the secondary actuators. These measurements are of the same predominant frequency as those measured at the AGC interface of Figure 49 although the polarity is reversed. Their peak amplitudes ranged between 0.35 and 0.7 volts.

Actuator Interface Measurements

To determine the magnitude of typical induced voltages appearing at the Secondary Actuators located in the wings and tail area, measurements were made at an interface with a Roll Actuator in the wing and the Yaw Actuator in the tail area. Break-out boxes were utilized to maintain circuit continuity and permit powered-up operation of the FCS system while the measurements were being made.

Roll Actuators.- Measurements were made at the left wing roll actuator since the left and right wing actuator circuits are identical. Nose-to-tail and nose-to-left wing tip lightning current conditions were applied in most cases, and measurements were made on the primary (DFCS) channel and two of the backup (BCS) channels. Figures 52 and 53 show the measurements made in the Active Valve and Pressure Transducer Excitation circuits in the three channels under both lightning current flow path conditions. Each of these is a two-wire circuit, and measurements were made between wires and also between each wire and FCS ground. Each of these measurements is important since the voltage between any wire and FCS ground is as important, from a component damage point of view, as the voltage between a functional pair. Such a combination of measurements also afforded an additional opportunity to check measurement validity, since the measured line-to-line voltage should be equal to the difference between voltages at either line and the FCS ground. This relationship is most apparent in the Pressure Transducer Excitation circuit measurements in the backup channel at J205, shown in

DFCS DIGITAL CONTROL
DIGITAL-TO-ANALOG CONVERTER
DFCS INTERFACE BOX

	J2	P2	P12		PRIMARY CONTROL ELECTRONICS #1
PITCH SERVO 1 HI	A		18	PITCH ACTIVE SERVO CMMD INPUT	(HI)
PITCH SERVO 1 LO	B		19	" " " "	(LO)
ROLL SERVO 1 HI	D		43	ROLL ACTIVE SERVO CMMD INPUT	(HI)
ROLL SERVO 1 LO	E		44	" " " "	(LO)
YAW SERVO 2 HI	G		67	YAW MONITOR SERVO CMMD INPUT	(HI)
YAW SERVO 2 LO	H		68	" " " "	(LO)
YAW SERVO 1 HI	X		65	YAW ACTIVE SERVO CMMD INPUT	(HI)
YAW SERVO 1 LO	Y		66	" " " "	(LO)
ROLL SERVO 2 HI	Z		45	ROLL MONITOR SERVO CMMD INPUT	(HI)
ROLL SERVO 2 LO	$\bar{A}$		46	" " " "	(LO)
PITCH SERVO 2 HI	$\bar{B}$		20	PITCH MONITOR SERVO CMMD INPUT	(HI)
PITCH SERVO 2 LO	$\bar{C}$		21	" " " "	(LO)

DFCS PALLET

LEFT GUN BAY

ALL MEASUREMENTS: 0.5 VOLTS/DIV, 1 μSEC/DIV.

PINS A-B

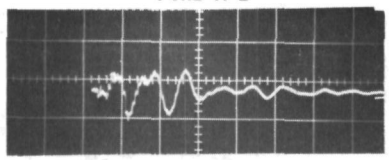

No. 514

PINS D-E

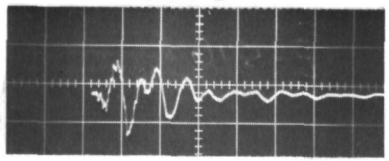

No. 516

PINS G-H

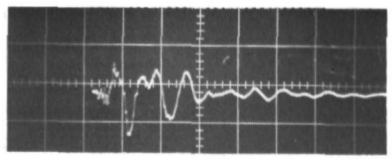

No. 518

PINS X-Y

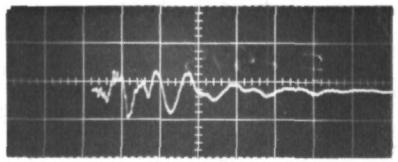

No. 515

PINS Z-A

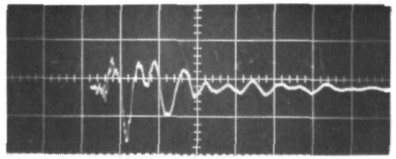

No. 517

PINS B-C

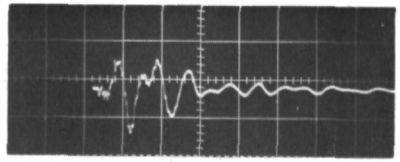

No. 519

FIGURE 51 - INDUCED VOLTAGES ON J2, DFCS DIGITAL CONTROL OUTPUT CIRCUITS, ON DFCS PALLET AT J2 BREAK-OUT BOX (LIGHTNING CURRENT PATH, NOSE TO TAIL).

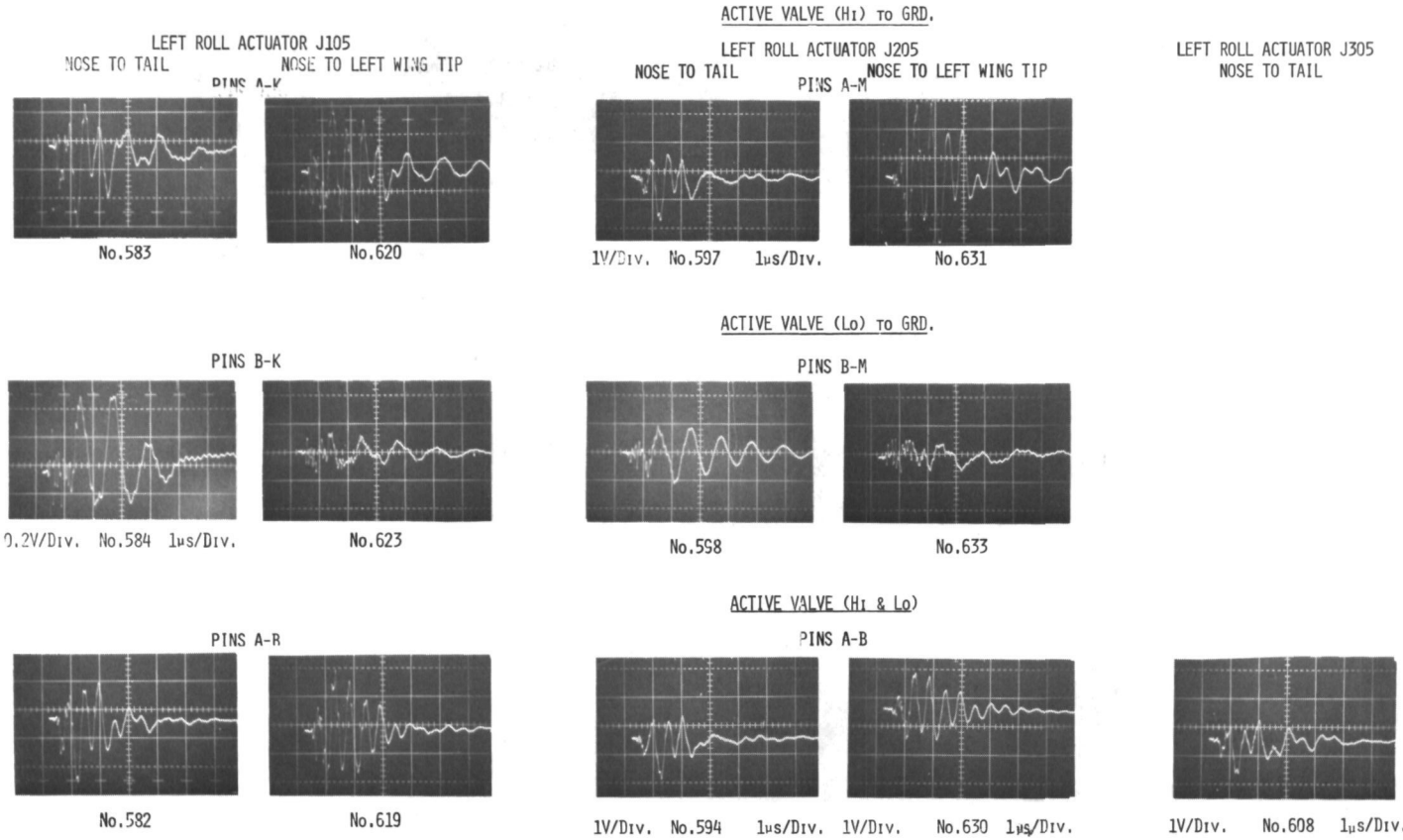

FIGURE 52- INDUCED VOLTAGES ON J105, J205, AND J305, LEFT ROLL ACTUATORS IN WING AREA AT J105, J205, AND J305 BREAK-OUT BOXES, ACTIVE VALVE CIRCUIT (LIGHTNING CURRENT PATH, NOSE TO TAIL AND NOSE TO LEFT WING TIP).

LEFT ROLL ACTUATOR J105

NOSE TO TAIL

NOSE TO LEFT WING TIP

LEFT ROLL ACTUATOR J205

NOSE TO TAIL

NOSE TO LEFT WING TIP

PRESS TRANS EXCIT (Hi) TO GRD.

PINS G-M

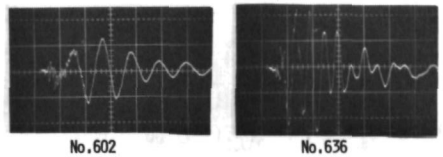

No.602

No.636

PRESS TRANS EXCIT (Lo) TO GRD.

PINS H-M

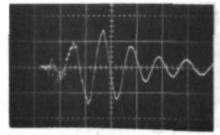

No.603

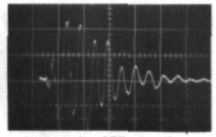

No.637

PRESS TRANS EXCIT (Hi & Lo)

PINS G-H

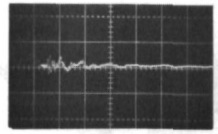

No.601

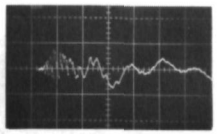

No.635

LEFT ACTUATOR J305

NOSE TO TAIL

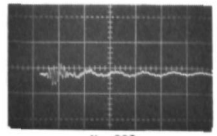

No.609

MONITOR VALVE (Hi) TO GRD

PINS C-K

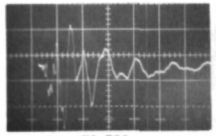

No.586

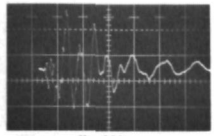

No.624

MONITOR VALVE (Hi & Lo)

PINS C-D

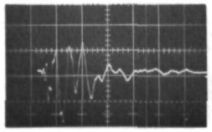

No.585

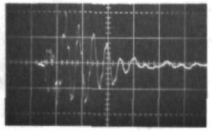

No.621

ALL OSCILLOGRAMS
0.5 V/Div, 1μs/Div,
UNLESS OTHERWISE NOTED

FIGURE 53 - INDUCED VOLTAGES ON J105, J205, J305, LEFT ROLL ACTUATORS IN WING AREA AT J105, J205, J305 BREAK-OUT BOXES, PRESS TRANS EXCIT AND MONITOR VALVE CIRCUITS. (LIGHTNING CURRENT PATH, NOSE TO TAIL AND NOSE TO LEFT WING TIP).

Figure 53, where, for example, the Hi to ground (oscillogram No. 602) minus the Lo to ground (oscillogram No. 603) equals the Hi-to-Lo measurement (oscillogram No. 601).

In Figure 52, the voltage at the Active Valve circuit Hi to ground (oscillogram No. 582) is much greater than that measured between the Lo terminal and ground (oscillogram No. 583 - note the more sensitive scale) so that a more substantial difference voltage results (oscillogram No. 582) than was the case for the Pressure Transducer Excitation Circuit (oscillogram No. 601).

Interesting comparisons also exist between measurements made on similar circuits in different channels. Figure 52 also shows these comparisons for the Active Valve circuits. Comparisons for the Pressure Transducer excitation circuits are shown on Figure 53. Close similarity in amplitude and waveshape is evident between voltages measured in the primary and two backup circuits for the Active Valve Hi-to-Lo measurements (Figure 52, oscillogram Nos. 582, 594 and 608) and also for the Pressure Transducer Excitation circuit Hi to Lo in the two backup circuits (Figure 53, oscillogram Nos. 601 and 609). The primary circuit was not measured.

Measurements in other Roll Actuator circuits are shown on Figures 53 and 54. Figure 54 shows the induced voltages at the LVDT SEC circuits in the Primary and a backup channel (oscillogram Nos. 588 and 600). The voltages are very similar in amplitude as well as waveform.

The induced voltage in the Pressure Transducer Output Circuit (Figure 54, oscillogram 605) is of particular interest because these are among the few shielded conductors in the cable. The voltage induced in this circuit was about one-twentieth of the amplitude of voltages induced in most of the other circuits. These conductors are individually shielded. The shields are not intentionally grounded to the airframe at the actuator but ohmeter checks with the other end of the cable unplugged indicate that the shields do contact the airframe at least once somewhere along the way back to the actuators.

Induced voltages resulting from both lightning current flow paths (nose-to-tail and nose-to-left-wing-tip) are presented side-by-side on Figures 52, 53 and 54. In nearly all cases the nose-to-left-wing-tip flow path caused the highest induced voltages. This is to be expected since passage of lightning current through the wings should cause a greater concentration of magnetic

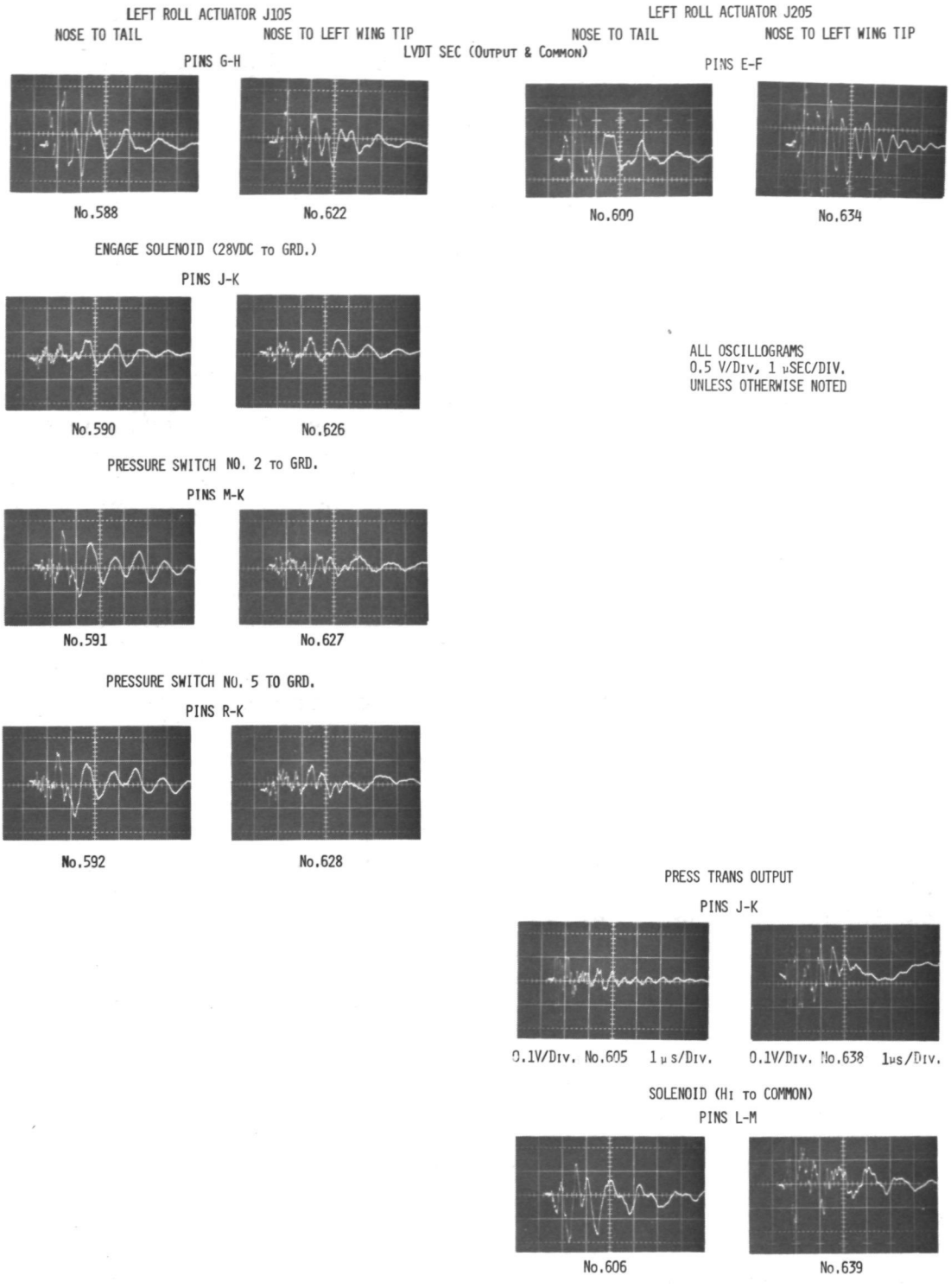

FIGURE 54 - INDUCED VOLTAGES ON J105 AND J205, LEFT ROLL ACTUATORS IN WING AREA AT J105 AND J205 BREAK-OUT BOXES, VARIOUS CIRCUITS (LIGHTNING CURRENT PATH, NOSE TO TAIL AND NOSE TO LEFT WING TIP).

flux in the vicinity of the Roll Actuator circuits located there. The predominant frequency of most of the induced voltages is the same for either flow path; however, the voltages induced by the nose-to-left-wing-tip strike indicate an additional component of somewhat higher frequency during the first 3 or 4 microseconds. This may result from increased aperture flux coupling, especially in the wing root area where lightning current is concentrated as it enters the wing from the fuselage. The same relationships discussed previously between line-to-line and line-to-ground measurements are evident.

The predominant frequency of voltages in the Roll Actuator circuits is about 0.9 megahertz, with the exception of the shielded circuit (Fig. 54, oscillogram No. 605) which has a predominant frequency of about 1.7 megahertz. All measurements have a lower amplitude 8 megahertz component superimposed during the first 2 microseconds or less. The fundamental frequency of unshielded circuit voltages is lower than the corresponding frequency of voltages induced in other circuits, especially those which travel shorter distances in the airframe. Peak amplitudes of voltages induced by the 300 ampere simulated lightning current ranged from 0.09 volts (in a shielded circuit) to 1.35 volts (in an unshielded circuit).

Yaw Actuator.- The Yaw Secondary Actuator is located in the vertical fin. Since lightning strokes often hit the vertical fin cap, a nose-to-vertical-fin lightning current flow path was applied as well as the nose-to-tail condition in which lightning current exited from the engine tail pipe. Measurements were made in primary circuits at the J107 interface and one of the backup channels at the J307 interface. Oscillograms are shown on Figures 55 and 56, respectively.

A few of the J307 interface measurements were also repeated with the very fast simulated lightning current waveform shown on Figure 16 applied for comparison of resulting induced voltages with those induced by the fast waveform. The main reason for this comparison was to determine if the predominant frequency of induced voltage is dependent on the lightning waveform or the actuator circuit characteristics. The very fast waveform has a maximum rate of current rise, di_L/dt, about two and one-half times that of the fast waveform.

The voltages induced by the very fast waveform are shown in Figure 56 (oscillogram Nos. 702, 699 and 700) next to those induced by the slow waveform in the same circuits. It is apparent that the predominant frequency is the same for voltages

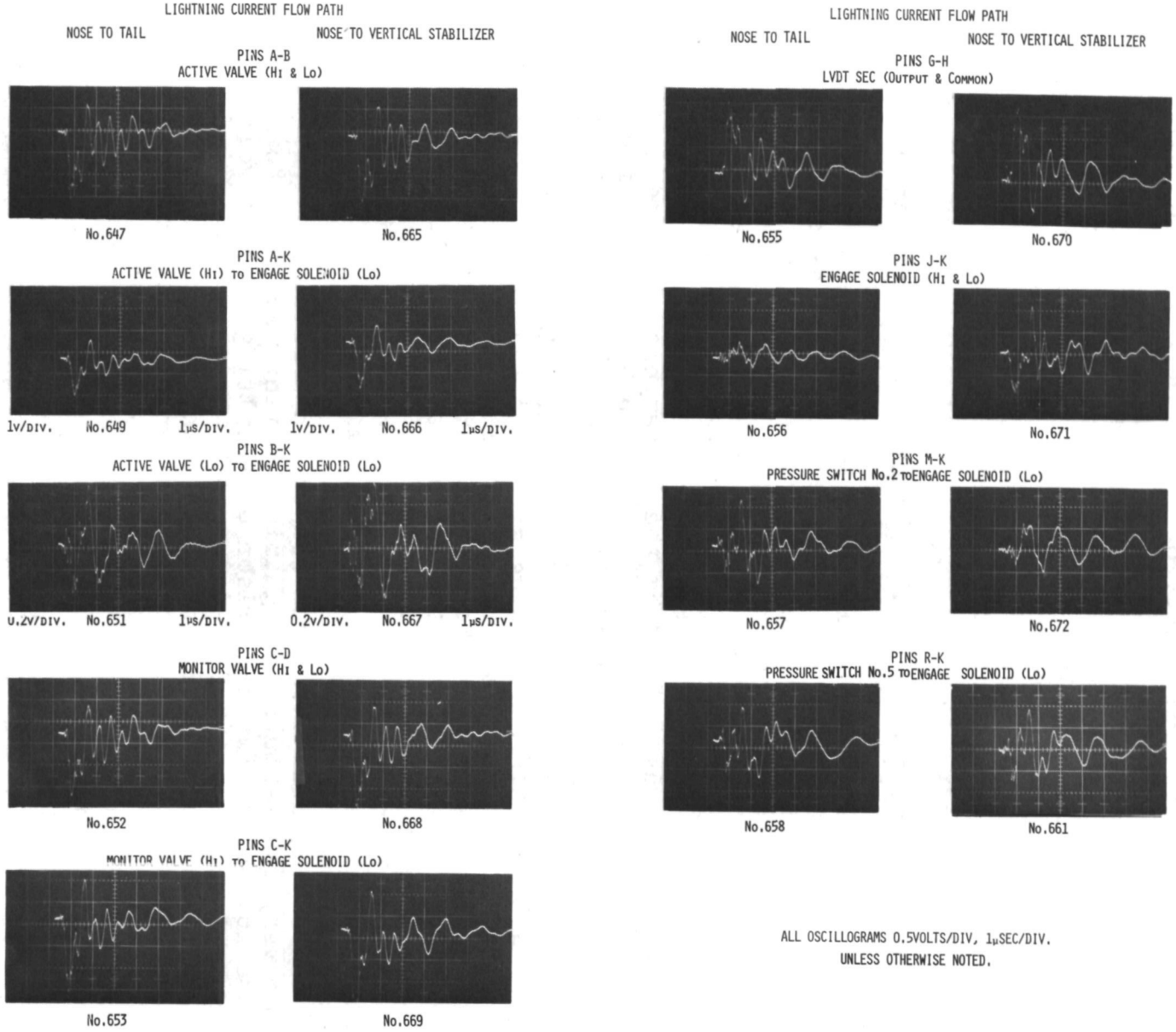

FIGURE 55 - INDUCED VOLTAGES ON J107, YAW ACTUATOR IN TAIL UTILIZING J107 BREAK-OUT BOX.

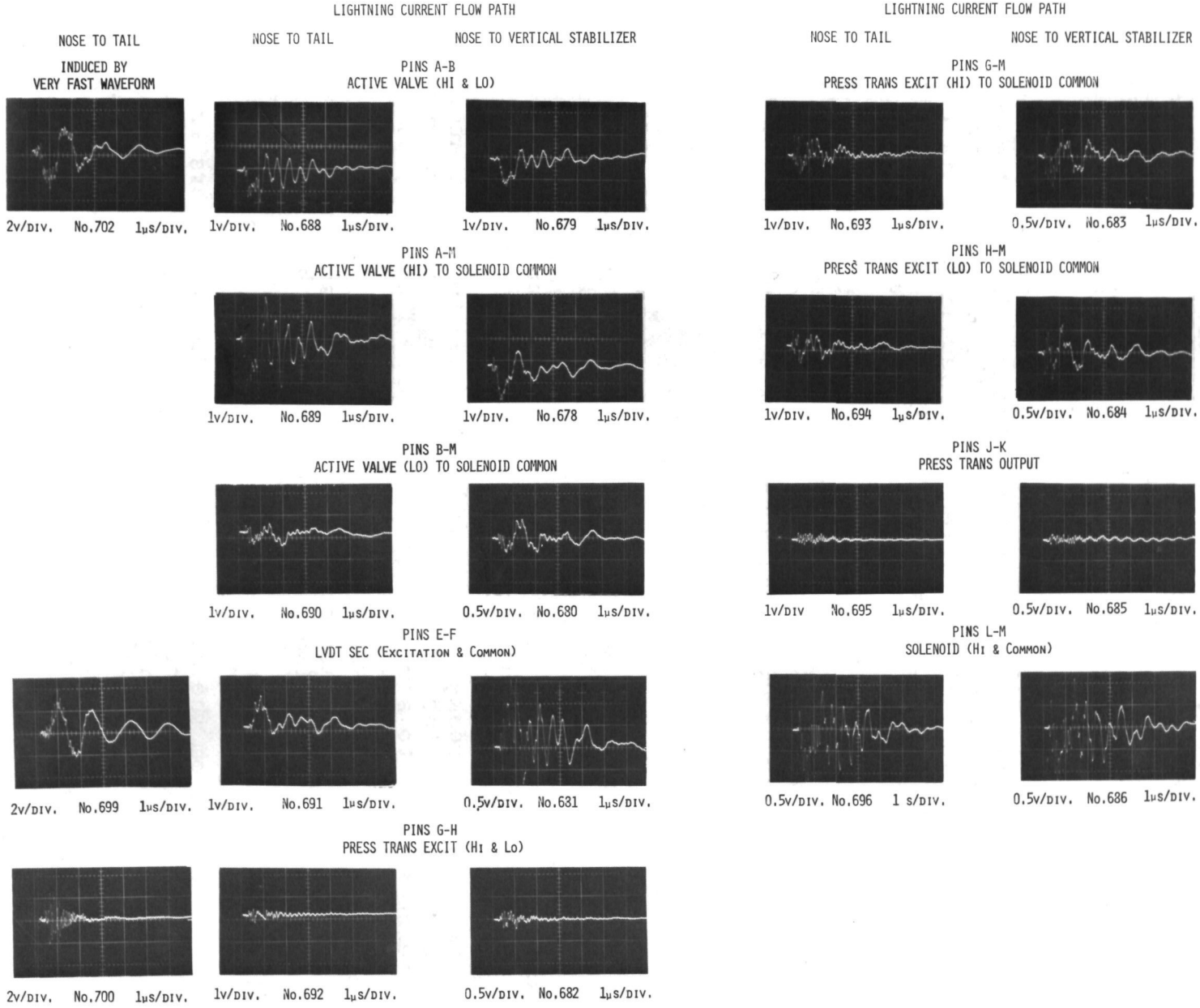

FIGURE 56 - INDUCED VOLTAGES ON J307, YAW ACTUATOR IN TAIL UTILIZING J307 BREAK-OUT BOX .

induced by each lightning waveform, although the amplitudes of voltages induced by the very fast lightning waveform are a little over twice as great as those induced by the fast waveform. Thus, the predominant frequency of the induced voltage is evidently a function of the actuator circuit characteristics, while the amplitude is nearly proportional to lightning current rate of rise.

The predominant frequency of all voltages induced in the Yaw Actuator circuits is about 0.7 megahertz. This is lower than the frequency of voltages induced in the Roll Actuator circuits in the wing. The difference may be due to the fact that the Yaw Actuator circuits are longer, requiring a longer period of oscillation and hence a lower ringing frequency.

Peak amplitudes of voltages induced by the fast lightning waveform in the Yaw Actuator circuits ranged from 0.12 volts to 2.8 volts. Those induced by the very fast waveform in a few of the J307 interface circuits ranged from 2.1 volts to 3.9 volts.

Cockpit Measurements

Measurements were made of induced voltages appearing at the J14 interface to the Mode and Power Control Panel in the cockpit. These measurements were made with a break-out box to maintain circuit continuity and permit powered-up operation while measurements were being made. Since the cockpit is not covered by metallic skin, the extra cable length provided by insertion of the break-out box may be expected to contribute excessive error to the aircraft circuit voltage by virtue of its being exposed to strong magnetic fields. Therefore, the box and its extension cables were wrapped tightly with aluminum foil which was grounded to the airframe. The instrument cable entered this package to obtain access to the desired measurement points on the break-out box. The measurements made at this interface are shown on Figure 57. Lightning current flow path was nose-to-tail,and only the fast lightning waveform was applied.

The cable from the J14 interface picks up conductors from other interfaces (Yaw trim, BCS trim, Stick, etc.) and runs to the DFCS pallet or gun bay. Predominant frequency of all voltages measured is 0.83 megahertz, although there are lower amplitude components of several different higher frequencies superimposed. Peak voltages ranged from 0.3 volts to 1.3 volts.

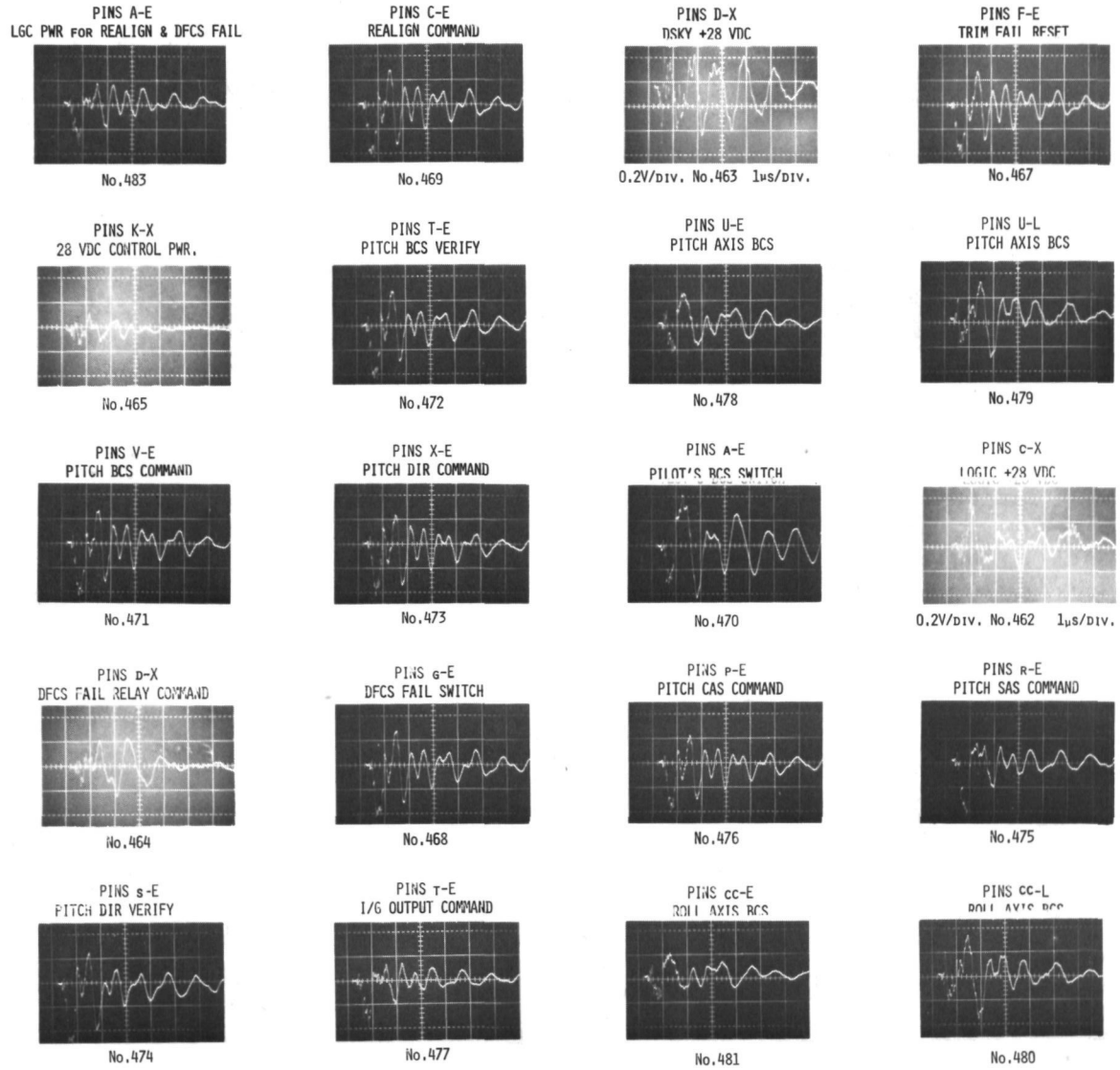

FIGURE 57- INDUCED VOLTAGES ON J14, MODE & POWER CONTROL PANEL, LOCATED IN THE COCKPIT UTILIZING J14 BREAK-OUT BOX (LIGHTNING CURRENT PATH, NOSE TO TAIL).

ALL OSCILLOGRAMS 0.5V/DIV, 1μSEC/DIV. UNLESS OTHERWISE NOTED.

TABLE II - Induced Voltages and Corresponding Analytical Expressions.

Osc. No.	FCS Sub-System	Circuit	Measurement Location	Interface Plug Terminals	System Status	i_L Path	Type of Meas.	e_1 Initial peak (volts)	Analytical Voltage Expression Parameters: Maximum Voltage Coefficient, E @ 300A	@ 30 kA	@ 200 kA	Decay Coefficient α	Radial Frequency β (MHz)
82	FCS DC Power System	Bus No.1(Green)	Gun Bay	Bus No.1 to FCS Grd	OFF	Fast Wave N-LWT	e_{oc}	1.7	2.05	205	1365	0.75	15.7
83	"	" "	"	" "	"	Slow Wave N-LWT	"	0.83	0.9	90	599	0.32	37.7
26	"	" "	"	" "	"	Fast Wave N-T	"	1.7	2.09	209	1392	0.41	15.7
45	"	" "	"	" "	"	Slow Wave N-T	"	0.7	0.73	73	486	0.34	37.7
81	"	Bus No.2(Blue)	"	Bus No.2 to FCS Grd	"	Fast Wave N-LWT	"	1.7	2.04	204	1359	1.39	12.6
80	"	" "	"	" "	"	Slow Wave N-LWT	"	0.79	0.89	89	593	0.46	37.7
23	"	" "	"	" "	"	Fast Wave N-T	"	1.4	1.5	150	999	0.67	12.6
86	"	Bus No.3(Yellow)	"	Bus No.3 to FCS Grd	"	Fast Wave N-LWT	"	1.45	1.8	180	1199	2.2	12.6
87	"	" "	"	" "	"	Slow Wave N-LWT	"	0.8	0.9	90	599	1.6	37.7
29	"	" "	"	" "	"	Fast Wave N-T	"	1.5	1.55	155	1032	0.36	12.6
48	"	" "	"	" "	"	Slow Wave N-T	"	0.82	0.99	99	659	0.62	12.6
85	"	Bus No.4(Red)	"	Bus No.4 to FCS Grd	"	Fast Wave N-LWT	"	1.3	1.69	169	1126	1.32	12.6
84	"	" "	"	" "	"	Slow Wave N-LWT	"	0.6	0.65	65	433	0.58	37.7
28	"	" "	"	" "	"	Fast Wave N-T	"	1.45	1.8	180	1199	2.4	12.6
47	"	" "	"	" "	"	Slow Wave N-T	"	0.8	0.9	90	599	0.9	12.6

TABLE II - Induced Voltages and Corresponding Analytical Expressions-(Continued)

Osc. No.	FCS Sub-System	Circuit	Measurement Location	Interface Plug Terminals	System Status	i_L Path	Type of Meas.	e_1 Initial peak (volts)	Analytical Voltage Expression Parameters: Maximum Voltage Coefficient, E @ 300A	@ 30 kA	@ 200 kA	Decay Coefficient α	Radial Frequency β (MHz)
121	FCS DC Power System	Bus No.1(Green)	Gun Bay	Bus No.1 to FCS Grd	ON	Fast Wave N-LWT	e	0.45	0.53	53	353	0.31	9.8
130	"	" "	"	" "	"	Slow Wave N-LWT	"	0.22	0.25	25	167	0.75	37.7
142	"	" "	"	" "	"	Fast Wave N-T	"	0.30	0.33	33	220	0.41	9.8
135	"	" "	"	" "	"	Slow Wave N-T	"	0.20	0.23	23	153	0.85	37.7
122	"	Bus No.2(Blue)	"	Bus No.2 to FCS Grd	"	Fast Wave N-LWT	"	0.5	0.53	53	353	0.28	9.8
128	"	" "	"	" "	"	Slow Wave N-LWT	"	0.16	0.18	18	120	0.78	37.7
141	"	" "	"	" "	"	Fast Wave N-T	"	0.46	0.55	55	367	0.92	9.8
136	"	" "	"	" "	"	Slow Wave N-T	"	0.20	0.23	23	153	1.28	37.7
123	"	Bus No.3(Yellow)	"	Bus No.3 to FCS GRD	"	Fast Wave N-LWT	"	0.4	0.43	43	287	0.36	9.8
131	"	" "	"	" "	"	Slow Wave N-LWT	"	0.12	0.13	13	87	0.61	37.7
140	"	" "	"	" "	"	Fast Wave N-T	"	0.28	0.31	31	207	0.55	9.8
137	"	" "	"	" "	"	Slow Wave N-T	"	0.14	0.16	16	107	0.93	37.7
124	"	Bus No.4(Red)	"	Bus No.4 to FCS GRD	"	Fast Wave N-LWT	"	0.55	0.64	64	427	0.76	9.8
132	"	" "	"	" "	"	Slow Wave N-LWT	"	0.20	0.21	21	140	0.56	37.7
139	"	" "	"	" "	"	Fast Wave N-T	"	0.38	0.42	42	280	0.24	9.8

TABLE II - Induced Voltages and Corresponding Analytical Expressions-(Continued)

Osc. No.	FCS Sub-System	Circuit	Measurement Location	Interface Plug	Interface Terminals	System Status	i L Path	Type of Meas.	e_1 Initial peak (volts)	Analytical Voltage Expression Parameters: Maximum Voltage Coefficient, E @ 300A	@ 30 kA	@ 200 kA	Decay Coefficient α	Radial Frequency β (MHz)
138	FCS DC Power System	Bus No.4(Red)	Gun Bay	Bus No.4	to FCS Grd	ON	Slow Wave N-T	e	0.20	0.23	23	153	0.73	37.7
253	Sperry Electronics Test Receptacle	Left Hor.FUP No.2	Gun Bay	Test Recept.	Pin 1-TB4 COM.	SAS	Fast Wave N-T	"	0.56	0.65	61	406	0.28	11.42
254	"	Right Hor.FUP No.2	"	"	2- "	"	"	"	0.56	0.65	65	433	0.49	11.42
257	"	Left Hor.FUP No.3	"	"	3- "	"	"	"	0.64	0.74	74	493	0.48	
256	"	" "	"	"	" "	"	Slow Wave N-T	"	0.2	0.24	24	160	1.7	
259	"	" "	"	"	" "	"	Fast Wave N-T	"	0.7	0.78	78	519	0.35	11.42
260	"	Right Hor.FUPNo.3	"	"	4- "	"	"	"	0.64	0.76	76	506	0.58	11.42
264	"	Right Hor.FUP No.1	"	"	8- "	"	"	"	0.58	0.66	66	440	0.45	11.42
267	"	L.Aileron FUP No.2	"	"	9- "	"	"	"	0.28	0.3	30	200	0.28	6.28
273	"	R.Aileron FUP No.2	"	"	10- "	"	"	"	0.32	0.35	35	233	0.31	6.28
335	"	Pitch Command Output No.2	"	"	21- "	"	N-LWT	"	0.4	0.45	45	300	0.36	11.42
276	"	Pitch Primary Command,Active	"	"	27- "	"	N-T	"	0.26	0.28	28	186	0.13	6.28
278	"	Pitch Primary Command,Monitor	"	"	28- "	"	"	"	0.28	0.32	32	213	0.28	6.28
316	"	Roll Primary Command,Active	"	"	35- "	"	N-LWT	"	0.32	0.34	34	226	0.10	11.42
315	"	Roll Primary Command,Monitor	"	"	36- "	"	"	"	0.32	0.34	34	226	0.24	11.42
342	"	Rudder Primary Command,Active	"	"	43- "	"	"	"	0.44	0.46	46	306	0.12	9.42

TABLE II - Induced Voltages and Corresponding Analytical Expressions-(Continued)

Osc. No.	FCS Sub-System	Circuit	Measurement Location	Interface Plug	Interface Terminals	System Status	i_L Path	Type of Meas.	e_1 Initial peak (volts)	Analytical Voltage Expression Parameters: Maximum Voltage Coefficient, E @ 300A	@ 30 kA	@ 200 kA	Decay Coefficient α	Radial Frequency β (MHz)
344	Sperry Electronics Test Receptacle	Rudder Primary Command, Monitor	Gun Bay	Test Rcpt.	Pin 44-TB4 Common	SAS	Fast Wave N-LWT	e	0.32	0.33	33	220	0.06	9.42
345	"	L.Pitch Servo Ampl.Test Input No.2	"	"	45- "	"	"	"	0.4	0.44	44	293	0.3	11.42
296	"	L.Pitch Servo Ampl.Test Input No.4	"	"	47-	"	"	"	0.44	0.48	48	320	0.16	11.42
289	"	Wing Down Switch	"	"	60-	"	"	"	0.48	0.5	50	333	0.18	11.42
284	"	PC No.1 Switch	"	"	61-	"	"	"	0.48	0.55	55	366	0.45	11.42
293	"	Weight-on-Wheels Switch	"	"	62- "	"	"	"	0.36	0.38	38	253	0.15	11.42
319	"	Wing Pos.Pot. Test Point	"	"	87- "	"	"	"	0.44	0.49	49	326	0.38	11.42
249	"	28 VDC Bus No.1 Input	"	"	88- "	"	N-T	"	0.38	0.47	47	313	0.72	11.42
326	"	28 VDC Bus No.2 Input	"	"	89- "	"	N-LWT	"	0.3	0.33	33	220	0.34	11.42
332	"	28 VDC Bus No.3 Input	"	"	90- "	"	"	"	0.48	0.52	52	346	0.24	11.42
334	"	28 VDC Bus No.4 Input	"	"	91- "	"	"	"	0.3	0.32	32	213	0.52	5.14
126	FCS System	FCS Grd to Aircraft Grd	"	TB4	FCS grd-airframe	PRI-SAS Batteries ON	"	"	0.6	0.63	63	420	0.23	8.05
133	"	" "	"	"	" "	"	Slow Wave N-LWT	"	0.2	0.3	30	200	0.8	52.3

TABLE II - Induced Voltages and Corresponding Analytical Expressions-(Continued)

Osc. No.	FCS Sub-System	Circuit	Measurement Location	Interface Plug	Interface Terminals	System Status	i_L Path	Type of Meas.	e_1 Initial peak (volts)	Analytical Voltage Expression Parameters: Maximum Voltage Coefficient, E @ 300A	@ 30 kA	@ 200 kA	Decay Coefficient α	Radial Frequency β (MHz)
143	FCS System	FCS Grd to Aircraft Grd	Gun Bay	TB4	FCS Grd - Airframe	PRI-SAS Batteries	Fast Wave N-T	e	0.95	0.98	98	653	0.14	8.05
134	" "	" "	"	"	" "	"	Slow Wave N-T	"	0.2	0.27	27	180	0.75	52.3
12	" "	" "	"	"	" "	De-energized	Fast Wave N-T	"	0.35	0.42	42	280	1.2	24.15
37	" "	" "	"	"	" "	"	Slow Wave N-T	"	0.3	0.33	33	220	0.81	31.4
78	" "	" "	"	"	" "	"	Fast Wave N-LWT	"	0.55	0.67	67	446	0.49	11.62
79	" "	" "	"	"	" "	"	Slow Wave N-LWT	"	0.25	0.3	30	200	0.17	31.4
355	" "	Left Pitch Valve Drive Output (High to Low)	"	P22	15 to 16	PRI-SAS Batteries	Fast Wave N-LWT	e_{oc}	0.10	0.103	10.3	69	0.19	11.42
359	" "	Left Roll Valve Drive Output Circuit (High to Low)	"	"	44 to 45	"	"	"	0.24	0.28	28	187	1.28	13.06
360	" "	" "	"	"	44 to 45	"	N-T	"	0.11	0.13	13	87	1.64	13.06
361	" "	Wing Pos. Ind. Switch (closed) (Line to Line)	"	"	" "	"	N-LWT	"	0.18	0.19	19	127	0.24	12.56
364	" "	Wing Pos. Ind. Switch (Closed) (Line-toAirframe)	"	"	" "	"	"	"	0.32	0.33	33	220	0.27	12.56
368	" "	Spare Conductors in FCS Cable (Line to Line)	"	"	24 to 25	"	N-T	"	0.20	0.24	24	160	1.73	15.70
367	" "	" "	"	"	24 to Airframe	"	"	"	2.5	2.96	296	1973	0.41	3.97

TABLE II - Induced Voltages and Coresponding Analytical Expressions-(Continued)

Osc. No.	FCS Sub-System	Circuit	Measurement Location	Interface Plug	Interface Terminals	System Status	i_L Path	Type of Meas.	e_1 Initial peak (volts)	Analytical Voltage Expression Parameters: Maximum Voltage Coefficient, E @ 300A	@ 30 kA	@ 200 kA	Decay Coeffi-cient α	Radial Fre-quency β (MHz)
373	FCS System	Spare Conductors in FCS cable Line to Airframe	Gun Bay	P22	24 to Airframe	PRI-SAS Batteries ON	Fast Wave N-T	e_{oc}	2.5	2.96	296	1973	0.41	3.97
370	" "	" "	"	"	" "	"	Slow Wave N-T	"	0.7	0.81	81	540	0.35	3.97
372	" "	" "	"	"	" "	"	" "	"	0.7	0.81	81	540	0.35	3.97
505	DFCS Apollo Guidance Computer	Yaw Gain Logic Power to FCS Grd	DFCS Pallet	J25	A - W	SAS	Fast Wave N-T	e	0.6	0.71	71	473	0.69	6.28
509	" "	Pitch Trim 2(BCS) to FCS Grd	" "	"	D - W	"	"	"	1.0	1.14	114	759	0.51	6.28
508	" "	Pitch Trim 2(BCS) to FCS Grd	" "	"	E - W	"	"	"	0.85	0.97	97	646	0.48	6.28
504	" "	Yaw Gain 4 to FCS Grd	" "	"	F - W	"	"	"	1.35	1.59	159	1059	0.66	6.28
501	" "	Logic Power-Pitch Gain to FCS Grd	" "	"	J - W	"	"	"	0.55	0.62	62	413	0.45	6.28
503	" "	Logic Power Roll Gain to FCS Grd	" "	"	L - W	"	"	"	0.75	0.95	95	633	0.83	6.28
500	" "	Pitch Gain 4 to FCS Grd	" "	"	T - W	"	"	"	0.85	0.97	97	646	0.53	6.28
502	" "	Roll Gain 4 to FCS grd	" "		V - W	"	"	"	1.0	1.14	114	759	0.51	6.28
506	" "	Pitch Trim 1 (DFCS) Up	" "	"	b - W	"	"	"	0.65	0.68	68	453	0.14	6.28
507	" "	Pitch Trim 1 (DFCS) Dwn	" "	"	c - W	"	"	"	0.5	0.53	53	353	0.22	6.28
510	" "	Yaw Trim (DFCS) LFT	" "	"	v - W	"	"	"	0.9	1.07	107	713	0.69	6.28

TABLE II - Induced Voltages and Corresponding Analytical Expressions-(Continued)

Osc. No.	FCS Sub-System	Circuit	Measurement Location	Interface Plug	Interface Terminals	System Status	i_L Path	Type of Meas.	e_1 Initial peak (volts)	Analytical Voltage Expression Parameters: Maximum Voltage Coefficient, E @ 300A	@ 30 kA	@ 200 kA	Decay Coefficient α	Radial Frequency β (MHz)
511	DFCS Apollo Guidance Computer	Yaw Trim (DFCS) RT	DFCS Pallet	J25	w ~ W	SAS	Fast Wave N-T	e	1.1	1.3	130	866	0.69	6.28
514	DFCS Digital Control, Digital to Analog Converters	Pitch Servo 1 (Hi & Lo)	" "	J2	A ~ B	"	"	"	0.4	0.43	43	286	0.26	6.3
516	" "	Roll Servo 1 (Hi & Lo)	" "	"	D ~ E	"	"	"	0.5	0.57	57	380	0.46	6.3
518	" "	Yaw Servo 2 (Hi & Lo)	" "	"	G ~ H	"	"	"	0.55	0.62	62	413	0.41	6.3
515	" "	Yaw Servo 1 (Hi & Lo)	" "	"	X ~ Y	"	"	"	0.35	0.43	43	286	0.39	6.3
517	" "	RollServo 2 (Hi & Lo)	" "	"	Z ~ a	"	"	"	0.7	0.84	84	559	0.63	6.3
519	" "	Pitch Servo 2 (Hi & Lo)	" "	"	b ~ c	"	"	"	0.6	0.69	69	460	0.49	6.3
524	" "	Yaw Pedal 1 (Hi & Lo)	" "	P4	A ~ B	OFF	"	e_{oc}	0.12	0.123	12.3	81.9	0.17	11.4
528	" "	Roll Stick 1 (Hi & Lo)	" "	"	D ~ E	"	"	"	0.1	0.11	11	73.3	0.56	15.0
525	" "	Pitch Stick 1 (Hi & Lo)	" "	"	G ~ H	"	"	"	0.13	0.14	14	93.2	0.33	15.0
527	" "	Yaw Pedal 2 (Hi & Lo)	" "	"	U ~ V	"	"	"	0.1	0.103	10.3	68.6	0.21	15.0
523	" "	Roll Stick 2 (Hi & Lo)	" "	"	W ~ X	"	"	"	0.06	0.07	7	46.6	0.68	15.0
526	" "	Pitch Stick 2 (Hi & Lo)	" "	"	Y ~ Z	"	"	"	0.1	0.103	10.3	68.6	0.21	15.0

TABLE II - Induced Voltages and Corresponding Analytical Expressions-(Continued)

Osc. No.	FCS Sub-System	Circuit	Measurement Location	Interface Plug	Interface Terminals	System Status	i_L Path	Type of Meas.	e_1 Initial peak (volts)	Analytical Voltage Expression Parameters: Maximum Voltage Coefficient, E @ 300A	@ 30 kA	@ 200 kA	Decay Coefficient α	Radial Frequency β (MHz)
582	Left Roll Actuator	Active Valve (Hi & Lo)	Wing Area	J105	A - B	SAS	Fast Wave N-T	e	1.1	1.17	117	779	0.24	5.7
583	"	Active Valve (Hi to Grd)	" "	"	A - K	"	"	"	1.4	1.56	156	1039	0.42	5.7
584	"	Active Valve (Lo to Grd)	" "	"	B - K	"	"	"	0.52	0.66	66	440	0.4	5.7
585	"	Monitor Valve (Hi & Lo)	" "	"	C - D	"	"	"	1.0	1.16	116	773	0.54	5.7
586	"	Monitor Valve (Hi to Grd)	" "	"	C - K	"	"	"	1.25	1.42	142	946	0.47	5.7
588	"	LVDT SEC (output & common)	" "	"	G - H	"	"	"	1.15	1.3	130	866	0.43	5.7
590	"	Engage Solenoid (28 VDC) to Grd	" "	"	J - K	"	"	"	0.4	0.43	43	286	0.24	5.7
591	"	Pressure Switch No.2 to Grd	" "	"	M - K	"	"	"	0.7	0.82	82	546	0.29	6.3
592	"	Pressure Switch No.2 to Grd	" "	"	R - K	"	"	"	0.75	0.88	88	586	0.63	6.3
594	"	Active Valve (Hi & Lo)	" "	J205	A - B	"	"	"	1.4	1.74	174	1159	0.77	6.3
597	"	Active Valve (Hi to Grd)	" "	"	A - M	"	"	"	1.5	1.76	176	1172	0.53	5.7
598	"	Active Valve (Lo to Grd)	" "	"	B - M	"	"	"	0.55	0.6	60	400	0.29	6.3
600	"	LVDT SEC (output & common)	" "	"	E - F	"	"	"	1.2	1.5	150	999	0.67	4.5

TABLE II - Induced Voltages and Corresponding Analytical Expressions-(Continued)

Osc. No.	FCS Sub-System	Circuit	Measurement Location	Interface Plug	Interface Terminals	System Status	i_L Path	Type of Meas.	e_1 Initial peak (volts)	Analytical Voltage Expression Parameters: Maximum Voltage Coefficient, E @ 300A	@ 30 kA	@ 200 kA	Decay Coefficient α	Radial Frequency β (MHz)
601	Left Roll Actuator	Press Trans. Excit (Hi & Lo)	Wing Area	J205	G - H	SAS	Fast Wave N-T	e	0.2	0.24	24	160	0.87	6.3
602	"	Press Trans Excit (Hi to Grd)	" "	"	G - M	"	"	"	0.65	0.67	67	446	0.1	5.7
603	"	Press Trans Excit (Lo to Grd)	" "	"	H - M	"	"	"	0.72	0.75	75	500	0.14	5.7
605	"	Press Trans Output	" "	"	J - K	"	"	"	0.09	0.11	11	76	1.5	10.5
606	"	Solenoid (Hi to Common)	" "	"	L - M	"	"	"	1.0	1.04	104	693	0.14	5.2
608	"	Active Valve (Hi to Lo)	" "	J305	A - B	"	"	"	1.2	1.4	140	932	0.45	5.7
609	"	Press Trans Excit (Hi & Lo)	" "	"	G - H	"	"	"	0.2	0.24	24	160	0.58	5.7
647	Yaw Actuator	Active Valve (Hi & Lo)	Tail Area	J107	A - B	"	"	"	1.5	1.79	179	1192	0.46	5.2
649	"	Active Valve (Hi to Grd)	" "	"	A - K	"	"	"	1.7	2.1	210	1399	0.55	5.2
651	"	Active Valve (Lo to Grd)	" "	"	B - K	"	"	"	0.52	0.78	78	519	0.82	3.9
652	"	Monitor Valve (Hi & Lo)	" "	"	C - D	"	"	"	1.4	1.46	146	972	0.1	5.2
653	"	Monitor Valve (Hi to Grd)	" "	"	C - K	"	"	"	1.65	2.05	205	1365	0.57	5.2

TABLE II - Induced Voltages and Corresponding Analytical Expressions-(Continued)

Osc. No.	FCS Sub-System	Circuit	Measurement Location	Interface Plug	Interface Terminals	System Status	i_L Path	Type of Meas.	e_1 Initial Peak (volts)	Analytical Voltage Expression Parameters: Maximum Voltage Coefficient, E @ 300A	@ 30 kA	@ 200 kA	Decay Coefficient α	Radial Frequency β (MHz)
655	Yaw Actuator	LVDT SEC (output & common)	Tail Area	J107	G - H	SAS	Fast Wave N-T	e	1.6	1.6	190	1265	0.46	5.2
656	" "	Engage Solenoid (Hi & Lo)	" "	"	J - K	"	"	"	0.4	0.42	42	280	0.14	5.2
657	" "	Pressure Switch No.2 to Grd	" "	"	M - K	"	"	"	1.0	1.26	126	839	0.61	3.9
658	" "	Pressure Switch No.2 to Grd	" "	"	R - K	"	"	"	0.9	1.09	109	726	0.24	3.9
665	" "	Active Valve (Hi & Lo)	" "	"	A - B	"	N-VS	"	1.65	2.04	204	1359	0.54	5.2
666	" "	Active Valve (Hi to GRD)	" "	"	A - K	"	"	"	2.1	2.56	256	1705	0.53	5.2
667	" "	Active Valve (Lo to Grd)	" "	"	B - K	"	"	"	0.6	0.75	75	500	0.3	3.9
668	" "	Monitor Valve (Hi & Lo)	" "	"	C - D	"	"	"	1.7	2.16	216	1439	0.6	3.9
669	" "	Monitor Valve (Hi to Grd)	" "	"	C - K	"	"	"	2.0	2.52	252	1678	0.6	3.9
670	" "	LVDT SEC (output & common)	" "	"	G - H	"	"	"	1.6	1.97	197	1312	0.55	3.9
671	" "	Engage Solenoid (Hi & Lo)	" "	"	J - K	"	"	"	1.1	1.52	152	1012	0.65	5.2
672	" "	Pressure Switch No.2 to Grd.	" "	"	M - K	"	"	"	0.6	0.71	71	473	0.2	3.9

TABLE II - Induced Voltages and Corresponding Analytical Expressions-(Continued)

Osc. No.	FCS Sub-System	Circuit	Measurement Location	Interface Plug	Interface Terminals	System Status	i_L Path	Type of Meas.	e_1 Initial Peak (volts)	Analytical Voltage Expression Parameters: Maximum Voltage Coefficient, E @ 300A	@ 30 kA	@ 200 kA	Decay Coefficient α	Radial Frequency β (MHz)
661	Yaw Actuator	Pressure Switch No.5 to Grd	Tail Area	J107	R - K	SAS	Fast Wave N-VS	e	0.95	1.18	118	789	0.48	3.9
688	" "	Active Valve (Hi & Lo)	" "	J307	A - B	"	N-T	"	1.4	1.6	160	1066	0.56	5.7
689	" "	Active Valve (Hi to Grd)	" "	"	A - M	"	"	"	2.8	3.01	301	2005	0.19	5.7
690	" "	Active Valve (Low to Grd)	" "	"	B - M	"	"	"	0.6	0.79	79	526	0.55	5.7
691	" "	LVDT SEC (Excit & Common	" "	"	E - F	"	"	"	1.4	1.74	174	1159	0.65	4.8
692	" "	Press Trans Excit (Hi & Lo)	" "	"	G - H	"	"	"	0.4	0.48	48	320	1.39	2.0
693	" "	Press Trans Excit (Hi to Grd)	" "	"	G - M	"	"	"	0.8	0.9	90	600	0.39	5.7
694	" "	Press Trans Excit (Lo to Grd)	" "	"	H - M	"	"	"	0.8	0.86	86	573	0.29	5.7
695	" "	Press Trans Output	" "	"	J - K	"	"	"	0.15	0.17	17	113	0.68	2.0
696	" "	Solenoid (Hi & Common)	" "	"	L - M	"	"	"	1.2	1.3	130	866	0.18	5.7
679	" "	Active Valve (Hi & Lo)	" "	"	A - B	"	N-VS	"	1.2	1.6	160	1066	0.78	5.7
678	" "	Active Valve (Hi to Grd)	" "	"	A - M	"	"	"	1.6	1.97	197	1312	0.55	5.7
680	" "	Active Valve (Lo to Grd)	" "	"	B - M	"	"	"	0.4	0.5	50	333	0.29	5.7

TABLE II - Induced Voltages and Corresponding Analytical Expressions-(Continued)

Osc. No.	FCS Sub-System	Circuit	Measurement Location	Interface Plug	Interface Terminals	System Status	i_L Path	Type of Meas.	e_1 Initial Peak (volts)	Analytical Voltage Expression Parameters: Maximum Voltage Coefficient, E @ 300A	@ 30 kA	@ 200 kA	Decay Coefficient α	Radial Frequency β (MHz)
681	Yaw Actuator	LVDT SEC (Excit & Common)	Tail Area	J307	E - F	SAS	Fast Wave N-VS	e	1.5	1.68	168	1119	0.40	4.8
682	" "	Press Trans Excit (Hi & Lo)	" "	"	G - H	"	"	"	0.2	0.24	24	160	0.99	2.0
683	" "	Press Trans Excit (Hi to Grd)	" "	"	G - M	"	"	"	0.6	0.69	69	469	0.45	5.7
684	" "	Press Trans Excit (Lo to Grd)	" "	"	H - M	"	"	"	0.6	0.71	71	473	0.3	5.7
685	" "	Press Trans Output	" "	"	J - K	"	"	"	0.12	0.126	12.6	84	0.3	2.0
686	" "	LVDT PRIM Excit & Common	" "	"	L - M	"	"	"	1.1	1.34	134	892	0.38	5.7
483	Mode & Power Control Pnl.	Logic Power for Realign & DFCS Fail to DSKY 0 VDC	Cockpit	J14	A - E		N-T	"	0.9	1.0	100	666	0.49	5.2
469	" "	Realign Command to DSKY 0 VDC	"	"	C - E	"	"	"	1.1	1.2	120	799	0.26	5.2
463	" "	DSKY +28 VDC to 0 VDC	"		D - X	"	"	"	0.46	0.48	48	320	0.08	5.2
467	" "	Trim Tail Reset to DSKY 0 VDC	"	"	F - E	"	"	"	1.1	1.23	123	819	0.45	5.2
465	" "	28 VDC Control Pwr to 0 VDC	"	"	K - X	"	"	"	0.3	0.31	31	206	0.23	9.0
472	" "	Pitch BCS Verify DSKY 0 VDC	"	"	T - E	"	"	"	1.1	1.23	123	819	0.45	5.2
478	" "	Pitch Axis BCS to DSKY 0 VDC	"	"	U - E	"	"	"	0.6	0.65	65	433	0.26	5.2
479	" "	Pitch Axis BCS to BCS Common Return	"	"	U - L	"	"	"	0.8	1.2	120	799	1.2	5.2

TABLE II - Induced Voltages and Corresponding Analytical Expressions-(Concluded)

Osc. No.	FCS Sub-System	Circuit	Measurement Location	Interface Plug	Interface Terminals	System Status	i_L Path	Type of Meas.	e_1 Initial Peak (volts)	Analytical Voltage Expression Parameters: Maximum Voltage Coefficient, E @ 300A	@ 30 kA	@ 200 kA	Decay Coefficient α	Radial Frequency β (MHz)
471	Mode & Power Control Pnl.	Pitch BCS Command to DSKY 0 VDC	Cockpit	J14	V - E	SAS	Fast Wave N-T	e	1.1	1.2	120	799	0.29	5.7
473	" "	Pitch BCS Command to DSKY 0 VDC	"	"	X - E	"	"	"	1.1	1.17	117	779	0.23	5.7
470	" "	Pilot's BCS to DSKY 0 VDC	"	"	a - E	"	"	"	1.1	1.28	128	852	0.25	5.2
462	" "	Logic +28 VDC to 0 VDC	"	"	c - X	"	"	"	0.36	0.5	50	333	0.44	5.0
464	" "	DFCS Fail Relay Command to 0 VDC	"	"	d - X	"	"	"	0.6	0.66	66	440	0.34	5.2
468	" "	DFCS Fail Sw. to DSKY 0 VDC	"	"	g - E	"	"	"	1.05	1.1	110	733	0.2	5.2
476	" "	Pitch CAS Command to DSKY 0 VDC	"	"	p - E	"	"	"	1.0	1.07	107	713	0.29	5.2
475	" "	Pitch SAS Cmmd. to DSKY 0 VDC	"	"	r - E	"	"	"	1.1	1.3	130	866	0.63	5.2
474	" "	Pitch DIR Verify to DSKY 0 VDC	"	"	s - E	"	"	"	1.3	1.4	140	932	0.24	5.2
477	" "	I/G Output Cmmd. to DSKY 0 VDC	"	"	t - E	"	"	"	1.0	1.2	120	799	0.63	5.2
481	" "	Roll Axis BCS to DSKY 0 VDC	"	"	cc - E	"	"	"	0.5	0.6	60	400	0.63	5.2
480	" "	Roll Axis BCS to BCS Common Return	"	"	cc - L	"	"	"	0.9	1.14	114	759	0.63	5.2

TABLE III - Predominant Frequency of Induced Voltage at Sperry Interface Electronics Test Receptacle

Freq.	0.82 Megahertz		1.0 Megahertz		1.5 Megahertz		1.82 Megahertz	
	Pin No.	Circuit	Pin No.	Circuit	Pin No.	Circuit	Pin No.	Circuit
	91	28 VDC BUS No.4 INPUT	9	LEFT AILERON FUP No.2	43	RUDDER PRIMARY COMMAND, ACTIVE	1	LEFT HOR. FUP No.2
			27	PITCH PRIMARY COMMAND, ACTIVE	44	RUDDER PRIMARY COMMAND, MONITOR	2	RIGHT HOR. FUP No.2
			28	PITCH PRIMARY COMMAND, MONITOR			3	LEFT HOR. FUP No.3
							4	RIGHT HOR. FUP No.3
							8	RIGHT HOR. FUP No.1
							21	PITCH COMMAND OUTPUT NO.2
							35	ROLL PRIMARY COMMAND, ACTIVE
							36	ROLL PRIMARY COMMAND, MONITOR
							45	L. PITCH SERVO AMPL. TEST INPUT No.2
							47	L. PITCH SERVO AMPL. TEST INPUT No.4
							60	WING DOWN SWITCH
							61	PC No.1 HYDRO SWITCH
							62	WEIGHT-ON-WHEELS SWITCH
							87	WING POSITION POT. TEST POINT
							88	28 VDC BUS No. 1 INPUT
							89	28 VDC BUS No. 2 INPUT
							90	28 VDC BUS No. 3 INPUT

DISCUSSION OF RESULTS

Induced Voltages

Origin.- Study of the induced voltages measured throughout the FCS system indicates that they are primarily of changing magnetic flux origin because the induced voltages and currents reach their maximums during the time when the lightning current is rising rapidly to its crest. Assuming that any induced voltages, by Faraday's Law, are proportional to rate of change of magnetic flux, this flux must therefore be changing at about the same rate as the total lightning current causing it.

If there are any holes in the aircraft skin, a portion of the exterior magnetic field can leak directly inside as was shown in Figure 10. This penetration of an external field into an interior region is called aperture flux. It is of a lower amplitude than the external field, but rises to its crest as fast as the external field. The measured voltages universally appear during the first microsecond of lightning current flow, which is when the lightning current is changing most rapidly, indicating they have been induced by this aperture flux. The magnetic flux measurements made inside the gun bay and battery compartment confirm these observations. The interior flux has a waveform similar to the external fluxwaveform, as was shown in Figures 29, 31 and 32.

There are no indications of long-duration, unidirectional induced voltage components induced by magnetic flux appearing inside the aircraft when lightning current has had time to diffuse to the inside of its skin. Such flux must, of course, exist inside the F-8 but because of the time required for significant currents to diffuse to the inside of an aircraft skin (Ref. 3) the total lightning current is diminishing by the time some of it reaches the inside surface of the skin. This reduces the amplitude and effective rate of rise of the current reaching the inside surface and therefore of the resulting diffusion magnetic flux. Accordingly, for significant voltages to be induced in an aircraft circuit by diffusion flux the circuit must encircle a relatively large area, linking a correspondingly large amount of diffusion flux. This is not usually the case with a single-point grounded system such as this FCS since dedicated parallel-pair return wires are utilized in system cabling, running next to each other in a single cable bundle.

Indications of structural IR voltage components are nearly absent, since the system is single-point grounded and has no direct reference to the airframe at locations remote from the DFCS pallet where the single-point ground to the airframe is made.

Verification.- To confirm that the measured induced voltages are in fact of aperture flux origin and that additional diffusion flux and IR voltages would appear if larger circuit loops were present (such as in airframe return circuits), some special tests were made in which such a circuit was created inside the F-8. The main FCS system cable between the gun bay and actuators in the tail area passes through the fuselage beneath the wing and thence to the Aft Disconnect located beneath the leading edge of the vertical tailfin. There are several spare conductors in this cable which are terminated at open pins in the Aft Disconnect plug. Two of the unused conductors were connected and grounded to the airframe at the Aft Disconnect to form a parallel pair with a common mode airframe return. These conductors are connected to pins 24 and 25 on plug P22 in the gun bay. The line-to-line voltage induced in the spare conductor circuit is shown on Figure 58. It is similar to voltages measured in other circuits in this cable, even though the circuit is connected to the airframe at the Aft Disconnect. Its predominant frequency is similar to that evident in the actuator circuits of Figures 39 and 40. However, the peak voltage induced between either conductor and the airframe is much greater, as shown in Figure 59, oscillogram No. 367. Here, over 20 times as much voltage appears. Its predominant frequency is much slower, at 0.63 megahertz. In addition, there is a long duration component apparent when the voltage is recorded at a slower oscilloscope sweep rate of 10 microseconds per division as shown on oscillogram No. 373. The long duration component is much lower in amplitude than the oscillatory component.

The high amplitude oscillatory component shown on oscillogram No. 367 is induced by aperture magnetic flux linking the circuit formed between the spare conductors and the airframe. Its frequency is not the same as the oscillatory voltages measured in other circuits; therefore, the frequency of this induced voltage must depend on peculiar characteristics of the common-mode circuit itself. The long duration component shown on oscillogram No. 373 is primarily the structural resistive voltage rise caused by lightning current flowing through the portion of airframe between the gun bay and the Aft Disconnect where the circuit is connected to the airframe. There is probably also a contribution to the long duration component from magnetic flux created by

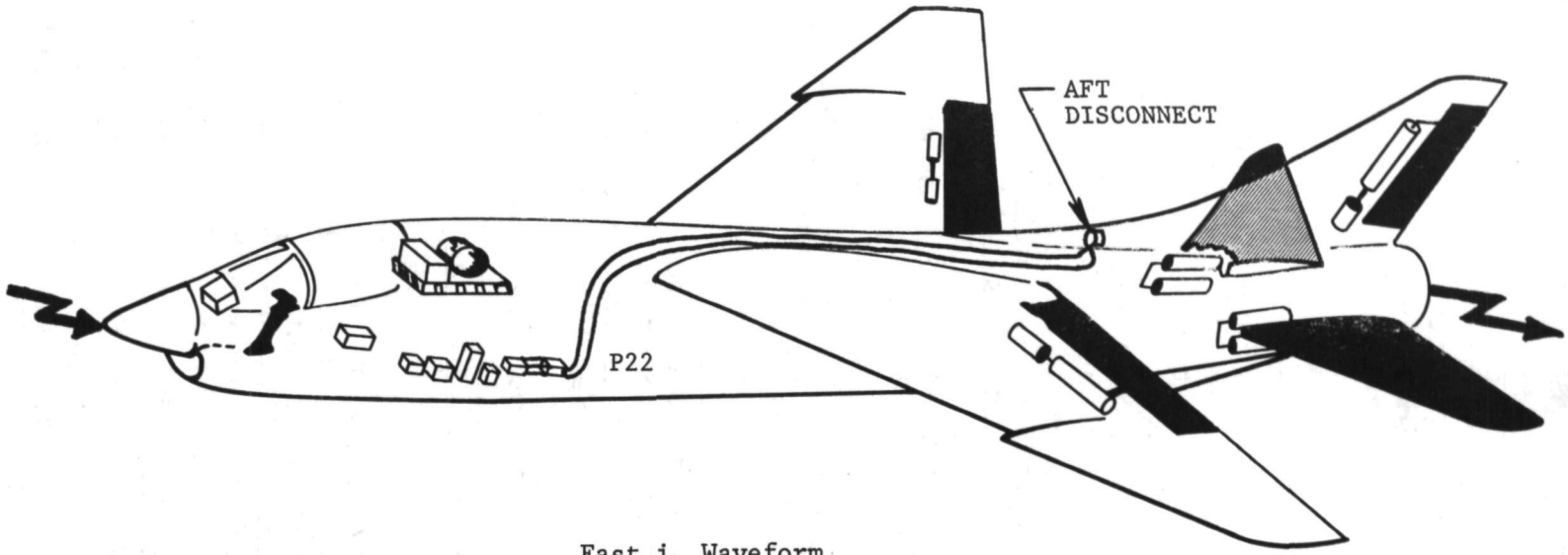

Fast i_L Waveform

Nose to Tail

Pins 24-25

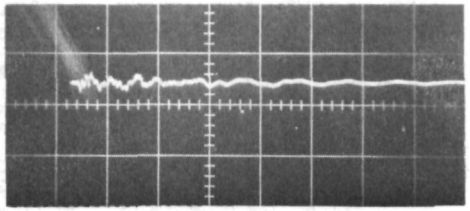

1V/div. No.368 1μs/div.

FIGURE 58- SPARE CONDUCTOR MEASUREMENT ON P22 (LINE-TO-LINE, PINS 24 to 25).

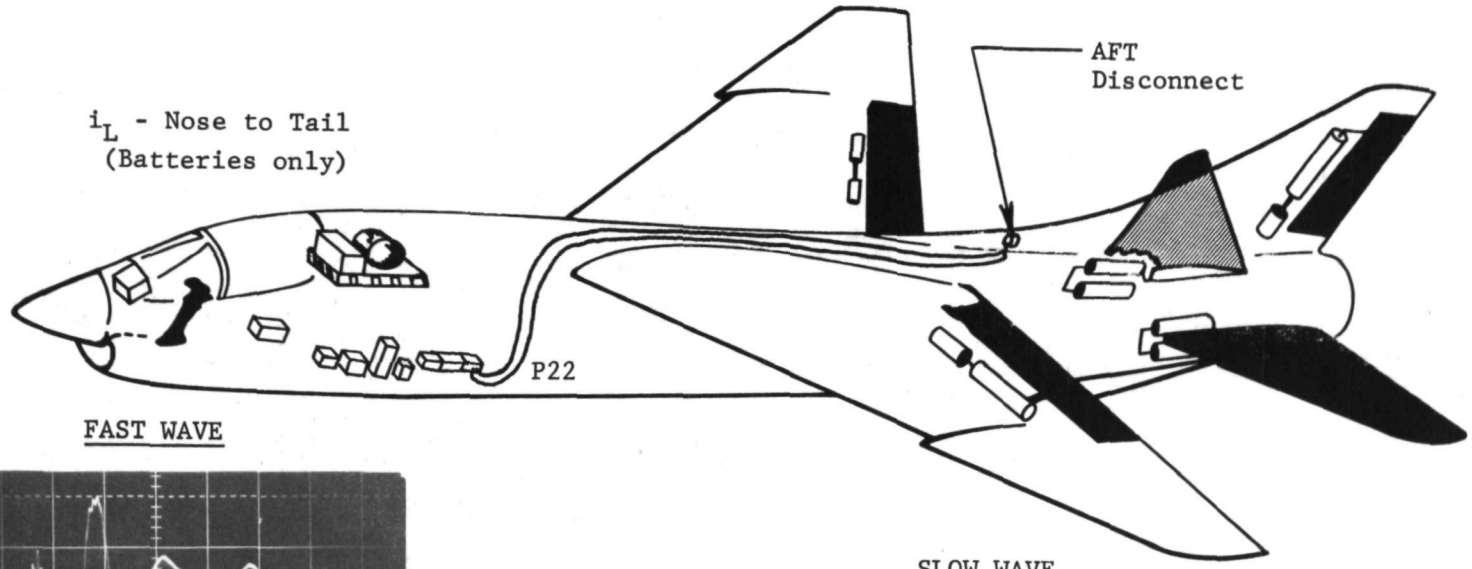

FAST WAVE

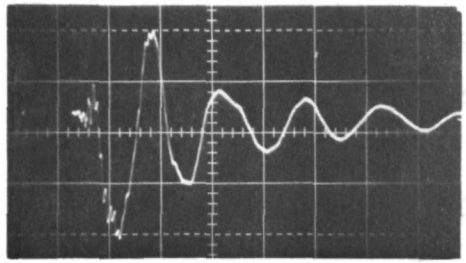

1V/div. No.367 1μs/div.

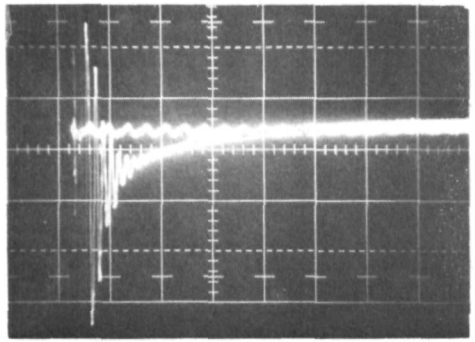

0.2V/div. No.373 10μs/div.

SLOW WAVE

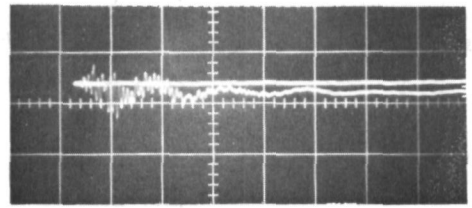

1V/div. No.370 1 μs/div.

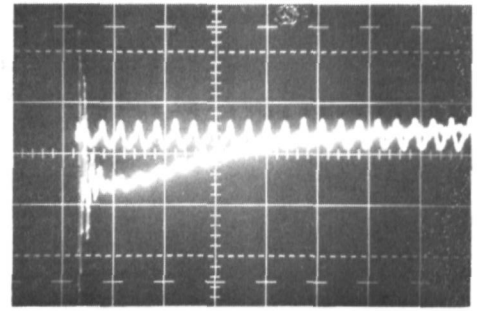

0.2V/div. No.372 10μs/div.

FIGURE 59 - SPARE CONDUCTOR MEASUREMENTS ON P22 (PIN 24 to AIRFRAME).

lightning current which has diffused to the inside of the aircraft skin. Such diffusion flux is of relatively low amplitude within cylindrical structures such as an airplane fuselage (Ref. 2), however, so its effects would not be expected to show up in a fuselage circuit nearly as much as they would in a wing circuit, for example.

Line-to-airframe measurements were also made in the spare conductor circuit with the slow lightning test waveform applied. These measurements are also shown on Figure 59, oscillogram Nos. 370 and 372. Here, the oscillatory component is much lower in amplitude than that induced by the fast lightning test waveform; however, it is apparently of the same frequency. This confirms an earlier observation that the frequency of induced voltage oscillation in these circuits is independent of the lightning current waveform. The amplitude of the long duration component produced by the slow lightning test waveform is the same amplitude as that produced by the fast waveform. This component must therefore primarily be airframe IR voltage, since the amplitude of the test current is the same for both fast and slow waveforms (300 amps).

The steady-state oscillation on the zero lines and induced voltage traces of oscillograms Nos. 373 and 372 of Figure 59 is induced interference from a neighboring conductor in the cable, since the FCS system was operating when these measurements were made. It is random interference and has no relationship to the lightning-induced voltages.

Common-Mode Voltages.- Figure 59 shows voltages that are induced between all conductors in a cable and the airframe. These common-mode voltages are much higher in amplitude than those appearing between any pair of wires in the cable. If no conductors in a cable are grounded to the airframe at either end, very little of the common-mode voltage will appear at a measurement oscilloscope connected to either end of the cable, since the impedance of the measurement system is normally lower than the nearly infinite impedance of open circuited conductors at the other end, and common-mode induced voltage would be expected to divide between the two ends of the cable in rough proportion to the terminating impedances. In other words, if a measurement were made at the Aft Disconnect end of the spare conductor circuit of Figure 59, instead of at P22, the measured voltage would be zero since the conductors are shorted to the airframe at the Aft Disconnect. But if the conductors had been shorted to the airframe at P22 and left open at the Aft Disconnect, induced voltage measured at the Aft Disconnect would be similar to those

shown on Figure 59, with the polarities reversed. These measurements have an important implication for design of single-point grounded systems as they illustrate that care must be taken to avoid excessive common-mode voltages at locations, such as actuators, remote from where the single-point ground is made to the airframe.

Frequencies.- Nearly all induced voltages measured in the FCS had damped oscillatory waveforms. The waveforms were characterized by a predominant frequency with one or more higher frequency components of lower amplitude superimposed. Predominant frequencies ranged from 0.8 megahertz to 2.08 megahertz and lower amplitude components ranged between 5 and 8 megahertz. Identical frequencies appeared in conductors within a single cable bundle, or in conductors following the same path between interfaces, although some exceptions were noted.

The oscillatory voltage waveforms are believed to be due to subsequent oscillation of induced energy between the inductive and capacitive elements of the cabling systems. Therefore, their frequency should be dependent primarily upon cable characteristics and not the waveform of the applied lightning current. As noted previously, however, there is an oscillatory component superimposed on the wavefront of the fast lightning current waveform shown on Figure 16 and the relationship between the frequency of this component and those of induced voltages is of interest. In an effort to determine what, if any, relationship(s) exist, several comparisons were made. First, the frequency of the lightning wavefront oscillations was compared with that of the induced voltages. Figure 60 is a large scale drawing of the simulated lightning current wavefront. It shows the frequency of the oscillatory component to be 2.63 megahertz. This is not the same as the predominant or higher frequency oscillations of any of the induced voltages measured in the FCS.

Second, a Fourier spectral transformation was made of the waveform of Figure 60 to determine if spectral energy peaks exist at any of the induced voltage frequencies. For comparison purposes, a transformation was also made of an idealized smooth-front waveform. The idealized waveform is also shown on Figure 60, and spectral distributions of both are shown on Figure 61. Figure 61 shows that the test waveform has spectral peaks above the idealized waveform at 2.5, 5 and 8 megahertz, but not at any of the induced voltage frequencies. These peaks are also of lower amplitude than the spectrum around 1 to 2 megahertz which is the region of most induced voltage frequencies. Here, the spectral distributions of test and idealized lightning current waveforms are nearly the same.

Third, comparison of the voltages induced by different lightning current waveforms, as is possible in Figures 56 and 59, shows

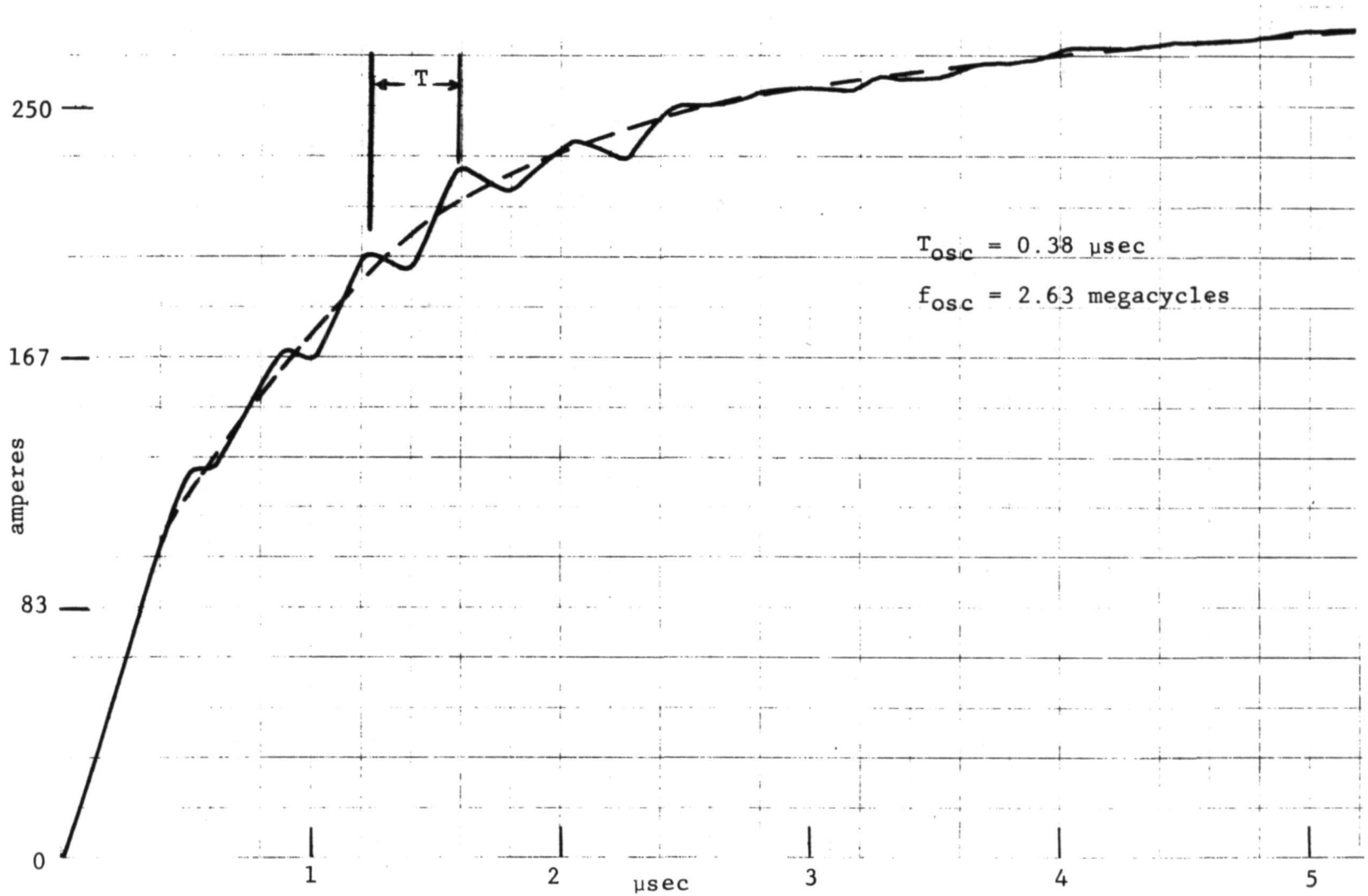

FIGURE 60 - FAST SIMULATED LIGHTNING CURRENT WAVEFORM AND IDEALIZED SMOOTH-FRONT WAVEFORM.

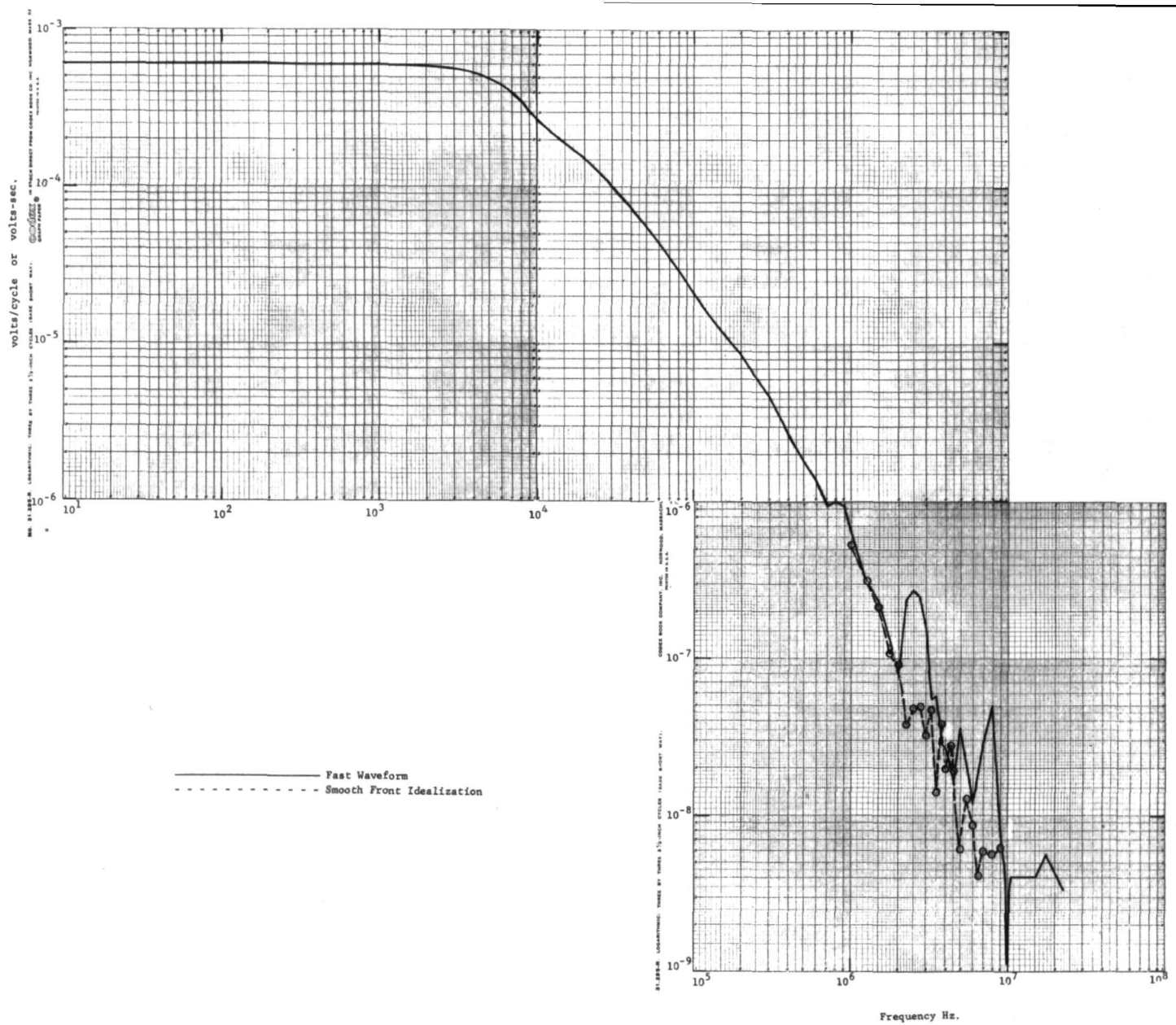

FIGURE 61 - FREQUENCY SPECTRAL DISTRIBUTIONS OF FAST SIMULATED LIGHTNING CURRENT WAVEFORM AND A SMOOTH-FRONT IDEALIZATION.

that the predominant frequency is the same, indicating that the frequency is independent of lightning current waveform.

If the above conclusions are correct, then the induced voltage frequency should be related to the FCS circuit characteristics. An obvious one is circuit length. Since the frequency of traveling wave reflections depends on circuit length, long circuits should exhibit lower frequencies and short circuits, higher frequencies. Table IV shows the predominant frequency of voltages induced in parallel pair circuits in each of the major FCS cables entering the gun bay, compared with the approximate length of each circuit. The circuit to the Wing Position Indicator switch received a voltage at 2 megahertz, whereas the longer circuits to the actuators had voltages of less than 1 megahertz; however, more detailed comparisons are difficult due to other circuit characteristics which are not common to each of those compared.

Voltage Amplitudes.- Peak amplitudes of each of the induced voltages have been presented in Table II along with coefficients of the damped oscillatory approximations extrapolated to correspond with 30,000 ampere and 200,000 ampere lightning stroke amplitudes. The ranges of peak induced voltages extrapolated for the 200,000 ampere stroke are presented in Table V. From this table it is apparent that induced voltages of similar amplitudes are simultaneously induced in each channel of the multi-channel FCS system.

Induced Cable Currents

Origin.- Study of the induced currents measured during the program also affords an opportunity to determine significant relationships. For example, Figure 62 shows two conductors located above a ground plane. One is connected to the ground plane at only one end and the other connected to the ground plane at both ends. These may be considered the open circuit and short circuit conditions. If a magnetic field links these conductors, and if the capacitance of the cable is temporarily ignored, a voltage will be induced between the end of the open-circuited conductor and the ground plane, but no current will flow in the conductor. In the short circuited condition this voltage will circulate a current along the conductor. The open circuit voltage will be proportional to the rate of change of magnetic flux linking the conductor or

$$e = -\frac{d\phi}{dt} = -\frac{d(AB)}{dt} \qquad (12)$$

Table IV - Frequency of Induced Voltages vs. Cable Length
(all circuits unshielded)

System	Circuit(s)	Cable Path	Cable Length (meters)	Predominant Frequency (megahertz)
Wing Pos. Indicator Circuit		Left Gun Bay to FWD Wing Root	3.4	2.0
Spare Conductors in Fuselage Cable		Left Gun Bay to Aft Disconnect	8.8	0.63
Roll Actuator	all	Left Gun Bay to Left Wing	9.4	0.90
Yaw Actuator	all	Left Gun Bay to Vertical Fin	11.4	0.80

Table V - Ranges of Peak Induced Voltages Measured at FCS Interfaces

Circuit	Location	INDUCED VOLTS SCALED to i_L = 200 kA	
		FAST i_L Waveform	SLOW i_L Waveform
	GUN BAY		
FCS Grd. to A/C Grd: (in Gun Bay)		420-653	180-200
28 VDC Busses		213-346	
Interface Electronics Test Receptacle		160-519	
	COCKPIT		
Mode & Power Control Panel	J14	206-932	
	DFCS PALLET		
DFCS (AGC)	J25	353-1059	
Pitch, Roll and Yaw Servos	J2	286-559	
	WING AREA		
Primary Circuits to Left Roll Actuator	J105	286-1039	
Backup (Channel 2) Circuit to Left Roll Actuator	J205	127-1172	
	TAIL AREA		
Primary Circuits to Yaw Actuator	J107	280-1705	
Backup (Channel 3) Circuits to Yaw Actuator	J307	84-2005	

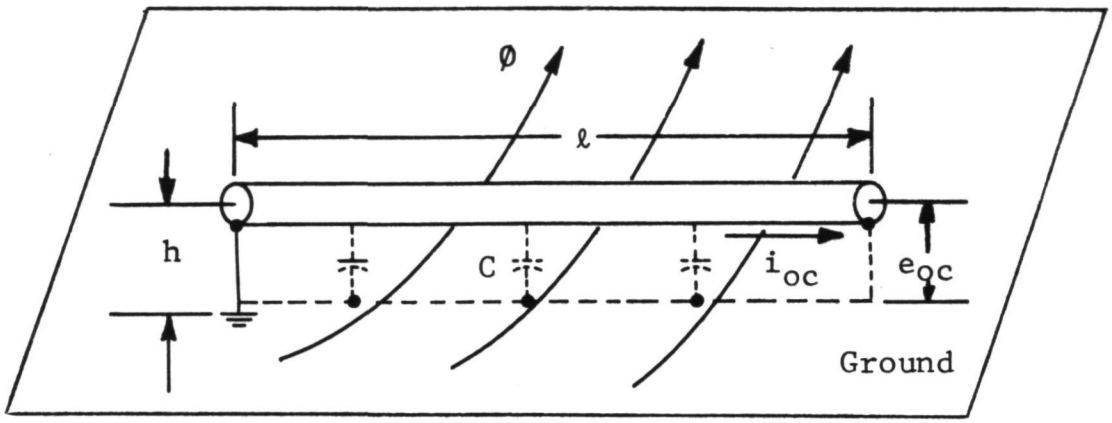

a) Open Circuit Voltage and Current

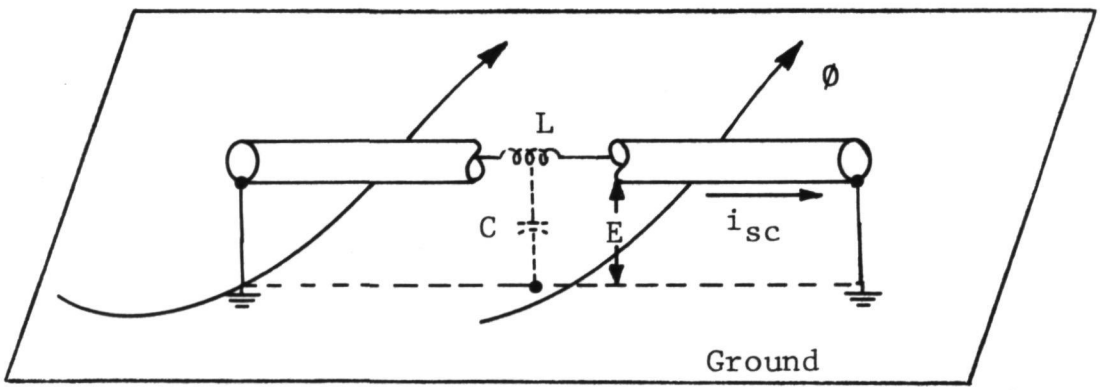

b) Short Circuit Current

FIGURE 62 - ORIGIN OF INDUCED VOLTAGES AND CURRENTS.

where:

e = induced voltage (volts)

ϕ = magnetic flux (webers)

B = magnetic flux density (webers/meter^2)

A = area between conductor and ground plane (meter^2)

which is also equal to

$$e = - A \frac{dB}{dt} = (h\ell) \frac{dB}{dt} \qquad (13)$$

where:

h = conductor height above ground plane (meters)

ℓ = conductor length (meters)

Assuming a constant h and uniform flux density, the induced voltage is proportional to conductor length. The current this voltage drives through a short circuited conductor is

$$i_{sc} = \frac{1}{L} \int e \, dt = \frac{(\ell h)}{L} \int \frac{dB}{dt} \, dt = \frac{AB}{L} \qquad (14)$$

where:

i = short circuit current (amperes)

L = self inductance of the complete circuit (henrys)

Thus the current that flows along the conductor in the short-circuited case tends to have the same waveshape as the magnetic field and be independent of conductor length. There is more voltage induced in the circuit if the conductor is longer, but this voltage must circulate current through a larger inductance, and the inductance increases in proportion to the conductor length exactly as does the induced voltage.

Equation (14) indicates that the short circuit current is also independent of the magnetic field rate of change. Instead, it is proportional to the magnetic field amplitude. Therefore, the open circuit voltage and short circuit current responses of a conductor to magnetic fields of different waveshapes should be as shown in Figure 63.

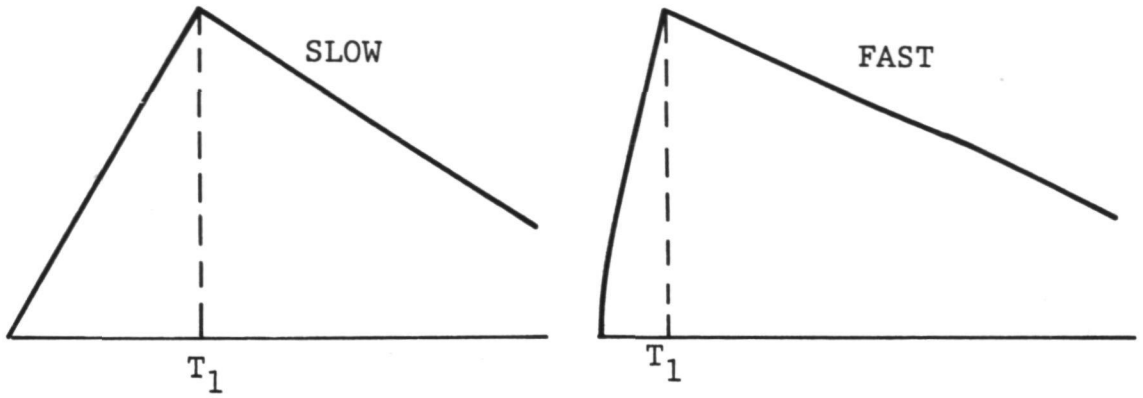

a) Magnetic Fields

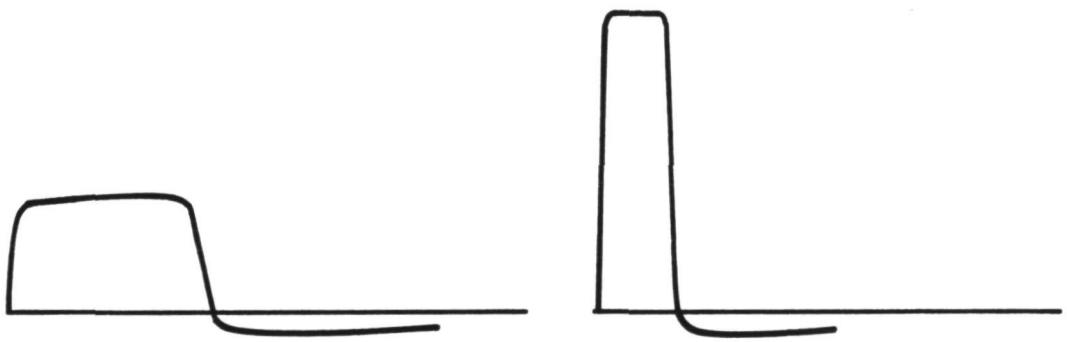

b) Open Circuit Voltage

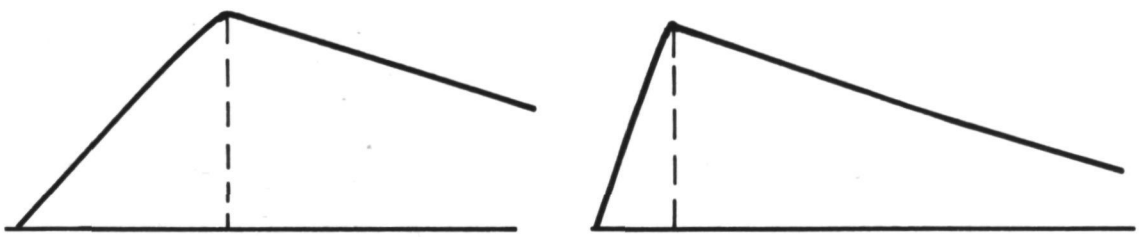

C) Short Circuit Current

FIGURE 63- RESPONSES TO DIFFERENT LIGHTNING CURRENT WAVESHAPES.

Figure 63 shows two magnetic fields of the same peak amplitude but rising to crest in different times. The open circuit voltage is predominantly affected by the magnetic field produced by the lightning current wavefront, assuming that the decay time of the lightning current would produce lower voltages, but of longer duration, than would a fast current of the same amplitude. The short circuit currents, however, would be of approximately equal amplitudes with rise times similar to those of the magnetic field.

Equations (13) and (14), of course, present only the first order characteristics of voltage and current. Resistance of the conductors and their distributed inductance and capacitance probably introduce important second order effects. These permit higher frequency oscillations to be superimposed upon the fundamental voltage and current waveforms shown in Figure 63.

Verification.- Some of the induced current exhibited the first order relationship described above, for example, in Figure 42 where short circuit currents induced by fast and slow lightning current waveforms are presented. In many other cases, however, a short duration oscillatory current is all that appears. These oscillatory currents were measured in functional circuits terminated with finite impedances, apparently high enough to eliminate long duration short circuit currents but low enough at higher frequencies to permit the oscillatory currents to flow into the terminations. These probably circulate through the distributed capacitances between conductors and the airframe. To confirm these observations, measurements were made in a dummy conductor grounded at each end to the airframe and placed beneath the wing adjacent to a portion of the main FCS cable running from the gun bay to the secondary actuators.

Since other aircraft electrical cables not related to the FCS also pass through this area, a comparison could be made with currents induced in these cables as well. A dummy conductor grounded at each end was also placed in the gun bay.

Figure 64 shows the location of the cables and the dummy conductor beneath the wing, where access for current measurements was possible. The FCS cable is carried beneath the wing in a thin wall aluminum conduit along the port side. The conduit is primarily to provide mechanical protection for the conductors and is not intentionally grounded to the airframe. A bundle of shielded instrumentation wires runs along the center. The exact treatment of the shields on these wires is not known but an ohmeter check

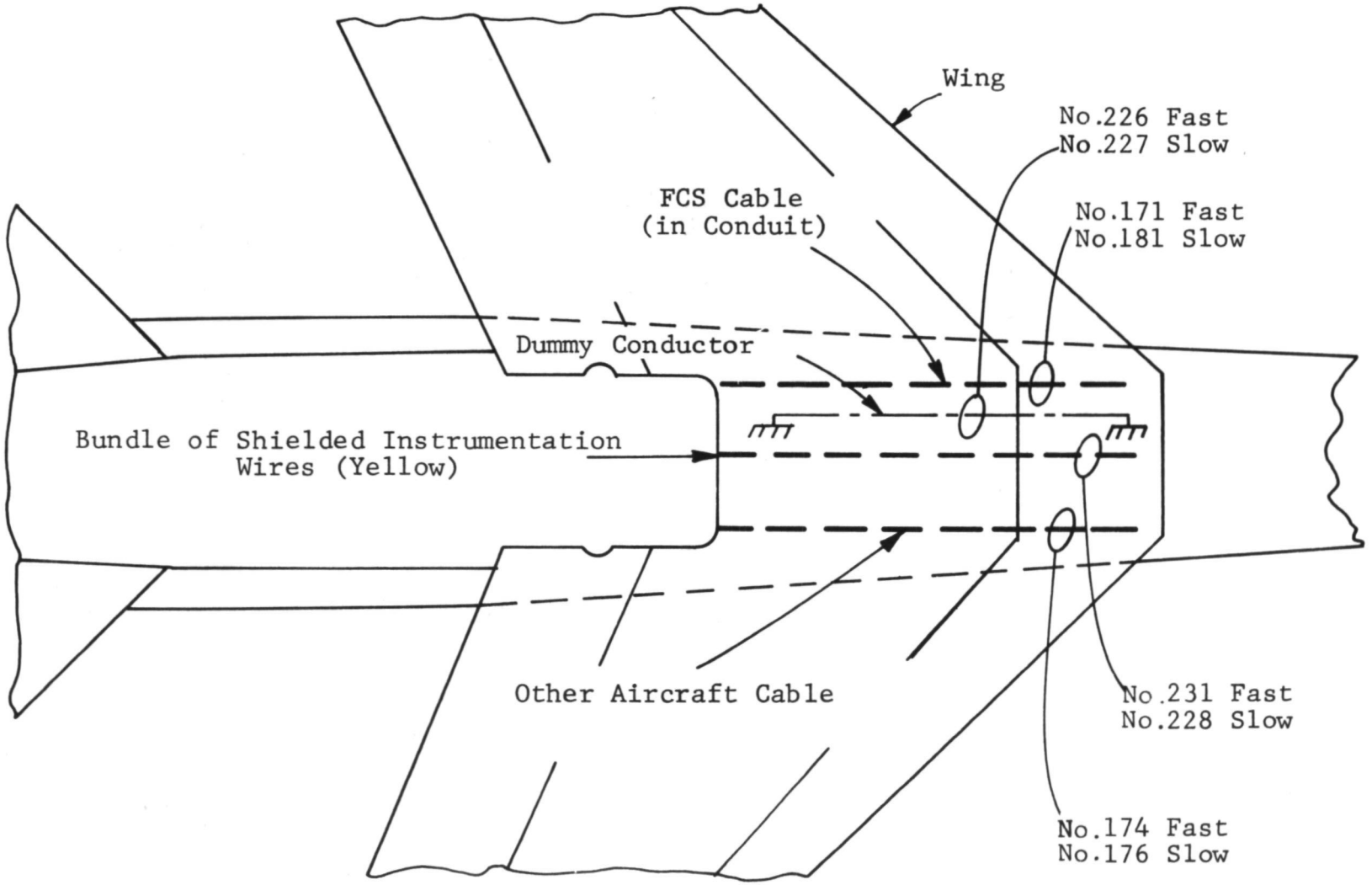

FIGURE 64 - FCS, DUMMY AND OTHER AIRCRAFT CABLE BUNDLES BENEATH WING.

indicates they are grounded somewhere. Another cable runs along the starboard side. These are original aircraft wires and are not shielded nor installed in a conduit.

Figure 65 shows the induced currents measured on these cables. Several significant points are to be noted. The first is that the currents measured on the shielded instrumentation wires, oscillogram Nos. 231 and 228, display the unidirectional component of current characteristic of a wire which has a ground at each end. The current waveforms are similar to the magnetic flux (and lightning current) waveforms and the amplitudes for fast and slow lightning currents are the same (note different scales). Another is that the induced currents on both of the other cables are of shorter duration and oscillatory, as measured on many other FCS cables. The FCS system is single-point grounded at the gun bay end, so the FCS cable is open-circuited with respect to the airframe at the other (aft) end. The oscillatory currents are secondary effects, as discussed previously. The other aircraft cable is also apparently ungrounded at least at one end.

Figure 66 shows the currents measured on each of the dummy wires. The location of the dummy conductor installed in the left gun bay is shown on Figure 67. This conductor was one strand of No. 18 AWG insulated wire running from a structural ground point on the DSKY unit to a ground stud in the gun bay. From the measurements on Figure 66 it is apparent that the amplitudes of the induced short-circuit currents are nearly the same for the fast and slow simulated lightning currents. Their waveforms are similar to the magnetic field waveforms causing them. With the gun bay door removed, the short circuit current waveform is similar to that of the lightning current, because the external field has directly entered the gun bay. With the door in place, the induced current rate of rise is much slower and the amplitudes are only one tenth as much as when the door was removed. This is a good example of diffusion flux coupling. Apparently the diffusion flux does not reach its crest until about 20 microseconds, whereas the aperture flux reached its crest at about 2.75 microseconds, the same as the fast lightning current waveform.

Some aperture flux does, of course, exist inside the gun bay with the door closed, as was evident in the measurements of Figure 29. The internal field measurements of Figure 29 do not show any diffusion flux, however. The reason for this is unclear, except that since the flux probe time constant is 4 microseconds it responds to the derivative of flux for much longer times, and the amplitude of the derivative of diffusion flux may have been much lower than amplitudes of the aperture flux itself. On the

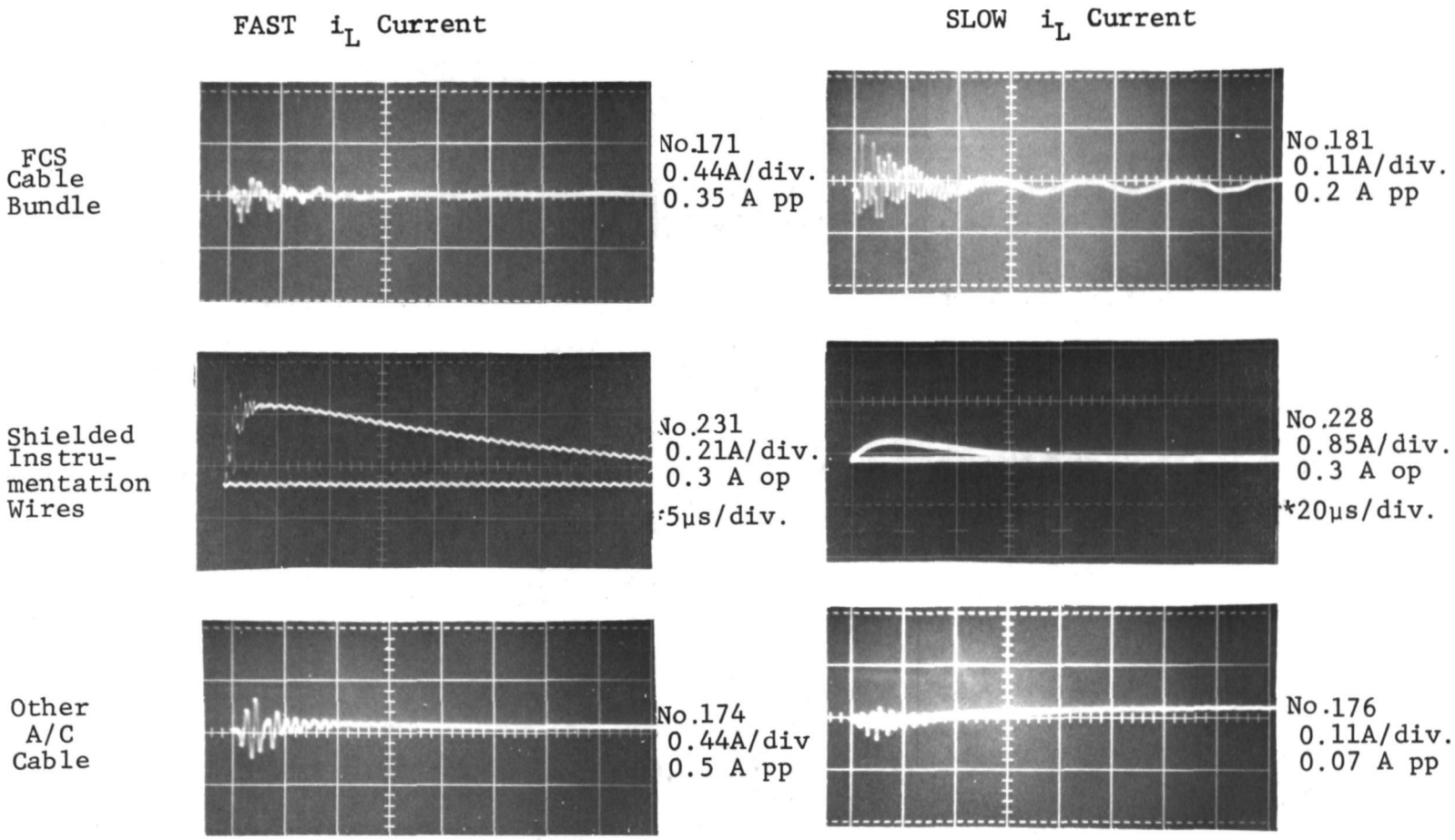

2μs/div. except as noted (*)

FIGURE 65 - INDUCED CURRENTS ON CABLE BUNDLES UNDER WING.

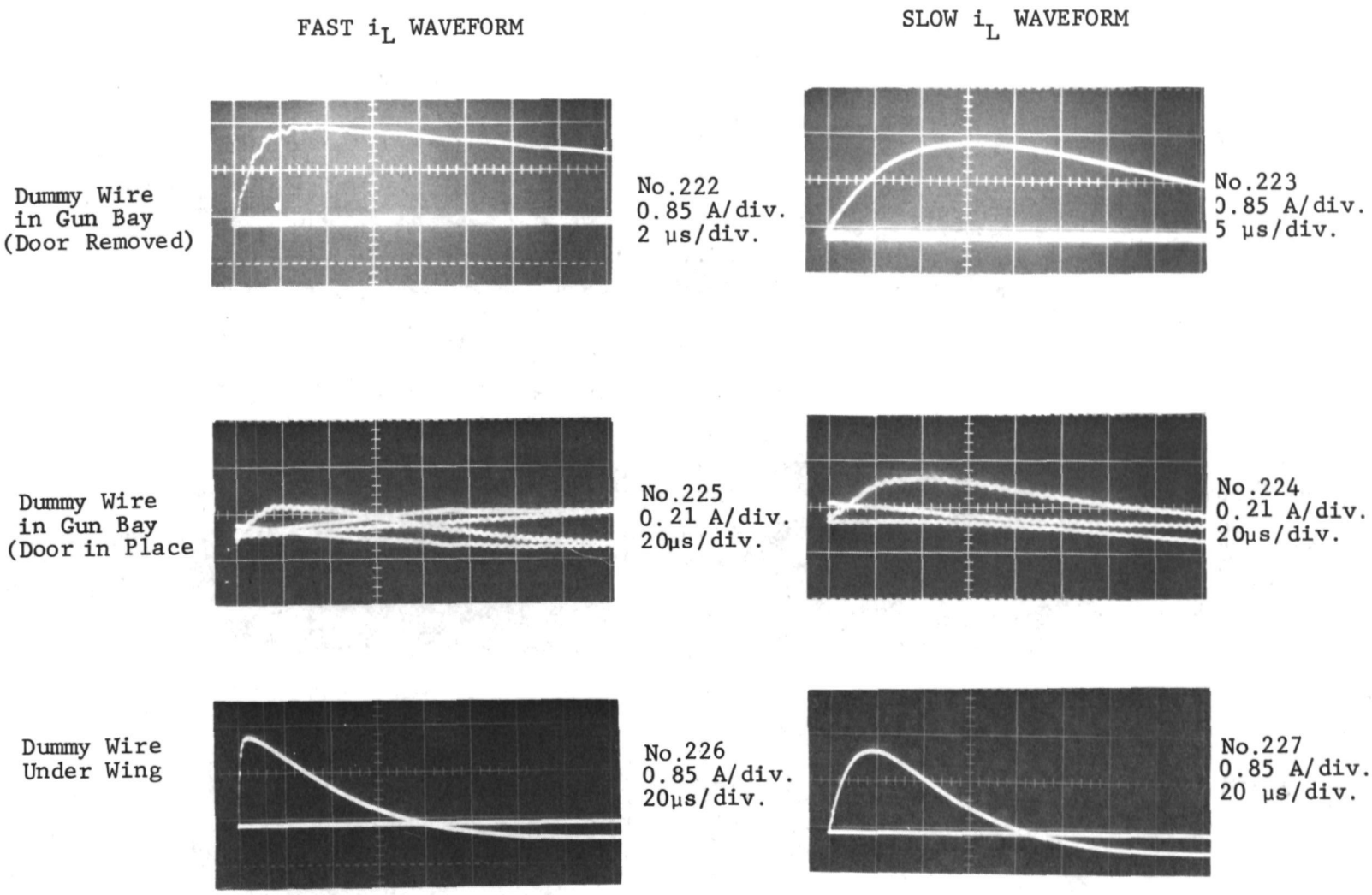

FIGURE 66 - CURRENTS MEASURED ON DUMMY WIRES GROUNDED AT EACH END.

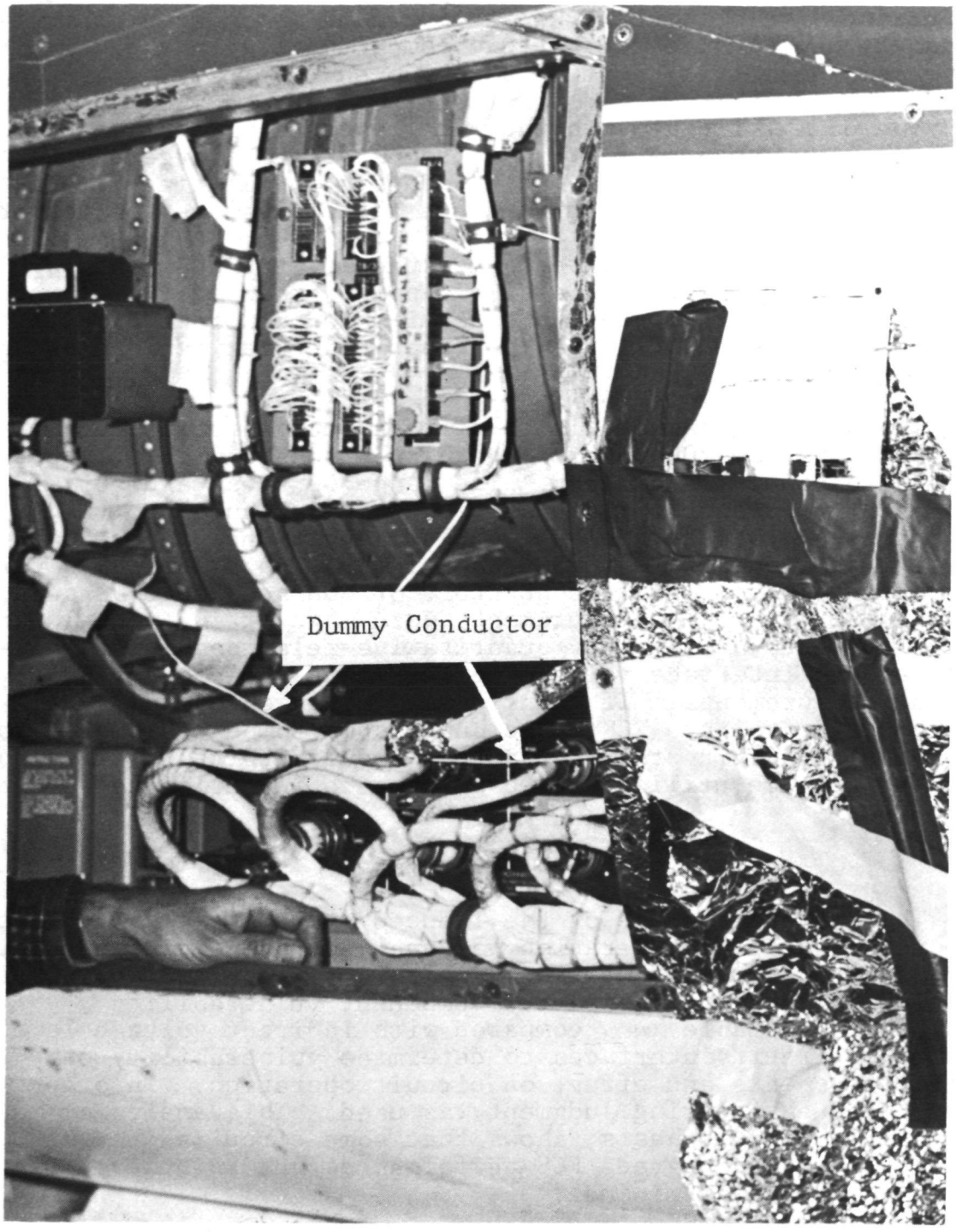

FIGURE 67 - DUMMY CONDUCTOR IN THE LEFT GUN BAY.

other hand, the presence of diffusion flux is apparent in measurements made inside the battery compartment with the same probe and sensitivity setting as shown on Figure 32.

The dummy wire beneath the wing responds primarily to aperture flux, because there is a comparatively large crack between the wing and these cables beneath, permitting direct flux penetration to the region where the cables are positioned.

Thus, the induced currents measured in the FCS cable system behave as expected for a single-point grounded system which limits first order currents but permits second order effects made possible by the distributed capacitance between cables and the airframe.

The peak-to-peak amplitude of total currents induced in the FCS cables by the 200 ampere lightning stroke ranged from 0.05 amperes to about 1.8 amperes. The range of these and corresponding extrapolated amplitudes is shown in Figure 68. Thus, the mean peak-to-peak amplitude of current induced by a 200,000 ampere lightning stroke in FCS cables would be about 267 amperes. The current on any single conductor, of course, would be some fraction of this. No measurements were made of individual conductor currents, nor is any quantitative relationship yet evident between interface voltage measurements and cable bundle current measurements. If transformer injection of full scale induced currents into FCS cable bundles is to be considered for future vulnerability testing, actual induced current data such as these must be utilized to establish the injection test levels.

Impact on DFCS System

The expected impact of the induced voltages measured in the FCS system on system operation was analyzed by Delco Electronics, manufacturer of the DFCS. This analysis is reported separately by Delco in Ref. 1. Individual component vulnerability data, when available, were compared with indirect voltage levels at single circuit interfaces to determine vulnerability of system components and effect on circuit operation. In other cases, best engineering judgment was used. This analysis, made on a single circuit basis, shows that some circuits are vulnerable enough to degrade FCS performance, but in others, the consequences appear minimal.

It is evident that lightning-induced voltages appear simultaneously in all DFCS circuits. They also appeared simultaneously in the three BCS channels. Simultaneous failures in many circuits may degrade redundance and backup capability as well as the primary DFCS. Thus, the consequences of various

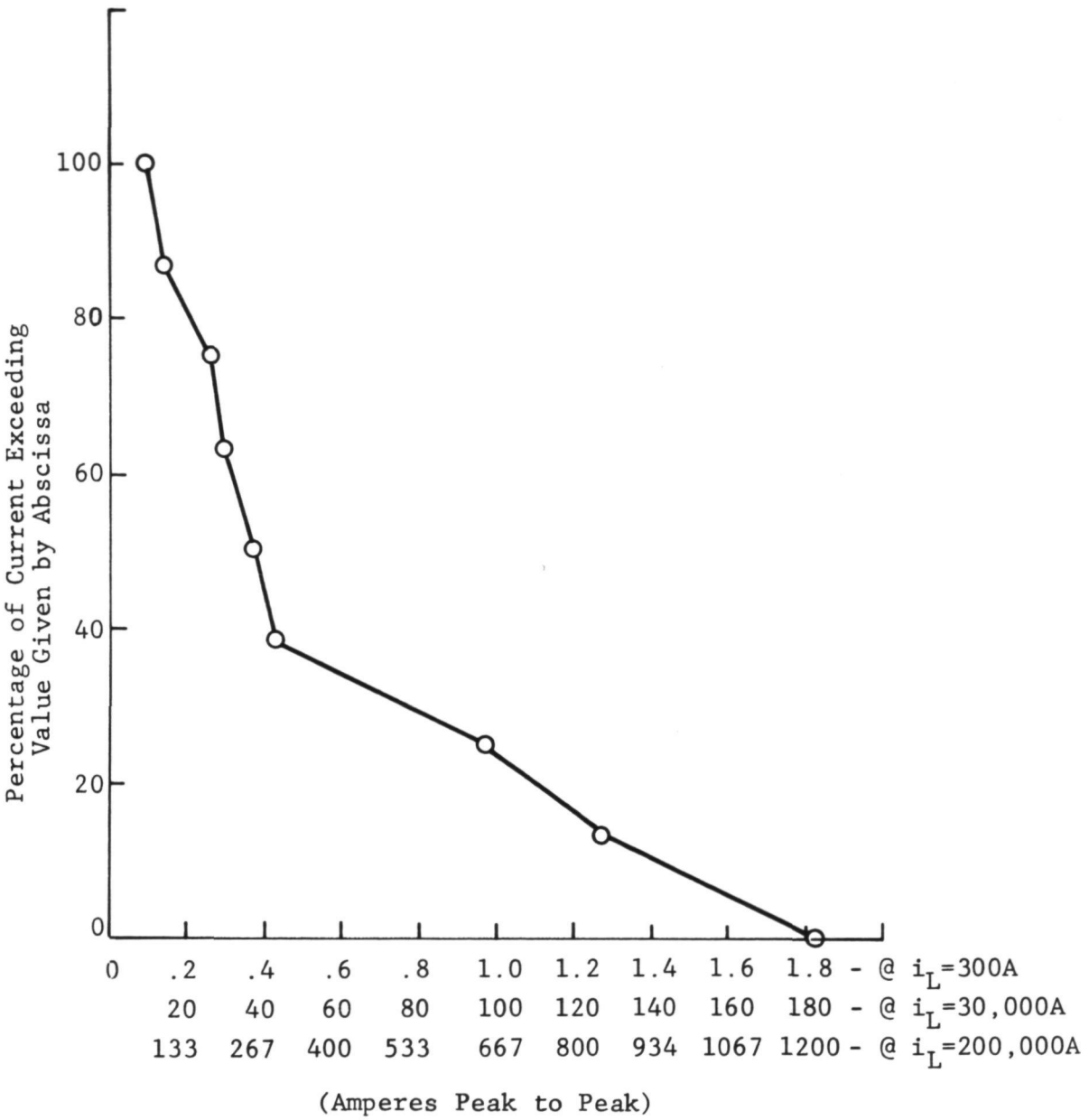

FIGURE 68 - DISTRIBUTION OF AMPLITUDES OF CABLE BUNDLE CURRENTS (MEASURED IN LEFT GUN BAY).

combinations of simultaneous failures must be assessed before the total impact of lightning on the FCS operation can be determined.

The experimental program described herein, of course, utilized single simulated lightning strokes. Since most lightning flashes convey more than one stroke in rapid succession (typical separations are 20 or 30 milliseconds) an FCS system subjected to a natural lightning flash is likely to experience multiple induced voltage surges in rapid succession. Such an environment may further compromise the FCS recovery ability. As noted in Reference 2, the Apollo Lunar Guidance Computer performs all flight control functions within a major cycle sample time of 30 milliseconds. Thus, more than one stroke could impact the system within one cycle. Computer computation times are between 23 and 82 microseconds and the memory cycle time is 11.7 microseconds. Nearly all of the induced voltages lasted for 10 microseconds or less, so they are within the time frame of computer computations.

CONCLUSIONS

This program represents the first experimental investigation of lightning-induced effects on a fly-by-wire flight control system. The results of this study are therefore significant, both for this particular aircraft and for future generations of aircraft and other aerospace vehicles such as the Space Shuttle, which will employ digital fly-by-wire flight control systems. Particular conclusions from this work are as follows:

1. Equipment bays in a typical metallic airframe are inadequately shielded and permit substantial voltages to be induced in unshielded electrical cabling inside.

2. A single-point ground does not eliminate lightning-induced voltages in aircraft electrical circuits. It reduces the amount of diffusion-flux induced and structural IR voltage but permits significant aperture flux induced voltages.

3. Typical voltages and currents induced in single-point grounded circuits are damped oscillatory waveforms excited by aperture magnetic fields, with frequencies and time durations dependent upon circuit physical and electrical characteristics.

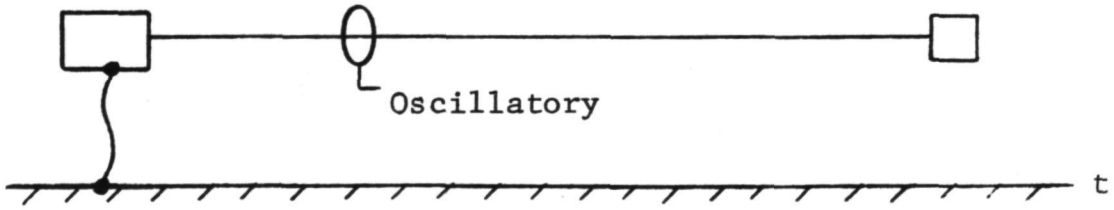

Voltage Amplitude - Proportional to Aperture Field Rate of Rise.
Current Amplitude - " " " " Amplitude

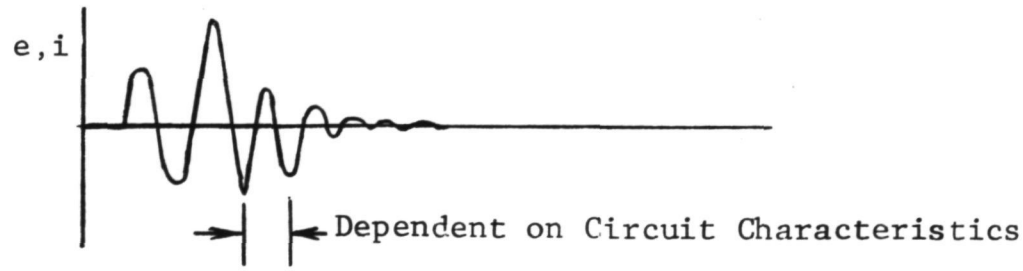

4. Typical voltages and currents induced in multiple grounded circuits are a double exponential unidirectional waveform induced by aperture and diffusion magnetic fields, whose duration is proportional to that of the diffusion magnetic field.

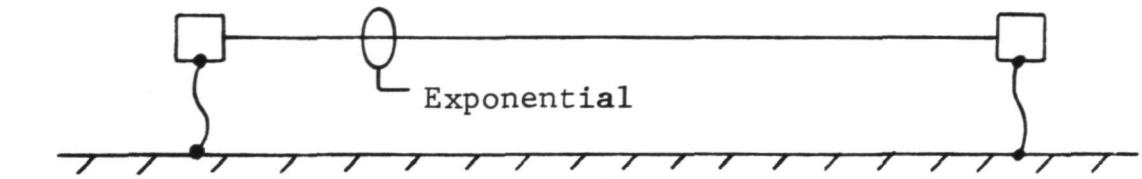

Voltage Amplitude - Proportional to Aperture Field Rate of Rise
Current Amplitude - " " " " Amplitude

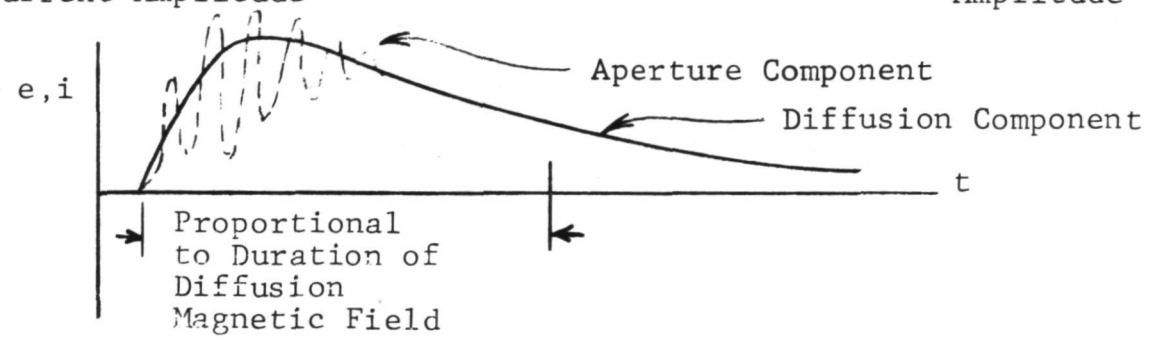

5. Induced voltages of similar magnitudes will appear simultaneously in all channels of a redundant system.

6. Lightning-induced voltages in the NASA F-8 DFBW electrical circuits pose a serious hazard to FCS operation.

It should be remembered that the DFCS equipment is an adaption of existing Apollo Lunar Module equipment that was not designed to survive lightning-induced voltages, nor were specific measures designed into the interconnecting cabling to reduce susceptibility to these effects.

RECOMMENDATIONS

For This Airplane

1. The NASA F-8 DFBW airplane should not be flown in thunderstorm areas unless positive measures are taken to minimize possible lightning effects.

2. If it is desired to minimize lightning effects on the NASA F-8 DFBW aircraft, the following modifications may be considered:

   - Place overall shields over all FCS system cables. These shields must be grounded to the airframe at each end.

   - Repeat some of the induced voltage tests to determine how much induced voltage remains, and then assess the impact of the remaining induced voltages on FCS operation.

   - Apply surge suppression and/or filtering at cable/electronics interfaces to limit remaining induced voltages to levels beneath those known to be hazardous to the FCS electronics.

For Future Fly-by-Wire Aircraft

Cable shielding, surge suppression, grounding and interface modifications offer means of protection of fly-by-wire flight control systems from the effects of lightning, but successful design will require a coordinated sharing of responsibility among those who design the interconnecting cabling and those who design the electronics. A set of Transient Control Levels for system cabling and Transient Design Levels for electronics, separated by a margin of safety, should be established as design criteria. Data from this and other experimental programs should be utilized to help establish these criteria.

Lightning protection design should be initiated very early in the design stages of the Flight Control System as well as the airframe in which it is to be installed. Protection against the indirect effects should therefore assume the same importance as protection against the direct effects of lightning has been given in the past.

REFERENCES

1. Anon: Lightning-Induced Voltage Impact on NASA F-8 Digital Flight Control System When Scaled to a 200,000 Ampere Stroke, Rep. R74-21, DELCO ELECTRONICS, February 1974.

2. Deets, D.A. and Szalai, K.J.: Design and Flight Experience With a Digital Fly-By-Wire Control System in an F-8 Airplane. AGARD paper reprinted from Conference Preprint No. 137 on Advances in Control Systems.

3. Plumer, J.A.: Analysis and Calculation of Lightning-Induced Voltages in Aircraft Electrical Circuits. NASA CR 2349, January, 1974.

4. Walko, L.C.: A Test Technique for Measuring Lightning-Induced Voltages in Aircraft Electrical Circuits. NASA CR 2348, February, 1974.

5. Berger, K.: Novel Observations on Lightning Discharges: Results of Research on Mount San Salvatore. Franklin Inst. vol. 283, pp. 478-525, June 1967.

6. Belevitch, V.: The Lateral Skin Effect in a Flat Conductor. Phillips Tech. Rev., vol. 32, no. 6/7/8, pp. 221-231, 1971.

7. Kaden, H.: Uber den Verlustwiderstand von Hochfrequenz-leiten. (Upon the Resistance of High Frequency Conductors). Archiv für Elektrotechnik, vol. 28, pp. 818-825, 1934.

APPENDIX - Derivation of Induced Voltage Expression Parameters.

A damped oscillatory voltage waveform of the form shown in Fig. 1

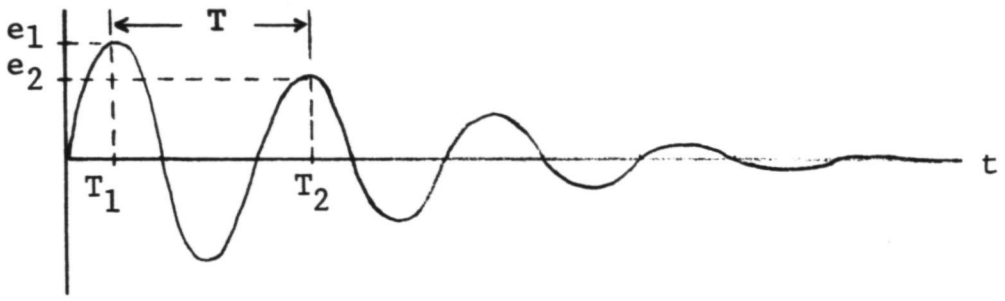

FIGURE 1 - DAMPED OSCILLATORY INDUCED VOLTAGE WAVEFORM

can be expressed analytically by

$$e = E(\sin\beta t)\varepsilon^{-\alpha t} \tag{1}$$

where,

$$E\varepsilon^{-\alpha t} \tag{2}$$

is the expression for the decaying envelope.

The radian frequency, B, is very nearly equal to

$$\beta = \frac{2\pi}{T} \tag{3}$$

where T is the period of oscillation.

At $t = t_1$ (the time of the first positive peak),

$$e_1 = E(1)\varepsilon^{-\alpha t_1} \tag{4}$$

since $\sin \frac{\pi}{2} = 1$.

Also, at $t = t_2$, (the time of the second positive peak),

$$e_2 = E(1)\varepsilon^{-\alpha t_2} \tag{5}$$

Equations (4) and (5) are two equations in two unknowns, E and α, since e_1, e_2, t_1 and t_2 are data points which can be taken from the induced voltage oscillogram. Thus, these two equations can be solved simultaneously for both unknowns.

The ratio e_1/e_2 is defined as the Decrement. Thus,

$$\text{Decrement} = \frac{e_1}{e_2} = \frac{E\varepsilon^{-\alpha t_1}}{E\varepsilon^{-\alpha t_2}} = \frac{\varepsilon^{-\alpha t_1}}{\varepsilon^{-\alpha t_2}} \tag{6}$$

or, simplifying,

$$\text{Decrement} = \varepsilon^{-\alpha t_1 + \alpha t_2} = \varepsilon^{\alpha(t_2 - t_1)} \tag{7}$$

and, from Fig. 1 and equation (3),

$$(t_2 - t_1) = T = \frac{2\pi}{\beta} \tag{8}$$

so, from equation (8),

$$\text{Decrement} = \varepsilon^{(2\pi\alpha/\beta)} \tag{9}$$

from which,

$$\alpha = \left(\frac{\beta}{2\pi}\right) \text{Log}(\text{Decrement}) \tag{10}$$

and, from equation (4),

$$E = \frac{e_1}{\varepsilon^{-\alpha t_1}} \tag{11}$$

E, α and β have been calculated by the above expression and tabulated with the measured peak induced voltages in Table II.

APPENDIX - Block Diagram of Flight Control System